Mechanisms of mu opioid receptor mediated protection from multiple models of acute injury

Jason Rosenbaum Goldsmith

A dissertation submitted to the faculty of the University of North Carolina at Chapel Hill in partial fulfillment of the requirements for the degree of Doctorate in Philosophy in the Department of Pharmacology (School of Medicine)

Chapel Hill
2012

Approved by:

Christian Jobin, PhD

Ryan Balfour Sartor, MD

T. Kendall Hardin, PhD

Lee Graves, PhD

Andrea Nackley, PhD

ABSTRACT

JASON ROSENBAUM GOLDSMITH: Mechanisms of mu opioid receptor mediated protection from multiple models of acute injury
Under the direction of Christian Jobin

Numerous intestinal pathologies involve breakdown of the intestinal barrier, including Inflammatory Bowel Diseases and ischemia/reperfusion injury. Damage to the intestinal barrier leads to immune system activation, resulting in further damage to the intestinal epithelium; this generates a positive feedback-loop leading to sustained intestinal injury. Current therapies focus on treating the symptoms of intestinal damage or suppressing the immune system, and do not treat the underlying intestinal damage. This work explores the role of mu opioid receptor (MOR) signaling in the protection and recovery from acute intestinal injury. MOR signaling is responsible for the analgesic properties of opiates such as morphine. This work establishes for the first time that MOR signaling promotes intestinal epithelial survival and restitution during and after acute intestinal injury, using multiple models of injury in two different animal species. In zebrafish larvae, we created a model of acute intestinal injury using the non-steroidal anti-inflammatory drug (NSAID) glafeinine, which was shown to involve induction of cell stress with blockade of proper endoplasmic reticulum (ER) and mitochondrial stress responses, leading to intestinal epithelial cell (IEC) apoptosis. Administration of the MOR agonist DALDA protected against this

injury by restoring the proper cellular stress responses. In mice, we established that DALDA administration could protect and enhance recovery from a chemical (dextran sodium sulfate) model of acute colitis. This effect correlated with increased IEC STAT3 phosphorylation, an effect known to be protective in the intestine. Additionally, we established that DALDA administration protected mice from small intestine ischemia/reperfusion-induced injury. Using an IEC-specific MOR knockout strain of mice that we developed, we established that the DALDA-mediated protection was due to IEC-specific MOR signaling. Pharmacological blockade of PI3K signaling demonstrated that MOR-mediated protection from ischemia/reperfusion injury is also PI3K-dependent. Together, this work establishes for the first time that enterocyte-mediated MOR signaling is intestinal-protective, engaging numerous, likely related pathways in the intestinal epithelium. This suggests that opioid-based therapy should be explored in patients for the treatment pathologies involving intestinal injury.

To my wife Rachel Goldsmith; without her love and support, I would not be the scientist or person I am today. She has been by my side since I developed ulcerative colitis, and it is my hope that one day, work such as this dissertation will prevent other couples from being put through the hardship my disease has put her through.

ACKNOWLEDGEMENTS

Numerous people have helped make this work possible, beyond what can written here. However, there are still many individuals I would like to thank specifically.

First, I would like to thank my dissertation committee and in particular my advisor Dr. Christian Jobin, who has been a source of both great support and inspiration, and for teaching me the art of science. I would like to thank Dr. Balfour Sartor, who has graciously let me work in his IBD clinic for the last three years, providing me with an amazing education in IBD patient care, and serving as inspiration of what can be accomplished while being inflicted with IBD. I would like to thank Dr. Andi Nackley for teaching me the tissue culture techniques I still use to this day. I would like to thank Dr. Ken Harden and Dr. Lee Graves for keeping this work “pharmacological.”

I would also like to thank the UNC-CH MD/PhD program, and in particular Dr. Orringer, for their support of my studies and their help and support in my successful pursuit of an F30 grant. Similarly, I would like to thank the Pharmacology Department at UNC-CH, for their support in the production of this work.

Numerous other scientists have helped me in this work as well, and they also greatly deserve my thanks. First, I would like to thank my current and past

lab mates, for their support in this work. In particular, I would like to thank Dr. Javier Rivera-Guzman, who has been both a friend and colleague throughout my studies. I would also like to thank Dr. John Rawls for support, guidance, and keen critical eye. Additionally, I must thank both Ed Flynn and Dr. Jordan Cocchiaro of the Rawls lab for their support and assistance in the zebrafish project. I am grateful to the lab of Dr. Bryan Roth, and Dr. Prem Yadav specifically, for their assistance with the radioligand binding assays, and I would like to thank Dr. Jennifer Whistler for her generous donation of the Floxed-MOR mice prior to publication. The staff of the Microscopy Services Laboratory: Dr. Robert Bagnell, Victoria Madden, and Steven Ray, have also played a crucial role in the success of this work, and I am grateful for their assistance. Greg Gipson, my undergraduate assistant and good friend, was also helpful to the publication of one of the manuscripts that makes up this work. Additionally, he offered his assistance on other occasions when my lab mates were unavailable during the radioligand binding studies. I would also like to thank Drs. Ian Carroll and Yehuda Ringel for inviting me to join them in their clinical IBS studies.

Outside of my scientific family, I would like to thank both my parents and my in-laws, for their steady support (in terms food, phone calls and vacations) and editing of this work over the years.

Finally, I must thank my martial arts school, who are my second Ohana and my primary source of stress relief. You have been my extended family throughout my time in North Carolina, and are a source of daily strength in my life.

TABLE OF CONTENTS

LIST OF TABLES

LIST OF FIGURES

LIST OF ABBREVIATIONS AND SYMBOLS

5-ASA: 5-aminosalicylic acid

ALD: Alcoholic liver disease

ANOVA: Analysis of variance

APC: Adenomatous polyposis coli

BF: Bright-field

COX: Cyclooxygenase

DALDA: Dermorphin [D-Arg2, Lys4] (1-4) amide

DAPI: 4',6-diamidino-2-phenylindole

DCM: Dilated cardiomyopathy

DMSO: dimethyl sulfoxide

DNA: Deoxyribonucleic acid

DOR: Delta opioid receptor

Dpf: Days post-fertilization

DTT: Dithiothreitol

DSS: Dextran sodium sulfate

EDTA: Ethylenediaminetetraacetic acid

Edu: 5-ethynyl-2'-deoxyuridine

EGF: Epidermal growth factor

EGFP: Enhanced green fluorescent protein

ENU: *N*-ethyl-*N*-nitrosourea

ER: Endoplasmic reticulum

Foigr: Foie gras mutation

GF: Germ-free

GFP: Green fluorescent protein

GI: gastro-intestinal

GPCR: G-protein-coupled-receptor

GSK3β: Glycogen synthase kinase 3 beta

GZM: Gnotobiotic zebrafish media

HCC: Hepatocellular carcinoma

HCV: Hepatitis C virus

HGPS: Hutchinson-Gilford progeria syndrome

HIF: Hypoxia inducible factor

Hpf: Hours post-fertilization

IBD: Inflammatory bowel disease

IBS: Irritable bowel syndrome

IEC: Intestinal epithelial cell

IHC: Immunohistochemistry

IFN: Interferon

IKKβ: IκB kinase beta

IL: Interleukin

I/R: Ischemia/reperfusion

JAK: Janus kinase

KOR: Kappa opioid receptor

LPS: Lipopolysaccharide

MAPK: Mitogen-activated protein kinase

MODS: Multi-organ dysfunction syndrome

MOR: Mu opioid receptor

MPO: Myeloperoxidase

MW: Molecular weight

NAFLD: Non-alcoholic fatty liver disease

NEC: Necrotizing enterocolitis

NF-κB: nuclear factor kappa-light-chain-enhancer of activated B cells

NIH: National Institutes of Health

NK: Natural killer

NSAIDs: non-steroidal anti-inflammatory drugs

Oprm1: Murine mu opioid receptor gene

PBS: Phosphate-buffered saline

PCR: Polymerase chain reaction

PI: Propidium ioidide

PI3K: Phosphoinositide 3 kinase

PKA: Protein kinase A

PLC: Phospholipase C

PTU: Phenylthiouria

ROI: Region of interest

RNA: ribonucleic acid

RT-PCR: Real-time polymerase chain reaction

SAA: Serum amyloid A

SCID: Severe combined immunodeficiency

SNP: Single nucleotide polymorphism

SPF: Specific-pathogen free

STAT3: Signal transducer and activator of transcription

TEM: Transmission electron microscopy

TILLING: Targeting induced local lesions in genome

TNBS: 2,4,6-trinitrobenzene sulfonic acid

TNF: Tumor necrosis factor alpha

TLR: Toll-like receptor

TRIF: TIR domain-containing adaptor inducing IFN-β

TxR: Texas red

UPR: Unfolded protein response

VEGF: Vascular endothelial growth factor

XBP1: X-box binding protein-1

WHO: World Health Organization

Zfin: Zebrafish

CHAPTER 1

INTRODUCTION

Human intestinal pathologies and the need for new therapeutics

The gastrointestinal system is responsible for the absorption of nutrients and excretion of waste products. Therefore, preserving intestinal homeostasis plays a central role in the overall health of an organism. Intestinal homeostasis is achieved in part by the maintenance of a functional barrier composed of a single monolayer of IECs, which isolates the host from the highly antigenic luminal milieu [1]. Numerous events can lead to an impaired mucosal barrier including genetic predisposition [1], radiation exposure [2], ischemic episodes [3], and medication use (non-steroidal anti-inflammatory drugs—ie NSAIDs [4]). Events leading to compromised barrier function have also been associated with inflammatory bowel diseases (IBD) [1, 5]. Additionally, loss of the intestinal barrier is the principle driver of the more serious complications of ischemia and radiation induced injury in the intestine—specifically sepsis and subsequent organ failure [2, 6-9]. Unfortunately, there is a near complete absence of pharmacological agents to enhance epithelial restitution in the face of these conditions. Current treatment strategies involve only supportive care or eliminating the source of intestinal injury.

One of the most notorious examples of an intestinal disorder involving a compromised barrier is IBD. In humans, IBD is the result of dys-regulated interactions between a genetically susceptible host and their commensal gut microbiota [1, 10, 11]. IBD affects 1.4 million Americans and there is no cure for the disease [12]. Pharmacological treatment centers around the use of anti-inflammatories and immunosuppressants [13]. However, current drugs are non-specific and have deleterious side-effects, such as serious and opportunistic infections, increased risk of lymphoma, and death [14]. Additionally, patients often become non-responsive to therapies over time [14-16], leaving surgery and its associated risks as the only recourse [14].

The current model of IBD pathogenesis involves an improper, sustained immune response to commensal bacteria in a genetically susceptible host [1, 11]. This sustained immune reaction results in epithelial damage, which leads to further immune activation due to loss of the intestinal barrier—creating a vicious positive-feedback loop. The intestine itself is under constant cellular stress, and proper responses to this stress are critical for maintaining an intact barrier. Recently, one set of genetic susceptibility factors in the pathogenesis of IBD that have gained increasing focus are primary defects in the maintenance of the intestinal barrier resulting from hampered cell stress responses such as autophagy [17, 18]. Specifically, single nucleotide polymorphisms (SNPs) in x-box binding protein-1 (XBP1) have been linked with IBD [19]. XBP1 is a downstream mediator of the unfolded protein response (UPR) that occurs in the face of ER (endoplasmic reticulum) stress and leads to autophagy [20]. In mice,

loss of intestinal epithelial cell (IEC)-specific XBP1 results in increased ER stress and Paneth cell apoptosis [19]. These mice develop spontaneous enteritis and have enhanced susceptibility to dextran sodium sulfate (DSS)-induced colitis, suggesting that loss of proper UPR responses can lead to a defective intestinal barrier, including loss of the intestine-protective Paneth cells [18].

Another gastro-intestinal pathology characterized by compromised barrier function is radiation-induced intestinal injury. More than 50% of cancer patients receive radiation as part of their therapeutic regime [2]. While the small bowel is rarely a target of such treatment, its size and location results in it receiving significant doses of ionizing radiation, leading to subsequent collateral damage in the gut [2]. Even with the low-doses typically used in modern therapy (< 2 Gy per treatment), over 70% of patients are estimated to have GI side effects within 3 weeks of therapy [2]. These symptoms typically include abdominal pain, diarrhea, nausea, vomiting and dehydration; while more severe, chronic symptoms include dysmotility, strictures and fistulae [2]. Particularly high levels of radiation can also lead to bacteremia and sepsis, although such radiation levels tend to be the result of accidental exposure—whether from medical error or a nuclear accident [2]—and not from deliberate therapeutic interventions. Radiation-induced small bowel injury is generally understood to result from damage to and loss of the rapidly proliferating intestinal stem cells. This leads to depletion of differentiated epithelial cells and loss of barrier function [7]. Currently, there are no treatments for radiation-induced intestinal injury, and patient care centers around the management of the resulting symptoms [2].

Ischemia-reperfusion (I/R) injury is a third source of intestinal barrier damage. The intestine can become hypoxic from a variety of sources, including atherosclerotic blockade, hemorrhage, veinous emboli, surgical clamping, and cardiac tamponade [3]. In all of these cases, enteric blood supply must be reduced by at least 50% to overcome compensatory mechanisms [8]. Additionally, ischemia is seen during chronic inflammation, which occurs during colitis [3], and is one of the driving factors in the pathogenesis of the newborn disease, necrotizing enterocolitis (NEC) [21]. Paradoxically, the restoration of blood flow (reperfusion) enhances the damage to the intestine through the introduction of oxygen free-radicals and increase in immune activation [3]. In severe cases, I/R injury can result in multiple organ dysfunction syndrome (MODS), with a mortality rate of approximately 30% [6].

I/R injury is currently believed to occur in a ‘three-hit’ model. In the first hit, blood flow is lost, resulting in signaling events directed towards the prevention of further injury, such as the activation of transcription factors including hypoxia-inducible factor (HIF) [22] and nuclear factor kappa-light-chain-enhancer of activated B cells (NF-κB) [23]. The second hit in this model is reperfusion, as the rapid introduction of oxygen enhances and sustains the inflammatory response [3]. The third hit is a chronically sustained intestinal immune response that results from intestinal barrier damage, due to bacterial translocation across the mucosa, bacteremia, and sepsis—all of which support further inflammatory responses and resulting intestinal damage—creating a positive feedback loop (like in IBD) of inflammation and intestinal damage [3]. In

I/R injury, the consequences of this positive feedback loop are perhaps most typified by NEC [21], where the sustained response results in progressive loss of a newborn's intestinal track, resulting the death of 2-4% of all very low birth weight infants [24]. At the molecular level, the dual-edged nature of the inflammatory response is best typified by studies of the NF-κB pathway. In a definitive study by Chen et al., enterocyte-specific loss of the essential catalytic activator of NF-κB, IKKβ (IκB kinase β), resulted in decreased systemic inflammatory responses that can lead to MODS during I/R injury but also resulted in several apoptotic damage in the enterocytes [23]. This dual-edged nature of the inflammatory response and its signaling effectors add to the complexity of treating this pathology.

IBD, radiation-injury, and I/R injury all provide clear examples of the type of profound human pathology that can occur with loss of the intestinal barrier compounded by a sustained immune reaction (Figure 1). Unfortunately, current management of such diseases is mostly supportive, focusing on treating the resulting symptoms (radiation, I/R injury, and IBD) as well as suppressing the inflammatory responses that leads to further intestinal damage (generally seen in IBD). Treatments that enhance epithelial healing and restore barrier function represent a novel means to approaching these severe GI illnesses and if validated, could radically alter patient therapy. Treatments focused on healing have seen some initial validation in both murine models of intestinal inflammation and in human IBD patients with the use of trophic factors that promote wound healing and restore the intestinal barrier function [5, 25, 26]. However, more

work needs to be done before restoration of barrier function can become a mainstay of intestinal therapy.

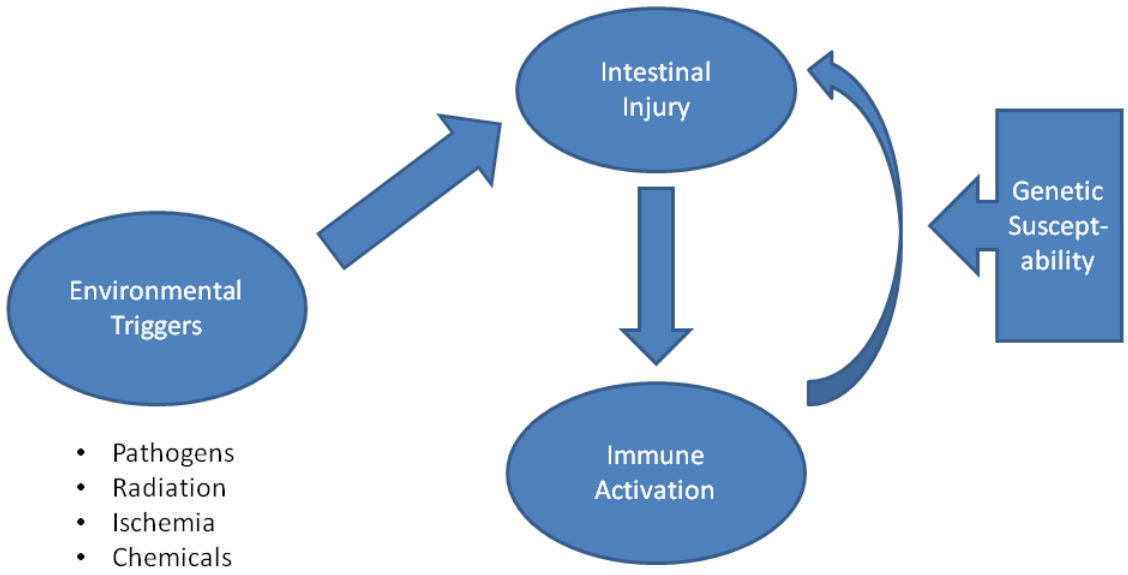

Figure 1: Intestinal injury and immune activation lead to a cycle of intestinal damage. In IBD, genetic susceptibility is generally viewed as required to have sustained inflammation. In ischemia/reperfusion and radiation-induced injury, the immune activation and resulting enhancement of intestinal injury is part of the acute, pathogenic process.

Wound healing, epithelial restitution and related signaling

Development of therapies that target intestinal healing requires an understanding of the host response to intestinal injury. This healing process and host response is also termed restitution/wound-healing [10]. At baseline, the gut is already highly migratory and proliferative—the monolayer of IECs migrates at a rate of 5-10 μm/hr and is renewed every 2 to 5 days [27]. During injury, this baseline process is enhanced further. Once a restitution response has been engaged, cells at the edge of the wound undergo a de-differentiation process and migrate into the wounded area. They then undergo cytoskeletal rearrangement [28], re-differentiate, and finally re-establish tight junction barriers with their neighboring cells [10, 29]. This process does not require epithelial proliferation, but cellular renewal is needed to replenish the decreased enterocyte pool after injury [28]. Numerous signals are implicated in the maintenance of the mucosal barrier such as epidermal growth factors (EGF) [7], transforming growth factors (TGF-β) [30, 31], and cytokines such as IL-22 [32]; they act through a combination of pro-migratory, proliferative and/or anti-apoptotic activities. A variety of pathways including NF-κB, MAPK, STAT3, GSK3β/β-catenin [33] and PI3K/Akt [10, 34] have been demonstrated to be involved in intestinal wound healing.

Regardless of the upstream factors that lead to the initiation of wound healing, the result is specific set of programmed cellular events that occur during the restitution process. Upon initiation of wound healing cells lose their columnar polarity, undergoing massive restructuring of their actin cytoskeleton [27]. This is

controlled by the Rho family of small GTPases (Rho, Rac, Cdc42) [27]. Rho regulates the presence of stress fibers and adhesions, while Rac regulates the formation of lamellipodia and membrane ruffles and Cdc42 initiates filopodial extensions at the migrating cell edge [27]. The activity of these small GTPases drives cellular migration into the wound, after which the cell regains its columnar polarity and re-establishes adhesions and tight junctions with its neighbors [27]. Proliferation then ensues hours to days after injury, replenishing the population of enterocytes [31].

Relevant models of wound healing/restitution

This dissertation involves numerous model systems to explore wound healing and restitution in the intestinal epithelium (Table 1). *In vitro* the main assay used is the scratch assay, where a monolayer of IECs is grown in culture, and then subjected to a scratch, usually with a pipette tip [27]. The migration distance or the speed of cells moving into the wound is then measured. The central role of TGF-β in intestinal wound healing was first established with such a system [30, 31].

Model	*In vivo/in vitro*	Key Features	Weaknesses
Scratch Assay	*In vitro*	- Rapid and easy to use - Directly measures migration rate	- Artificial system - Uses cell lines
DSS Colitis	*In vivo*	- Rapid, reproducible injury - Low background for signaling - innate-immune-dependent - adaptive-immune-independent	- Chemical-based injury - Not physiologically relevant - Background and sex-specific severity
I/R injury	*In vivo*	- Physiologically and clinically relevant	- Labor-intensive - Noisy background for signaling studies
Glafenine/Zebra-fish injury	*In vivo*	- Rapid injury (12 hours) - Can use zebrafish imaging modalities	- New, unexplored system - Non-mammalian

Table 1: Models used in these studies.

One of the standard animal systems for the study of wound healing is DSS-induced colitis. Administration of the detergent DSS in the drinking water for several days results in acute colitis characterized by bloody diarrhea, weight loss, ulcerations, and granulocyte infiltration [35]. DSS is believed to be directly toxic to enterocytes in the basal crypts [35], and damage is thought to be exacerbated through innate immune activity. Specifically, blockade of neutrophil recruitment via knockout or antibody neutralization of the chemokine receptor CXCR2 abrogated DSS-induced damage [36]. However, studies in mice with conditionally depleted macrophages and dendritic cells (created using a transgenic line with Fas-mediated apoptosis of these cell lineages) demonstrated that macrophages/dendritic cells are important in protection from DSS-mediated injury, and that their loss enhances injury and neutrophil activity [37]. In contrast to the important role of the innate immune system in this model, DSS-colitis is largely adaptive-immune independent, as T-cell and B-cell deficient severe combined immunodeficiency (SCID) mice also develop severe colitis with DSS administration [38].

The roles of the numerous signaling pathways involved in wound healing have been explored in the DSS model of colitis. Transgenic mice with a dominant negative TGF-β receptor demonstrate enhanced injury in this model [39]. Similarly, enterocyte-specific STAT3-knockout mice [32] and enterocyte-specific NF-κB (RelA-subunit) knockout mice [40] both experience enhanced DSS-injury. Functional β-catenin is also important in protection from DSS-injury, as transgenic mice with reduced expression of the Wnt anatgonist Dkk1 have

enhanced recovery [41]. The presence of commensal bacteria in the intestine drives some of these protective pathways, demonstrated by exacerbated DSS-colitis in germ-free mice [42]. This pattern was also observed in mice deficient for the Toll-like receptor (TLR) adaptor MyD88 (myeloid differentiation primary response gene). These mice lack the ability to sense many bacterial products [43] and activate downstream signaling including the NF-κB pathway.

The second model explored in these studies is the ischemia-reperfusion model of injury. In this injury model, anesthetized animals (usually mice or rats) have branches of the superior mesenteric artery (along with collateral branches) clipped with aneurysm clamps for 30-60 minutes [23]. After the ischemic period, the clamps are removed for a variable amount of time before sacrifice, to induce the reperfusion phase of injury [23]. This system is in general less well-studied than the DSS-model of injury. NF-κB-mediated signaling was shown to be important in the protection of enterocytes during I/R injury, but also to potentiate the systemic inflammatory responses characteristic of this model [23]. GSK3β signaling has also been implicated in protection from ischemic injury, likely due to the sensing of bacterial products via the intracellular sensor Nod2 [33, 44]. These same studies showed that germ-free mice have enhanced damage due to I/R injury, suggesting that sensing the commensal microbiota is important in the wound healing response of this model [33, 44]. In contrast, however, $MyD88^{-/-}$ mice showed decreased susceptibility to I/R injury [45]. $MyD88^{-/-}$ mice are deficient in their ability to respond to bacterial products, including the potent endotoxin lipopolysaccharide through TLR4, and TLR4-deficient mice are also

less susceptible to I/R injury [46]. The contrasting data between the germ-free and MyD88$^{-/-}$ and TLR4-null mice demonstrate that the role of the microbiota in protection from intestinal I/R injury is still poorly understood (reviewed extensively by Kinross, et al. 2009 [3]).

While these two models of intestinal injury have provided key insights into the wound healing response, direct *in vivo* observation of the restitution response in real-time is not possible with murine systems. In recent years, the zebrafish (*Danio rerio*) has gained significant attention as a model organism [47]. It has numerous strengths that make it particularly well-suited for its use in the study of wound healing, including transparency through early adulthood. Significant key findings, including the role of H_2O_2 signaling in the wound healing process, were first discovered in the zebrafish [48-50]. A detailed review of the zebrafish as a model organism, with particular focus on the gastrointestinal system and the wound healing response, is presented in Chapter 2.

Mu-opioid receptor mediated signaling

This work explores the role of mu-opioid receptor activation in the wound healing response. The opioid receptors, consisting of the mu, delta, and kappa subtypes, are G-protein coupled receptors (GPCRs) of the rhodopsin subfamily. These receptors were named for the opiate class of drugs which signal through them. Opioids are widely used analgesics and have long been known to affect the development, differentiation and function in a variety of immune cells, typically in an immunosuppressive manner [51, 52]. Many of these effects have been linked to the mu-opioid receptor (MOR), while opposing effects by the delta

and kappa opioid receptors (DOR and KOR, respectively) are also observed [51-55]. Opioid receptors are classic G_i/G_o-coupled receptors, known to inhibit adenylate cyclase and increase intracellular [Ca^{2+}] and [K^+] [54], as well as to activate phospholipase C (PLC) [54, 56, 57]. Interesting, MOR has also been shown to induce cAMP by switching coupling from G_i to G_s, especially in the case of chronic morphine treatment [54, 58-60]. MOR has also been shown to activate the mitogen-activated protein kinase (MAPK) pathway through the extracellular-signal-related kinases (ERKs) [54, 61], a potential source of the receptor's immunomodulary properties [62] and a pathway known to be protective against DSS-colitis [63]. Finally, MOR can activate the phosphoinositide 3-kinase (PI3K)/Akt pathway through the Gβγ subunit in multiple cell types [55, 64, 65], including immune cells [66]. MOR activity is regulated in the canonical manner typical of GPCRs by down-regulation, desensitization and internalization of the receptor, often involving β-arrestin binding, which also induces downstream signaling events [54, 67, 68]. Hence, MOR affects numerous signaling cascades and likely impinges on a wide spectrum of cellular functions.

Due to the immunosuppressive properties of opioids, specific MOR agonists have recently been explored in murine systems as potential therapeutics for IBD. Subcutaneous administration of the highly specific peripheral MOR agonist, DALDA, [69] reduces inflammation in two T-cell dependent models of murine colitis (TNBS-induced colitis and in T-cell transfer-induced colitis [70]). DALDA also reduced TNF mRNA production in cultured

colonic biopsies from CD and UC patients [71]. Other work showed that in a small, open-label clinical trial, low-dose therapy of the non-specific opioid antagonist Naltrexone decreased inflammation in the DSS murine model of acute colitis, and ameliorated Crohn's Disease in patients [72, 73]. The activity of Naltrexone was postulated to work through DOR [72, 73], but the observations could be due to potentiation of endogenous MOR activity and prevention of G_s-coupling [74].

Interestingly, MOR mRNA expression levels were shown to be modulated by cytokines important in IBD [15, 16, 75] such as interleukin-1β [54], IL-4 [76], IL-6 [77], and TNF [78], in both murine models of colitis and human IBD patient samples [71, 72, 79]. At least one study has shown that changes in MOR mRNA correspond to equivalent changes in functional receptor number and activity, as determined by radioligand binding assays of ^{3}H-DAMGO and by [^{35}S]GTPγS binding assays [80]. This suggests that MOR activity may be regulated in part at the mRNA level, which would be unique for a GPCR.

Altogether, the current literature supports the concept that MOR signaling modulates intestinal inflammation; however, the therapeutic effect of MOR activation in intestinal injury is still unclear and somewhat controversial. Moreover, the signaling pathways responsible for MOR-mediated therapeutic effect in the intestine are currently undetermined, although several candidates do exist (outlined in Figure 2).

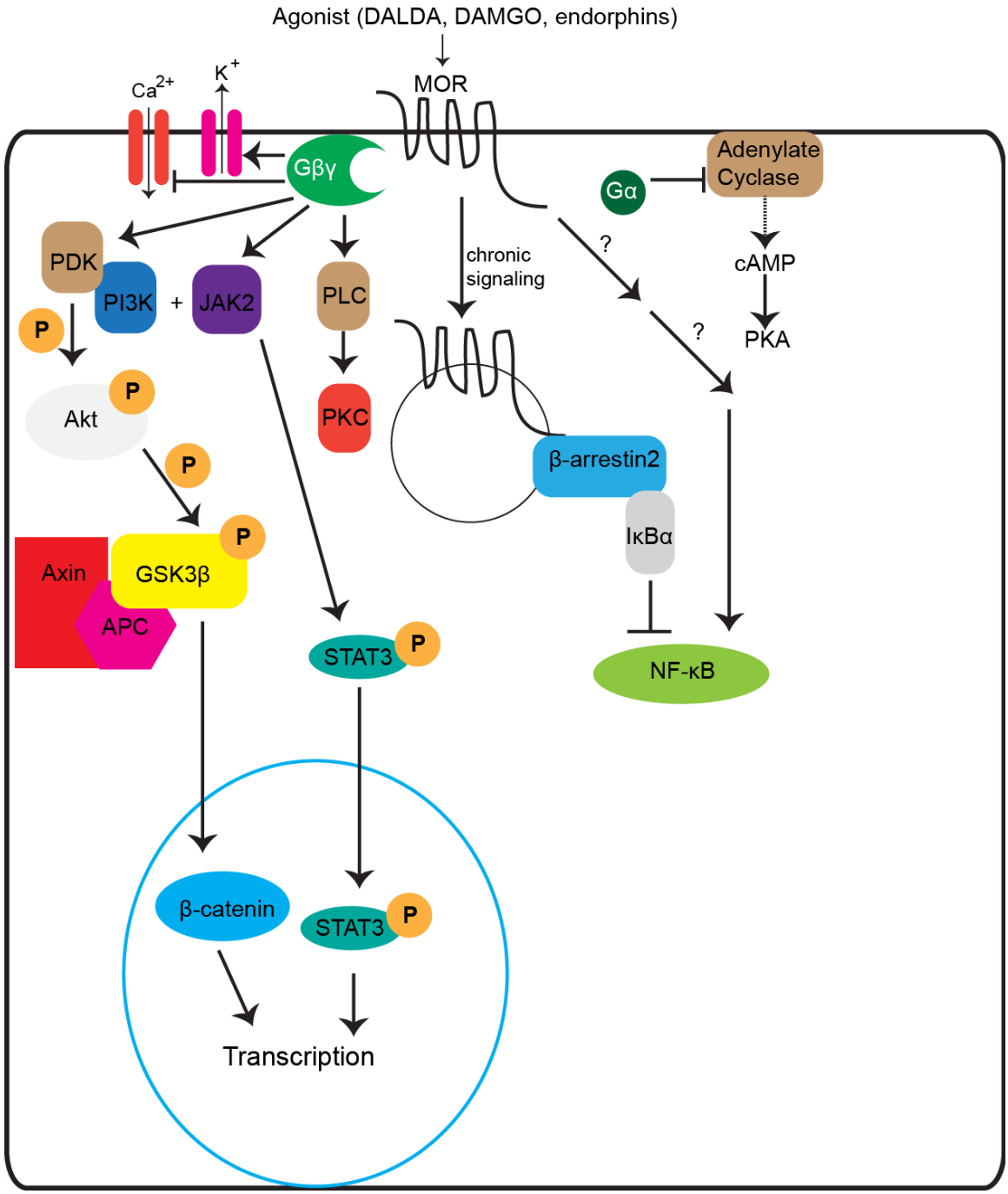

Figure 2: MOR signaling can impinge on a variety of signaling pathways. Activation of MOR can result in numerous downstream signaling events, a subset of which are shown here. Ligand binding results in nucleotide exchange and dissociation of the Gα and Gβγ subunits. The Gα unit (a G_i-subclass) inhibits adenylate cyclase, resulting in decreased levels of cAMP and diminished PKA (protein kinase A) activation. The Gβγ subunit activates protein lipase C (PLC), the PI3K/Akt pathway, STAT3 (through Janus Activating Kinase 2—JAK2), as well as the outward rectifying K^+ channel. It inhibits influx Ca^{2+}. MOR activation

can also affect NF-κB activation, both positively and negatively. Negative regulation has been demonstrated to involve β-arrestin signaling, which usually occurs as a result of chronic activation of the receptor, leading to internalization of MOR.

MOR has numerous downstream secondary messengers that are known to be protective in the intestine. NF-κB for example, has been shown to be both positively and negatively regulated by MOR-mediated signaling events [55, 81], sometimes in a concentration-dependent manner [82]. Similarly, G_i-coupled receptors have shown to activate STAT3 in other GPCR systems [83, 84], and DOR has specifically been shown to activate STAT3 [85]. Additionally, while MOR-activation is known to induce PI3K/Akt signaling [54], downstream activation of β-catenin is only presumed at this point. More globally, opioids have been used to protect brain and cardiac tissue from ischemia/reperfusion injury [86-88], and in the heart this process requires PI3K/Akt-dependent activation of the JAK/STAT3 pathway [89].

Unfortunately, a paucity of information exists on MOR-specific activation, especially in the intestine. Most work studying opioids in the intestinal system has focused on their alterations to gut motility [90]. Opiates in numerous mammalian systems decrease gut motility; in humans this results in increased tonic contractions of the intestine and increasing transit time of the lumenal contents [90]. This has been established as primarily an effect of the delta and mu receptors, while the kappa receptor has the opposite effect [90]. Opiates also decrease intestinal secretions by acting on both the enteric and central nervous systems [90]. In patients who experience both chronic pain and diarrhea (especially those with IBD), the use of opiates for these symptoms must be carefully managed, as colonic dyskinesia can predispose patients to toxic megacolon, a serious condition characterized by systemic toxicity and severe

colonic distension [91]. A second complication of chronic opiate use is narcotic bowel syndrome, characterized chronic or frequently occurring abdominal pain that worsens with continued or increasing opiate usage [91]. This is likely a result of chronic-opiate mediated desensitization and hyperalgesia [54, 91].

Due to the potential for serious complications, the role of opiates in enterocyte signaling has largely been ignored. However, these admittedly serious side effects are usually the result of *chronic* opiate use. In the studies presented here, we focus on the potential benefits of *acute* opiate use in the prevention of and recovery from acute intestinal injury. The current lack of available therapeutics that target epithelial restitution requires the exploration of every possible therapeutic agent. Furthermore, opiates are well-understood and available drugs, with consequently rapid bench-to-bedside potential. The use of restitution enhancing drugs to treat intestinal pathologies such as IBD, radiation-induced injury, and I/R injury remain a potent, but a relatively unexplored possibility due to the difficulty in finding non-opiate drugs outside of widely acting (and expensive) growth factors that can target this cellular response. MOR-specific agonists, particularly peripheral-only acting compounds such as those used in this dissertation work, could offer a new therapeutic avenue. The work presented here establishes the presence of MOR-mediated protection from intestinal injury in three different models of acute intestinal injury across two species, and provides the bench-side justification for the pursuit of clinical trials exploring the use of MOR agonists in the treatment of a significant array of intestinal pathologies.

CHAPTER 2

THINK SMALL: ZEBRAFISH AS A MODEL SYSTEM OF HUMAN PATHOLOGY[1]

Introduction

Although human pathologies have mostly been modeled using higher mammal systems such as mice, the lower vertebrate zebrafish has gained tremendous attention as a model system. The advantages of zebrafish over classical vertebrate models are multifactorial and include high genetic and organ system homology to humans, high fecundity, external fertilization, ease of genetic manipulation, and transparency through early adulthood that enables powerful imaging modalities. This review focuses on four areas of human pathology that were developed and/or advanced significantly in zebrafish in the last decade. These areas are 1) wound healing/restitution, 2) gastrointestinal diseases, 3) microbe-host interactions, and 4) genetic diseases and drug screens. Important biological processes and pathologies explored include wound-healing responses, pancreatic cancer, inflammatory bowel diseases, non-alcoholic fatty liver disease, and mycobacterium infection. The utility of zebrafish in screening for novel genes important in various pathologies such as polycystic kidney disease is also discussed.

---

[1] *Journal of Biotechnology and Biomedicine*, In Press.

Background

Investigators have long utilized reductionist systems and animal models to mimic and study basic processes regulating cellular biology, organ function and host homeostasis. While much work has been accomplished and continues to be undertaken in higher mammalian systems such as mice, rats, and rabbits, important discoveries have also been made using invertebrate systems such as Caenorhabditis *elegans* and Drosophila *melanogaster*. For example, RNA interference technology was first discovered in C. *elegans* [92], as was the initial caspase enzyme, caspase-1 (*ced-3* in C. *elegans*) [93]. Similarly, it was in Drosophila *melanogaster* that the innate signaling Toll-like receptors (TLR) were first identified via the discovery of the Toll gene, as was its linkage to the nuclear factor kappa-light-chain-enhancer of activated B cells (NF-κB) signaling cascade [94]. In the last ~15 years, there has been a growing appreciation for the vertebrate organism Danio *rerio* (zebrafish) as a tool to study human disease [95]. As opposed to C. *elegans* and Drosophila *melanogaster*, zebrafish is a vertebrate organism with physiological and anatomical characteristics of its higher organism counterparts (see Figure 3 for a diagram of larval zebrafish anatomy), while maintaining the ease of use of a lower organism. The characteristics of zebrafish that make them desirable tools for the study of embryogenesis/development also make them useful for the study of human pathologies. Zebrafish have a fully mapped genome (http://www.sanger.ac.uk/Projects/D_rerio/), which has significant homology with the human genome, including non-coding regions (~60 per gene globally across

all genes) [96] suggesting that numerous genes involved in human diseases could be matched in the zebrafish genome. Reverse (morpholino knock-down, Targeting Induced Local Lesions in Genome—TILLING [97]) and forward genetic (mutagenesis, transgenic) approaches are well established and commonly used to manipulate and characterize zebrafish gene function.

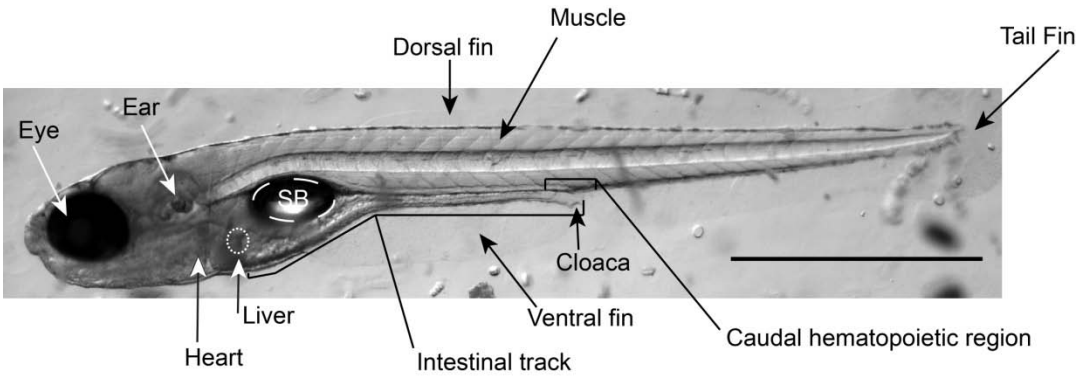

Figure 3: Diagram of zebrafish anatomy. A representative image of a transparent, 6 dpf larvae captured with brightfield microscopy. Organs and anatomical features are denoted in the figure. SB = swim bladder. Scale bar is 1 mm.

Zebrafish are highly fecund and breed rapidly; a pair of zebrafish produces over 100 embryos per clutch that are usable for larval experiments as early as 3 days post fertilization (dpf). These larvae are transparent through 7 dpf, and this can be extended to up to 9-14 dpf with the addition of the melanocyte inhibitor phenylthiouria. Moreover, the recent generation of transparent adult zebrafish such as the *Casper* line adds new imaging possibilities [98]. The transparency of zebrafish, in conjunction with sophisticated utilization of fluorescent technology to mark signaling proteins or cellular entities allows for powerful time-lapse imaging of biological and disease processes. Additionally, the vertebrate zebrafish has many features commonly found in mammals, including an innate immune system composed of neutrophils, NK cells, and monocyte/macrophages with functionality by 48 hours post-fertilization (hpf) [99, 100], and an adaptive immune system that is fully functional at 4-6 weeks post-fertilization [101]. The adaptive immune system is highly analogous to that of mammals, with T-cells and B-cells that have Rag-dependent V(D)J recombination (reviewed extensively in [100]). Finally, the zebrafish research community benefits from an up-to-date database of techniques, genetic strains and other useful resources at www.zfin.org.

In this review, we focus our discussion on larval and adult zebrafish models that recapitulate human diseases, focusing on four separate branches of pathology: wound healing/restitution, gastrointestinal disease, microbe-host interactions and genetic diseases and drug screens.

Wound Healing/Restitution

Wound healing represents a critical biological response of injured tissues and organs. Events causing epithelial injury and barrier breakdown initiate a biological response known as "restitution," which is aimed at resealing the damaged region and re-establishing host homeostasis. This “wound healing” response involves migration of epithelial cells toward the injured regions as well as epithelial cell proliferation to replenish the cell pool. Understanding the cellular and molecular mechanisms regulating this response could have profound translational impact for patients suffering from chronic inflammation, ischemia/hypoxia, burn injury and cancer. The powerful imaging modalities available to zebrafish researchers alongside their ease of genetic manipulation makes this vertebrate system an ideal model for studying wound healing response to various injuries [49]. Additionally, the ability of zebrafish to regenerate both limbs and cardiac tissue [102] make them a powerful animal model for understanding the molecular mechanisms involved in regenerative signaling.

The most popular zebrafish injury model is the larval tail wounding model, where a segment of the tail fin is resected. Using this injury model with transgenic zebrafish expressing EGFP under the transcriptional controlled of the neutrophil-specific myeloperoxidase (MPO) promoter—*Tg(BACmpx:GFP)i114*—investigators studied real-time neutrophil chemotaxis to the site of injury [48]. In this study, they observed retrograde chemotaxis of neutrophils towards the vasculature alongside where injury resolution was observed, suggesting for the

first time that retrograde chemotaxis may play an important role in the resolution phase of the inflammatory response [48]. To determine the function of the reactive oxygen species H_2O_2 in the wound healing response, investigators injected mRNA encoding for the hydrogen peroxide sensor HyPer to one-cell stage developing zebrafish embryos [103]. Upon tail wounding of 3 dpf larvae, the HyPer sensor demonstrated increased H_2O_2 production along a gradient decreasing away from the wound site, which signaled leukocyte chemotaxis to the injured location [49]. Using pharmacological and morpholino blockade, the authors showed that generation of the H_2O_2 gradient is dependent on the activity of the dual oxidase (*duox*) gene. This HyPer reporter system has also been utilized in the study of neuronal regeneration, an important area of study for the treatment of many human diseases. H_2O_2 produced by injured keratinocytes was shown to induce somatosensory axonal regeneration in zebrafish. Similar to the tail fin wounding model, neuronal regeneration required activation of *duox* [50]. Moreover, H_2O_2 administration promoted axonal regeneration following neuronal injury, even without accompanying keratinocyte injury [50]. These results expand the understanding of post-traumatic nerve injury and subsequent loss of limb function in humans. The healing-enhancing properties of H_2O_2 have since been extended to studies in both rabbits [104] and horses [105], as well as one reported case study in a human patient [106].

Beyond cutaneous wounds, zebrafish have been used for the ability to regenerate cardiac tissue. Unlike mammals, which form scars and do not regenerate cardiac tissue following injury, zebrafish are able to fully regenerate

their heart within 2 months after 20% ventricular resection [107]. This ability for zebrafish to overcome scar formation requires activation of Mps1, a mitotic checkpoint kinase [107]. Additionally, cardiac regeneration involves up-regulation of wound healing genes and proliferative factors including *apoeb, vegcf and granulina* (all of which have human analogs) and likely activation of platelet-derived growth factor B signaling [108]. Cardiac regeneration studies in zebrafish could produce novel paradigms and identify unique pathways/targets with profound translational impact for patients suffering from ischemic heart disease.

Gastrointestinal Diseases

The zebrafish gastrointestinal system is highly homologous to that of mammals, containing a liver, pancreas, gall bladder, and a linearly segmented intestinal track with absorptive and secretory functions [109, 110]. The intestinal epithelium displays proximal-distal functional specification, and contains many of same epithelial cell lineages found in mammals including absorptive enterocytes, goblet cells, and enteroendocrine cells [109, 110]. Enterocytes have a basolateral nuclei and form tight junctions, apical microvilli and an intestinal brush border [111]. In the last decade, numerous gastrointestinal pathologies have been modeled in the zebrafish, as summarized in Table 2.

Model	Mechanism of pathology	Human relevancy/key features	Key references
Pan-GI neoplasias	Heterozygotic APC mutation	APC mutations drive spontaneous and genetic intestinal adenocarcinomas.	Haramis, 2006. [112]
Hepatocellular carcinoma	Thioactemide +/- HCV-core-protein-zebrafish	Human genetic overlap. Rising prevalence of HCV-driven HCC in humans.	Lam, 2006. [113] Rekha, 2008. [114]
Pancreatic cancer	Transgenic *ptf1a*-KRAS zebrafish	Recapitulates hedgehog signaling aberrations found in humans. Elucidates a potential cellular origin for pancreatic cancers.	Park, 2008. [115]
Inflammatory bowel disease	TNBS in the media of zebrafish larvae	Model inflammatory and goblet cell hypertrophy. Responds to bacterial status and IBD medications	Flemming, 2010. [116] Oehlers, 2011. [117]
Inflammatory bowel disease	Oxazolone enema in adult zebrafish	Goblet cell depletion and eosinophil infiltration. Responds to antibiotic therapy.	Brugman, 2009. [118]
NAFLD	Mutation in a novel gene: *foigr*^{hi1532b}. Alternative model involves chemical induction with thiactemide	Large lipid filled hepatocytes and cellular apoptosis; pathology linked to ER stress responses. Alternative model generates a fatty liver and hepatocyte apoptosis.	Cinaroglu, 2011. [119] Amali, 2006. [120] (alternative model)
Alcoholic liver disease	2% ethanol to the water of 4 dpf zebrafish for 32 days	Hepatomegally and steatosis, with up-regulation of genes involved in toxic alcohol metabolism. Model is sensitive to sterol regulatory binding protein, important in human disease.	Passeri, 2009. [121]

Table 2: Zebrafish gastrointestinal models of pathology. Abbreviations: GI, gastrointestinal; APC, adenomatous polyposis coli; HCV, hepatitis C virus; TNBS, 2,4,6-trinitrobenzene sulfonic acid; IBD, inflammatory bowel diseases; NAFLD, non-alcoholic fatty liver disease; ER, endoplasmic reticulum.

Interestingly, a forward genetic mutagenesis screen (*N*-ethyl-*N*-nitrosourea (ENU), see Genetic Diseases and Drug Screens, below) generated zebrafish mutants that develop spontaneous intestinal, pancreatic and hepatic neoplasias [112]. These mutants were later found to be heterozygotic for a truncated form of APC, thereby leading to accumulation of nuclear β-catenin and increased expression of downstream genes such as *cmyc* and *axin2* [112]. Adding the carcinogen 7,12-dimethylbenz[a]anthracene to these mutant zebrafish increases the frequency of tumor development. Since germ-line truncated APC mutations in both humans [122, 123] and mice [124] result in the spontaneous development of a large numbers of intestinal polyps, the APC zebrafish model could be useful in genetic, drug screening and toxicology studies.

There are roughly 24,000 new cases of hepatocellular carcinoma (HCC) annually in the United States, resulting in over 18,000 deaths per year [125]. World-wide, the disease incidence can be as much as 30-fold higher due to the increased prevalence of hepatitis infections [126]; globally an estimated 564,000 new cases occur per year, accounting for 5.6% of all human cancers [126], and resulting in similar rates of mortality as seen in the US [126]. Oncogenomic profiling of liver tumors showed a significant overlap between human and zebrafish in 132 genes [113]. These genes included those involved in β-catenin and Ras-MAPK signaling pathways, as well as genes implicated in cellular adhesion, apoptosis, and liver-specific metabolism found in both organisms

[113]. HCC can be induced in zebrafish with the liver toxin thioacetamide, resulting in HCC-related pathology within 12 weeks of exposure. The timeline of thioacetamide-induced HCC could be significantly accelerated (6 vs 12 weeks) by using transgenic fish expressing the hepatitis C virus (HCV) core protein (HCP-transgenic fish) [114]. The increasing prevalence of HCC in humans has been attributed to the rise of HCV infection [127], in particular through the oncogenic action of the HCV core protein [128], making this model particularly relevant to human disease.

Pancreatic cancer represents the fourth most common cause of cancer-related mortality in the western world, likely due to limited diagnostic tools and inability to survey the disease. Exocrine pancreatic cells are responsible for more than 95% of pancreatic cancer [125]. The cell population in the pancreas that gives rise to human exocrine pancreatic cancer remains unknown and investigators have turned to zebrafish models to investigate this important question. Transgenic zebrafish were generated using a bacterial artificial chromosome (BAC) approach that expressed EGFP-KRAS fusion protein under the control of the zebrafish pancreatic locus *ptf1a* (*Tg(pft1a:EGFP-Hsa.KRAS^{G12V})jh7* [115]. Using these fish, investigators found that while normal pancreatic cell progenitors differentiated normally, KRAS-transgenic fish had blocked cellular differentiation, producing a pool of undifferentiated progenitors that progressed to invasive pancreatic cancer over a course of 3 to 9 months. These cancer cells also had increased expression of multiple hedgehog genes (*shh*, *dhh*, *ihha*, *ihhb*) as well as the downstream hedgehog targets Ptc2, *ptc1*

and *gli1*. This aberrant signaling pattern seen in these pancreatic tumor cells was also typical of human pancreatic cancer [115]. This zebrafish model established for the first time that oncogenic exocrine pancreatic progenitor cells could be the cellular origin for pancreatic cancer.

Outside of cancer models, one area of gastrointestinal disease that has received significant attention in recent years is the development of zebrafish models of Inflammatory Bowel Disease (IBD). In humans, IBD is the result of dys-regulated interactions between a genetically susceptible host and their commensal gut microbiota [1, 10, 11]. IBD is primarily a disease of the Western world; it affects 1.4 million Americans and there is no cure for the disease [12]. Outside of North America, similar disease burdens are seen in Europe but are ~3-fold lower in Asia and the Middle East, with the exception of Japan [129]. Pharmacological treatment centers around the use of anti-inflammatories and immunosuppressants, and surgical management of the disease is also possible though not always curative [13]. Numerous chemicals and genetic approaches are currently used by the IBD research community to study this pathology. These models mimic various aspects of the disease, such as disrupted barrier function and impaired innate and adaptive immune responses [35, 130]. Among the chemical models, the hapten oxazolone has been used for studies of acute intestinal inflammation. This murine model consists of rectal administration of a single dose of oxazolone dissolved in ethanol, resulting in an acute colitis lasting up to 10 days, with peak inflammation at 2 days post-administration in mice [131]. The model is characterized by a strong Th2-dependent immune response

that can be abrogated by IL-4 neutralizing antibodies, and has similar characteristics to human ulcerative colitis [35].

Investigators have tried to adapt the hapten oxazolone model of colitis to adult zebrafish. Brugman et al. showed intestinal epithelial damage and goblet cell depletion in oxazolone-treated fish within 5 hours of treatment, which lasts for up to 7 days [118]. This was accompanied by eosinophil infiltration into the intestine with increased *il1b*, *tnf*, and *il10* gene production compared to untreated zebrafish. The inflammatory phenotype was reduced by the administration of the gram-positive specific antibiotic vancomycin, suggesting a role for commensal bacteria in the inflammatory process of this model. The main constraint of this model is the need to use adult, non-transparent zebrafish which severely limits imaging capability. In addition, the need to rectally administer each individual zebrafish with oxazolone represents a technical challenge.

The hapten 2,4,6-trinitrobenzene sulfonic acid (TNBS) is another popular mammalian model of colitis characterized by a Th1-driven immune response [35] that is used for the study of both acute and chronic intestinal inflammation. In the acute model, TNBS is dissolved in ethanol and rectally administered in a single dose, while the chronic model can have multiple administrations weekly over a period of months [132]. The ethanol is responsible for disrupting the intestinal barrier while the TNBS serves to activate the immune system [35]. Two research groups have developed a larval model of colitis by exposing 3 dpf zebrafish for 3-5 days to TNBS in the fish media [116, 117]. Using the MPO reporter strain (*Tg(BACmpx:GFP)i114*) these investigators noticed neutrophil infiltration

throughout the zebrafish [48], gut-specific increases in *il1b* expression, altered intestinal lipid metabolism, goblet cell hypertrophy, and intestinal shortening. This larval TNBS model presents several advantages, including a dose-dependent phenotype, a sensitivity to antibiotics treatment and a response to anti-inflammatory agents (5-ASA and prednisolone) widely used to treat human IBD [117]. However, the intestinal histo-pathologies are poorly characterized in this model. In addition, the inflammatory component appears mostly to be non-intestine-specific. Furthermore, no intestinal epithelial cell damage is observed histologically [117], suggesting a lack of significant intestinal injury. Finally, it is unclear how a hapten could cause an inflammatory reaction in larvae missing a functional adaptive immune system.

We have recently established a model of epithelial injury in zebrafish using the NSAID glafenine [133]. Administration of glafenine to 5 dpf zebrafish for 12 hours results in a dramatic increase in intestinal epithelial cell apoptosis. This intestinal-specific apoptotic response is mediated by induction of endoplasmic reticulum (ER) stress and is accompanied by attenuation of the unfolded protein response (UPR) coupled to an improper activation of downstream UPR mediators such *atf6* and *s-xbp1*. Interestingly, loss of XBP1 in IECs results in the development of spontaneous enterocolitis in mice [19] and polymorphisms of this gene are associated with human IBD [17].

Chronic liver disease is responsible for over 25,000 deaths annually in the United States and represents the tenth leading cause of death, with a prevalence of over 5.5 million patients in 1998 [134] and that has since been estimated to

affect up to 30% of the US population [135]. In the UK, the picture is grimmer, as it is the fifth leading cause of death [136]. Non-alcoholic fatty liver disease (NAFLD) is a highly prevalent form of severe chronic liver disease, affecting 3% of all adults in America [137]. It also has significant associated mortality, with a 5-year survival of 67% and 10-year survival of 59% [137]. Additionally, up to one-third of all Americans have some level of NAFLD [136]. Outside of the US, where obesity is less prevalent, rates are also increasing. In Italy, which is traditionally considered low risk, an incidence of NAFLD of 20-25% of the population has been recently been reported [136]. In China and Japan, the disease incidence has been reported at 15% and 14% of the population, respectively [136]. There is no identifiable cause of NAFLD, but the pathology is linked to obesity, diabetes, and hyperlipidemia. Treatment involves managing these complex etiologies, and pharmacological therapies specific for NAFLD are not available for these patients [137]. Consequently, significant work has been invested to develop reliable zebrafish larvae models of liver pathology that could be easily utilized for drug targeting and screening.

The most characterized zebrafish model of NAFLD involved a forward genetic screen using viral insertion and screening for hepatomegally. In the case of the NAFLD model, a 172 bp gene trap cassette was found to be inserted in the intron between exons 11 and 12 of the recently discovered zebrafish gene *foie gras* (*foigr*) [138], which results in a frame shift mutation, and generation of a stop codon. This mutation ($foigr^{hi1532b}$) results in the development of steatosis (fatty liver disease) resembling human NAFLD, characterized by large lipid filled

hepatocytes and cellular apoptosis in larvae as young as 5 dpf [138]. However, the exact function of this gene, which is highly conserved across species including humans, is not yet determined. Further studies with the *foigr* mutant have shown that the apoptosis observed involves increased ER stress and is regulated in part through the UPR gene *atf6*. Morpholino blockade of *atf6* ameliorates liver injury during chronic ER stress in the *foigr* mutants [119]. However, *atf6* blockade potentiates steatosis during acute ER stress induced by the toxin tunicamycin [119], suggesting that *atf6* may have variable effects in different phases (acute/chronic) of liver injury. Hepatic steatosis has also been induced in zebrafish larvae using thioacetamide [120]. Investigators have showed that administration of 0.025% thioacetamide into the fish media at 3 dpf resulted in liver damage by 5 dpf, characterized by increased accumulation of fatty droplets, hepatocyte apoptosis and up-regulation of apoptotic genes such as *bad, bax, p-38a, caspase-3* and *8,* and *jnk-1*. Overall, the availability of NAFLD zebrafish models is burgeoning, and they are poised to be screened for pharmacological compounds that could for the first time effectively treat this disease.

Alcoholic fatty liver disease (ALD) is estimated to be involved in over 50% of all deaths due to liver failure secondary to liver cirrhosis, but accurate estimates for prevalence are unavailable [134]. Binge drinking leads to transient fatty liver disease, but chronic alcohol consumption can lead to fibrosis, cirrhosis, and steatohepatitis [139]. An ALD model has also been developed in zebrafish with administration of 2% ethanol to the water of 4 dpf zebrafish for 32 days.

This regimen results in hepatomegally and steatosis, alongside up-regulation of hepatic *cyp2e1*, *sod*, and *bip* gene expression—indicating hepatotoxic metabolism of the ethanol [121]. Importantly, ethanol-induced steatosis was prevented by morpholino blockade of the sterol regulatory binding protein (Srebps). Because Srebps activation is important in chronic alcoholic liver disease [121] in humans, the zebrafish ALD model could be utilized to identify new therapeutic mechanisms and to screen for therapeutic agents.

Microbe-Host Interactions

The ability to generate germ-free and gnotobiotic zebrafish [140] has led to an increasing interest in understanding cellular and molecular mechanisms of microbial-host interactions using zebrafish. Microbial-host interactions have received significant interested in recent years and have been implicated in a wide variety of human diseases, including CRC [141], IBD [1, 11], obesity and diabetes [142], intestinal healing [2], irritable bowel syndrome [143] and inflammatory nociception [144]. Zebrafish are host to gram-positive and gram-negative bacteria, mycobacteria, protozoa, and viruses [145], also allowing for their use as a model for infectious diseases. In most cases, microorganisms associated with these pathologies are not intrinsically pathogenic, but are rather part of the normal, commensal biota. The organ exposed to the highest amount of microorganisms in the human body is the gastrointestinal (GI) tract, especially the distal ileum and colon. Because of the high prevalence of bacteria and bacterial products in the GI tract, investigators have studied mechanisms controlling homeostasis in the face of such highly antigenic materials. The

zebrafish GI tract also harbors the highest concentration of bacteria and as such represents an interesting model to study bacterial/host interactions.

Bacteria and their associated products such as DNA, RNA and membrane structures (peptidoglycans, LPS--lipopolysaccharide) are typically detected by a series of innate sensors that are evolutionary conserved. A survey of the zebrafish genome has identified numerous innate sensors from the TLR and the Nod-like receptor family, as well as their associated signaling pathways [146]. An almost complete set of TLRs (TLR1-5, 7-9, 21 [147]) exist in zebrafish, as do the intracellular sensors Nod1 and Nod2 [148]. Associated innate signaling proteins have also been identified in zebrafish such as myeloid differentiation primary response gene (MyD88) [147, 149], TIR domain-containing adaptor inducing IFN-β (TRIF) [150] and NF-κB [151, 152].

The most studied bacterial product is arguably the gram-negative derived LPS. In mammals, LPS is detected by TLR4, in association with the co-receptors MD2 and CD-14 [153]. Once engaged, TLR4 recruits the adapter protein Myd88 or TRIF to propagate the signal to NF-κB [154] and the interferon responsive factor (IRF) 3, respectively [155]. This signaling cascade plays a critical role in host response to microbes and microbial products. As in humans, high doses of LPS are toxic to zebrafish [156]. Studies using commensal and germ-free zebrafish established that intestinal alkaline phosphatase (*iap*), known to detoxify the endotoxic lipid moiety A of LPS in mammals, is induced following microbial colonization [156]. Knockout of *iap* resulted in excessive intestinal neutrophil

infiltration, a process involving functional *myd88* and *tnfr* as determined by morpholino blockade [156].

Another important TLR system is TLR5, which detects flagellin and activates various signaling pathways including NF-κB [153]. Similarly to mammals, zebrafish detect flagellin (*Salmonella*-derived in these experiments) to induce multiple matrix metalloproteinase genes, as well as the inflammatory markers *il1b, il8*, *ifn* and *cxcl-C1c* [157]. Morpholino blockade showed that flagellin-induced *Il1b* and metalloproteinase 9 (*mmp9*) were *myd88* dependent whereas *ifn* and *il8* were activated through another signaling system [157].

The function of some of these TLR downstream signaling adaptors have also been studied in zebrafish. Both red and green transgenic Myd88 reporter strains such as*Tg(myd88:EGFP)z163* and *Tg(myd88-DsRED2)z164* have been developed [149]. These strains have been crossed to both macrophage (*Tg(lyz:DsRED2)nz50* [158]) and neutrophil (*Tg*(BAC*mpx:GFP*)i114 [48]) reporter strains to monitor myd88 signaling. Studies with these dual-reporter fish demonstrated that MyD88 co-localized with both macrophages and neutrophils, and that these *myd88*-expressing leukocytes migrated to wound sites and were involved in bacterial phagocytosis [149].

Another downstream mediator of LPS signaling, acting independently of MyD88, is TRIF. While zebrafish TRIF shares only 32% homology with the human protein, like in mammalian systems it can induce IFN and NF-κB luciferase-reporter responses as seen using an over-expression system in human HEK293T cells [150]. Interestingly TRIF-dependent gene induction

through the TLR4 pathway was found to be non-functional in experiments with adult zebrafish stimulated with LPS [150]; however, this is to be expected given that zebrafish TLR4 paralogues (*tlr4a* and *tlr4b*) do not recognize LPS [159, 160]. Outside of the TLRs, the intracellular sensors Nod1 and Nod2 are critical innate signaling systems in mammals. Importantly, Nod2 was the first innate signaling molecule to be genetically linked to Crohn's disease susceptibility [161]. The exact protective role of Nod proteins in mammals is not fully understood but defective bacterial killing appears to be an important factor [161-163]. Both *nod1* and *nod2* genes are expressed in IECs and neutrophils of zebrafish. Functional studies using morpholino blockade showed that Nod2 plays an important role in setting host anti-microbial properties [148]. Interestingly, Nod1 or Nod2 depletion resulted in increased susceptibility to *Salmonella* infection in a zebrafish embryonic infection model [148]. This study suggests that the anti-microbial properties of Nod2 are conserved in zebrafish.

As mentioned above, NF-κB signaling is an important effector pathway downstream of numerous innate sensor systems [164]. Colonization of germ-free NF-κB;EGFP reporter zebrafish *Tg(NFkB:EGFP)*^{nc1} with a commensal microbiota induced NF-κB activation and expression of NF-κB target genes including *complement factor b (cfb)* and *serum amyloid a (saa)* in intestinal as well as in extra-intestinal tissues of the GI tract [165]. Activation of NF-κB signaling in zebrafish indicates an important role of this transcription factor in maintaining host homeostasis that is conserved across species. The ability to longitudinally study NF-κB activation in a cell-type specific fashion in response to

various microbial stimuli makes the zebrafish a powerful system to decipher complex host-microbe interaction. Overall, the recent development of the aforementioned technologies makes the study of microbial-host interactions in zebrafish a burgeoning area of research.

Response to infection is another area of microbial-host interaction that has received significant attention in zebrafish. The most studied and prominent zebrafish infectious model is the *M. marinum* model, which is highly analogous to the human infectious agent *M. tuberculosis*, the etiologic agent for Tuberculosis (TB). TB is a growing epidemic worldwide, with over 83 million cases reported between 1990 and 1999, resulting in over 3 million deaths annually [166]. Many strains of the infectious bacteria are becoming drug resistant, resulting in an increase in global disease burden, including in the Unites States [167]. Finding new drugs to combat the ongoing threat of TB is consequently essential, as the disease can no longer be contained with current medications [168]. Co-incubation of *M. marinum* with 5hpf embryos results in the formation of macrophage-driven granulomas within 5 dpf [169], a hallmark of TB pathology. *In vivo* imaging and macrophage depletion showed that granulomas, traditionally thought to be a host-protective mechanism, may in fact be a source of early TB tissue dissemination by passing *M. marinum* into uninfected macrophages during phagocytosis [170] [171]. Consequently, this system has provided novel insights into the pathological mechanisms of TB infection and its interactions with the host immune system, and is poised to be used as a drug screen to identify novel anti-TB compounds.

Other pathogens have also been studied in zebrafish. These include *S. aureus*, *S. pyogenes*, and *S. typhimurium*. These and other infectious models in zebrafish have recently been reviewed in detail by Meeker, et al [100]. Although very informative, these studies were not performed using a natural route of infection but rather by using direct delivery (injection) into embryos at various developmental stages. However, oral gavage technology in larvea would likely improve the physiological relevance of infectious models perform in zebrafish. Another limitation of zebrafish infection models is the difference in host temperature; zebrafish and their natural pathogens exist at a temperature of 28°C, while many human-relevant pathogens are only infectious at 37°C [100]. Finally, there is some evolutionary divergence in TLR signaling that must be taken into account when working with this organism. Specifically, in contrast to mammals, LPS is not sensed by zebrafish TLR4 and the sensor negatively regulates MyD88 signaling [159]. Despite these limitations, zebrafish remain a powerful tool for studying microbe-host interactions [146].

Genetic Diseases and Drug Screens

Because of their high fecundity, transparency and ease of imaging, zebrafish are particularly well suited for genetic screening approaches. Forward and reverse genetic approaches can be undertaken to generate new zebrafish phenotypes and identify new genes of interest with potential relevance to human disease phenotypes. Zebrafish disease models can also be screened in a cost- and time-effective manner to discover disease-suppressing compounds. Using a

whole organism is a particularly appealing aspect of zebrafish-based screens, since complex cell-cell and organ-organ interactions are kept intact.

There are two main approaches to forward-genetic screens in zebrafish that have been undertaken thus far. The first involves exposing males to the mutagen ethylnitrosourea (ENU) and then screening for a phenotype [172, 173] shared by all mutants, such as renal cysts or heart failure. ENU is an alkylating agent that typically induces A→T base transversions. Zebrafish are relatively resistant to the ENU toxic side effects, allowing for higher dosages and thus increased rates of mutation [47]. An alternative mutagenesis approach employs random retroviral insertion [174, 175]. While this retroviral method is only one-ninth as efficient at generating a mutation as the ENU approach, it circumvents the need for positional cloning by tagging each insertion event, saving significant screening effort once a phenotype is found.

Duchenne muscular dystrophy (DMD) affects 1 in 3500 males and causes progressive muscle degeneration that can lead to death. DMD is the result of mutations in the sarcolemmal protein dystrophin located on the X-chromosome [176]. During an ENU screen of zebrafish [173], a mutation referred to as *sapje* [177] was discovered. This mutation was later found to be located in the zebrafish Duchenne muscular dystrophy (*dmd*) gene and causes progressive muscular degeneration in zebrafish larvae [178]. Electron microscopy showed that muscular degeneration was the result of failure to form proper muscle attachments at the myotendinous junction. This pathological mechanism was hypothesized to occur in mammals but was lacking concrete evidence, making

the zebrafish a novel system for studying the pathophysiology of this devastating disease.

The most common form of heritable polycystic kidney disease (PKD) is autosomal dominant PKD. This disease affects more than 1 in 1000 live births and approximately 10% of patients with PKD will require kidney transplant due to renal failure [179]. PKD has been linked to defects in primary cilia formation and function in humans [179]. This disease has also been successfully modeled in zebrafish by using retroviral insertion mutagenesis and screening for cystic kidneys in 5 dpf larvae [180]. The screen discovered 12 genes whose loss formed cysts in the glomerular-tubular region, including two already associated with human disease (*vhnf1* and *pkd2*), demonstrating genetic and phenotypic homology between humans and zebrafish. Three of the 10 remaining genes are homologues of *Chlamydomonas* (a genus of green algae) genes, which encode components of intraflagellar transport particles involved in cilia formation [180], but have yet to be analyzed in human PKD patients. The other 7 genes discovered provide completely novel targets for studying the underlying genetics and mechanisms of PKD, as many of the genes that can result in PKD remain unidentified in humans [179].

Dilated cardiomyopathy (DCM) is the cause of at least half of the 5.8 million heart failure cases in the US, typically resulting from prior heart damage due to a myocardial infarction or an infection [181]. World-wide, DCM is the leading indicator for heart transplant [182]; with incidences to be as high as 9.6 per 100,000 person-years in Europe [182] and China [183]. DCM results in poor

heart function that eventually leads to death [181]. ENU zebrafish screens discovered numerous fish with cardiac abnormalities [172, 184, 185]. Two of these mutants, *sih* and *pickwickm171*, were found to have dilated hearts with thin walls and defective contractility [186, 187]. Further analysis showed that the *sih* (silent heart) mutants had a mutation in cardiac troponin T gene [186], while the *pickwickm171* mutants had a mutation in the *titin* gene [187]. Since both of these genes are known to be important in human DCM, these mutants zebrafish represent interesting and complementary models to study this pathology.

All of the aforementioned models demonstrate that forward genetic screens in zebrafish can generate specific phenotypes that are highly homologous to human diseases. Further analysis of these mutants almost invariability lead to the identification of a gene with high homology and relevance to corresponding human disease.

Targeted, reverse genetic approaches are also quite successful in generating models of disease, especially if a homolog exists between the human gene(s) driving the disease and the zebrafish. One disease that has recently been modeled in zebrafish using a reverse-genetic approach is Hutchinson-Gilford progeria syndrome (HGPS), a rare (1:4,000,000 people) premature senescence syndrome that generally results from sporadic mutations that disrupts conversion of prelamin A to mature lamin A [188]. HGPS patients have markedly aberrant development characterized by lipodystrophy, osteolysis that is most pronounced in the cranium, and coronary dysfunction [188]. The mean life expectancy for patients with HGPS is less than 13 years. In zebrafish,

investigators were able to use a combination of directed loss of function mutations and morpholino knockdowns of prelamin and progerin to generate zebrafish that were able to live to adulthood (though with shortened lifespans). These fish had both phenotypic and molecular signs of early senescence, including lipodystrophy, aberrant musculature and craniofacial skeletal structure, increased cellular apoptosis, and cell-cycle arrest [189]. These phenotypic manifestations align remarkably well with those seen in human HGPS, demonstrating a proof of concept for reverse genetic approaches to developing zebrafish models of human diseases.

Some of the mutants generated during forward-genetic screens have been subsequently subjected to drug screening methodologies. The ability to rapidly and easily image large numbers of developing zebrafish makes them highly tractable as a pre-clinical system for drug screens [190]. A prototypical example of drug screening in mutant zebrafish discovered with the ENU forward-genetic approaches involves the *gridlock* (*grl*) mutant. The *grl* mutant lacks blood flow to the posterior trunk and tail due to a localized block in caudal blood flow at the base of the dorsal aorta [191]. This model has many characteristics similar to the human congenital disease coarctation of the aorta, making it of significant clinical interest. Coarctation of the aorta involves narrowing of the aorta that affects 1 in 2,500 live births [192]. It is the fifth most common form of congenital heart defect, and without surgical treatment the mean age of survival is only 31 years of age [192]. Surgical intervention can prevent early death, but significant morbidity, usually in the form of hypertension, can persist and results in

decreased life expectancy [192]. Unfortunately, no clear etiology of the disease exists, and the *grl* model in zebrafish is the best animal model currently in existence for the study of this disease [192].

The *grl* zebrafish has a hypomorphic mutation in the *hey2* gene, a basic helix-loop-helix protein involved in aortic development [193]. Gene titration studies using morpholino technology demonstrated that dose-dependent loss of this gene results in ablation of progressively larger sections of the aorta and expansion of the contiguous region of vein [194]. A pharmacological screen, assessing restoration of blood flood and survival of larvae using bright-field microscopy, found that two structurally related compounds (GS3999 and GS4012, unknown targets) promoted activation of the vascular endothelial growth factor (VEGF) pathway and were able to rescue the phenotype [195]. Another unrelated screen found that phosphoinositide-3-kinase (PI3K) inhibitors were also able to rescue the phenotype by driving VEGF activation [83]. This included the uncharacterized flavone GS4898, a structurally similar compound to the PI3K inhibitor LY294002, and the PI3K inhibitor wortmannin. This work also demonstrated for the first time that ERK signaling in embryos drives aortic differentiation, while activation of PI3K signaling produces a veinous fate. These findings have since been recapitulated in a murine system and have provided new insights into arterial morphogenesis [196], as well as generated some of the first insights into the underlying mechanisms behind coarctation of the aorta in humans.

A pair of robust screens has also been performed to evaluate compounds known to induce prolonged QT intervals in humans in the hopes of developing a pre-clinical cardiac toxicity screen. Cardiac QT elongation, which can cause the fatal heart arrhythmia known as Torsade de Pointes, is required to be evaluated in clinical drug trials [197] and thus these screens are of great clinical importance. Two such screens to evaluate bradycardia, atrioventricular blockade and arrhythmias in zebrafish have been performed thus far [198, 199]. In the first study 100 biologically active compounds were screened and 18 of the 23 that caused arrhythmias in humans were also positive in the zebrafish, while post-screen analysis showed that poor absorption explained 4 out of 5 of the false-negatives [199]. Additionally, the combination of erythromycin and cisaperide was also positive during screening while each drug alone was not, recapitulating a known drug-drug interaction that causes arrhythmias in humans. Consequently, the zebrafish holds significant promise to be used as a screen to evaluate new drugs for their potential to generate this serious and often fatal side effect.

Overall limitations

The use of zebrafish as a model organism for studying human disease is a relatively new and emerging field of research. Consequently, the number of available zebrafish strains and facilities that house zebrafish is much smaller than for well-developed model higher vertebrate organisms such as the mouse. Additionally, very few validated zebrafish reagents such as antibodies and cell lines are available to the research community. This significantly curtails the in-

depth investigation of molecular and cellular details implicated in a given phenotypes.

Zebrafish also have numerous duplicate genes [200], which significantly complicate generation of knockout strains using either forward or reverse-genetic approaches. Forward-genetic approaches that disrupt one gene copy likely will not disrupt the second copy, and duplicate genes also make targeted knockout strategies more difficult as both copies must be deleted. Additionally, while the zebrafish genome has been fully sequenced, the annotation is still limited and more of a work in progress. Furthermore comparative genomic analyzes between zebrafish and the human or murine genome counterparts have yet to be performed.

Zebrafish also have environmental conditions that differ substantially from humans. They must be raised in water with specific ionic concentrations and temperature (28°C). Consequently, some water-insoluble small molecules cannot be administered to zebrafish because carrier solvents (such as EtOH or DMSO) would reach toxic levels before solubility is achieved. Additionally, since drugs are administered directly to the fish media, bathing the entire fish in the test compound can result in non-desired toxic side effects. An example in our hands was the attempt to use dextran sodium sulfate (DSS) to induce colitis in larval zebrafish. At concentrations as low as 0.01% (v/v) the surfactant properties of the DSS choked the gills of the zebrafish, resulting in their death before an intestine-specific effect could be observed (Goldsmith and Jobin,

unpublished observation). As discussed in a previous section, the development of an oral gavage approach could circumvent this important limitation.

Perspectives

Animal models have been used since the inception of medical research. For most models of human disease, the preferred and most utilized animal system of human disease is overwhelmingly the murine system. Despite the tremendous gain of knowledge provided by using murine experimental systems, the long gestation time (18-20 days), and sexual maturation rate (6-8 weeks) combined with high cost of housing and breeding represent significant limitations. Furthermore, experiments with mice are labor-intensive and not particularly well suited for high-throughput screening. These limitations have spurred the need to develop other model organisms that could be used to provide initial gene or drug targets information before beginning investigations in more expensive systems. Transparent, larval zebrafish models have the potential to fill this important niche in the study of human disease, enabling rapid, physiologically-relevant *in vivo* screening. The transparent nature of zebrafish also allows for real-time imaging of pathogenesis, which has already provided key insights into the molecular mechanisms of metastasis [201-204] and tuberculosis dissemination [169-171]. The recent advent of the *Casper* fish promises to extend the imaging capacity beyond larvae to adult fish, permitting studies in fish with a functional adaptive immune system. The zebrafish has already demonstrated profound bench-to-bedside power, as evidenced by the rapid translation time (~2-years) from the

initial reports of the role of H_2O_2 in neutrophil chemotaxis during wound healing in zebrafish [49] to the first utilizations of such knowledge in human patients [106].

The zebrafish remains a relatively underdeveloped model organism with large amounts of untapped potential. As more is understood about the comparative genome, anatomy and physiology of zebrafish to that of humans, the relevance and utility of this vertebrate model will only grow and provide a powerful complement to the murine system. Two decades of research has demonstrated the power and relevancy of the zebrafish in modeling human disease. Its unique properties make it an ideal *in vivo* system for initial use in the interrogation of a given pathology before translating the observations made in the model organism to more expensive murine systems.

CHAPTER 3

ZEBRAFISH GLAFENINE-INTESTINAL INJURY IS AMELIORATED BY MU-OPIOID SIGNALING VIA ENHANCED AUTOPHAGY[2]

Introduction

Beside their analgesic properties, opiates exert beneficial effects on the intestinal wound healing response. In this study, we investigated the role of mu-opioid receptor (MOR) signaling on the unfolded protein response (UPR) using a novel zebrafish model of NSAID-induced intestinal injury. The NSAID glafenine was administered to 5 days-post-fertilization (dpf) zebrafish larvae for up to 24h in the presence or absence of the MOR-specific agonist DALDA. By analysis with histology, transmission electron microscopy, and vital dye staining, glafenine-treated zebrafish showed evidence of endoplasmic reticulum (ER) and mitochondrial stress with disrupted intestinal architecture and halted autophagy, alongside accumulation of apoptotic intestinal epithelial cells in the lumen. While the early UPR marker BiP was induced with glafenine-injury, downstream *atf6* and *s-xbp1* expression were paradoxically not increased, explaining the halted autophagic responses. The mu-opioid agonist DALDA protected against glafenine-induced injury through induction of *atf6*-dependent UPR and

[2] Submitted to the *Disease Models and Mechanisms*

autophagy. Our findings show that DALDA prevents glafenine-induced epithelial damage through induction of effective UPR and autophagy.

Background

Intestinal homeostasis is achieved in part by the maintenance of a functional barrier composed of a single layer of intestinal epithelial cells (IEC), which separates the host from the highly antigenic lumenal milieu [1]. Events leading to compromised barrier function are associated with various intestinal disorders including inflammatory bowel diseases (IBD) [1, 5]. Conditions leading to an impaired mucosal barrier function are diverse and include medications (non-steroidal anti-inflammatory drugs or NSAIDs [4]), radiation exposure[2], ischemic episodes [3], and genetic predisposition [1]. Notably, genes that disrupt the unfolded protein response (UPR) and autophagy following cellular stress have recently been implicated in the pathogenesis of IBD [17, 18]. The disease etiology remains unclear, however genetic evidence and experimental models suggest that intestinal cell death due to improper responses to ER stress leads to impaired barrier function [19]. Because of the importance of the epithelium in maintaining intestinal homeostasis, understanding mechanisms involved in intestinal epithelial healing and autophagy responses, and the identification of compounds that promote these processes, could lead to new therapeutic strategies for IBD.

Epithelial barrier damage triggers a host response termed restitution/wound-healing [10]. In this response, cells at the wound edge migrate into the wounded area, undergo cytoskeletal rearrangement, and finally re-establish tight junction barriers with their neighboring cells [10, 29]. This initial phase does not require epithelial proliferation, but renewal of cells are needed to

replenish the decreased enterocyte pool after injury [10]. Various pathways including NF-κB, MAPK, STAT3, GSK3β/β-catenin [33] and PI3K/Akt [10] are involved in the wound healing response through a combination of pro-migratory, proliferative and/or anti-apoptotic activities. The mu opioid receptor (MOR) ligand DALDA has also recently been shown to activate the intestinal wound healing response in mice [205]. However, the mechanism of MOR-mediated protection is largely unknown at this point.

The wide array of upstream signals and downstream pathways has made the study of restitution/wound healing a complex and difficult area of research [10, 164]. The vast majority of our information on this complex process is derived from rodent models, which have limited capacity for imaging techniques and therapeutic investigation [35]. Zebrafish (*Danio rerio*) possess several features that make it an attractive model for *in vivo* investigation of intestinal injury. Zebrafish are transparent through early adulthood, allowing for the use of live, *in vivo* imaging techniques. Furthermore, the anatomy and physiology of their digestive tract is similar to mammals, with a pancreas, liver, gall bladder, and intestine [109, 110]. The zebrafish intestinal epithelium displays proximal-distal functional specification, and contains most of same cell lineages found in mammals including absorptive enterocytes, goblet cells, and enteroendocrine cells [109, 110]. The zebrafish digestive tract develops rapidly to permit feeding and digestive function by 5 days post fertilization (dpf). Zebrafish also possess innate and adaptive immune systems homologous to those of mammals [146, 206]. Previous studies have attempted to establish models of intestinal injury in

zebrafish larvae by immersion in the hapten TNBS; however, these models lack overt pathological changes to the intestinal tract based on histology, and the inflammation and injury produced is not intestine-specific [116, 117].

Here, we developed a novel larval zebrafish model of acute intestinal injury using the NSAID glafenine. NSAIDs are known to disrupt the intestinal epithelium, leading to ulceration and inflammation in both humans and in mice [4, 207]. Additionally, zebrafish have homologs for both cyclooxygenase (COX) isoforms (the targets of NSAIDs) that function similarly and display the same responses to prototypical pharmacological inhibitors as seen in mammals [208]. Our work establishes that administration of glafenine larvae for 1-12h results in profound intestinal injury, with limited evidence of damage in extra-intestinal location. Immersion in glafenine resulted in intestinal epithelial cell (IEC) apoptosis and sloughing due to induction of ER stress combined with inhibition of appropriate compensatory UPR and autophagic responses. In contrast to previous reports of 2,4,6-trinitrobenzene sulfonic acid (TNBS) injury in the zebrafish [116, 117], the glafenine injury model shows profound pathological changes to the intestine, and appears to be specific to the gastroenterological system. We demonstrate for the first time that MOR signaling induces the UPR and autophagic signals to enhance restitution, thereby protecting against glafenine-induced intestinal injury.

Materials & methods

Fish husbandry, zebrafish lines and drugs

All experiments using zebrafish were performed using protocols approved by the Animal Studies Committee of the University of North Carolina at Chapel Hill. Zebrafish were maintained as previously described[209] All experiments were performed on zebrafish at 5.5-6 days post-fertilization (dpf). Fish were plated into 10cm diameter petri dishes, with 20mL gnotobiotic zebrafish medium (GZM)[140], to a maximum of 20 fish/plate the day of the experiment, and all drugs (glafenine plus any therapeutics) were administered simultaneously to the water for the indicated period of time. Isovolumetric vehicle controls were used for all experiments. Wild-type TL zebrafish were used for most assays in these studies. Blood flow analysis was performed with *Tg(gata1:dsRed)*^{sd2}*;(kdr1:EGFP)*^{s843} [210, 211] zebrafish, and NF-κB activation was assessed with *Tg(NFkB:EGFP)*^{nc1} zebrafish[165]. Glafenine (Sigma-Aldrich, St. Louis, MO) was dissolved in DMSO, and administered at 25μM final concentration for all experiments unless otherwise noted. DALDA (US Biological; Swampscott, MA) administered at 10μM. Indomethacin and Naloxone were obtained from Sigma Aldrich. Sc-560, Ns-398 and dmPGE2 were obtained from Cayman Chemicals (Ann Arbor, MI); R-spondin1, hIGF1 and mEGF were obtained from R&D Systems (Minneapolis, MN); Q-VD-Oph was obtained from BioVision (Mountain View, CA).

Acridine orange tube assay

Fish were submerged in a 1µg/mL solution of acridine orange (AO) (Sigma-Aldrich) and were then anesthetized in 0.017% tricaine, and mounted in 3% methylcellulose for visualization using a Leica MZ16F fluorescence stereomicroscope with a dsRed filter. Larvae were scored for the presence of an AO-positive tube extending from the intestine out of the cloaca, or for the presence of a strong, red signal in intestinal segment 2. Zebrafish with one of these two characteristics were deemed “positive”.

Fish imaging and fluorescence quantification

Live zebrafish were anesthetized with 0.017% tricaine (MS-222; Sigma-Aldrich, St. Louis, MO), mounted on 3% methylcellulose, and imaged with a Leica MZ16F fluorescence stereomicroscope. Within a given experiment, exposure times and magnifications were held constant. Relative fluorescence intensity was determined with ImageJ [212], using equal-sized boxes for the region of interest (ROI).

Histology and immunohistochemistry

Larvae were collected and fixed in 4% paraformaldehyde/PBS overnight, then transferred to 70% ethanol for another 24 hours. Fish were then embedded axially in 1% agarose and paraffin embedded. Fish were serially sectioned axially and the distance from the cloaca of each section was established based on section thickness and section number, to determine the section being viewed. We developed a histological scoring system in conjunction with a veterinary pathologist (see **Figure 6**A), using only segment 2 sections due to their more

consistent histological presentation. Histological scores were verified by a blinded pathologist. IHC for activated caspase 3 (R&D Systems, Minneapolis, MN) was performed as described[213]. 5-ethynyl-2'-deoxyuridine (EdU) staining was performed using the Edu Click-iT® kit (Invitrogen; Carlsbad, CA), according to manufacturer's protocol, with a final EdU concentration of 15 μg/mL. Fish were exposed to EdU for the same duration as glafenine and any other treatments (12 hours). Bright-field histological images were taken on an Olympus IX70 (Olympus; Center Valley, PA) with the default Olympus DP Controller software. An Olympus, UpLan Fl 40X, 0.75 NA objective was used. For fluorescence images, a Zeiss 710 microscope with an oil immersion, 40X, 1.4 NA objective was used (Carl Zeiss; Thornwood, NY). Zeiss Zen 2009 software was used for image acquisition. All images were acquired at room temperature.

Electron microscopy

Zebrafish were collected, euthanized with tricaine (0.083%), and immersion-fixed in 2% formaldehyde/2.5% glutaraldehyde/0.1M sodium cacodylate buffer, pH 7.4, overnight to several days at 4˚C. Following post-fixation for 1 hour in potassium ferrocyanide-reduced osmium[214], specimens were dehydrated through a graded series of ethanol and embedded in Polybed 812 epoxy resin (Polysciences, Warrington, PA). Transverse 1μm sections were cut at several locations along the gut, stained with 1% toluidine blue/1% sodium borate and examined by light microscopy to confirm region of interest. Ultrathin sections were cut with a diamond knife (70-80 nm thickness), mounted on 200 mesh copper grids and stained with 4% aqueous uranyl acetate for 15 minutes

followed by Reynolds' lead citrate for 8 min[215]. The sections were analyzed using a LEO EM-910 transmission electron microscope (Carl Zeiss SMT, Inc., Peabody, MA), operating at an accelerating voltage of 80 kV. Digital images were taken using a Gatan Orius SC 1000 CCD Camera and DigitalMicrograph 3.11.0 software (Gatan, Inc., Pleasanton, CA). All images were acquired at room temperature.

Oral micro-gavage and barrier function assay

Wild-type TL zebrafish larvae at 6dpf were pre-treated in a petri dish containing 20mL of GZM plus 0.1mM PTU (to inhibit melanin synthesis) with Glafenine (25µM) or the equivalent amount of the DMSO vehicle control (0.025% v/v) for 1 or 3 hrs at 25^{o}C. Following treatment, larvae were gavaged as previously described (Cocchiaro and Rawls, in preparation) with 1% TxR-dextran (10,000 MW, D1863; Invitrogen/Molecular Probes) or 1% TxR-dextran plus 20mM EDTA (positive control). Briefly, larvae were anesthetized in 0.026% tricaine, and mounted in 3% methylcellulose layered on an agarose injection mold to position the larvae for gavage and hold them gently in place. Borosilicate glass capillary needles specifically designed for gavage were clipped as bluntly as possible. Using a Drummond Nanoject II microinjection apparatus and stereomicroscope, gavage needles were carefully maneuvered into the mouths of anesthetized larvae, through the esophagus, and just inside the anterior bulb of the intestine by gently depressing the esophageal sphincter. The dextran gavage solution (4.6 nl on the slow setting) was administered into the anterior bulb. Following gavage, fish were moved to fresh GZM/PTU media, washed

gently to remove methylcellulose, and revived from anesthesia. At 15-20 min post-gavage, larvae were re-anesthetized, mounted in 3% methylcellulose on top of a 3% agarose block (to reduce reflection glare), and imaged on a Leica M205C fluorescence stereomicroscope. The same magnification and gain settings were used for all images. ImageJ software was used to quantitate mean relative fluorescence in a region of interest in the larvae trunk above the posterior intestine (trunk ROI) and an ROI outside of the fish (background ROI). To ensure consistency in measurement, the posterior side of the trunk ROI was always aligned with the end of cloaca just above the intestine. GraphPad Prism 5.0 was used for graphs and statistical analysis. The assay was also performed for larvae pre-treated for longer at 12-14h (data not shown).

RT-PCR

Total RNA was isolated from either whole zebrafish larvae or microdissected digestive tracts using an Ambion Purelink Kit (Invitrogren) according to manufacturer's protocol and RT-PCR was performed as described[165], using a ABI Prism HT7700. Specificity and linearity of amplification for each primer set was determined by melting curve analysis and calculation of the slope from serial diluted samples. Relative fold-changes were determined using the ΔΔCT calculation method. Values were normalized to the internal control 18S RNA. Primers: *atf6* (5'-CTGTGGTGAAACCTCCACCT-3' and 5'-CATGGTGACCACAGGAGATG-3'), *xbp1* (5'-GGGTTGGATACCTTGGAAA-3' and 5'-AGGGCCAGGGCTGTGAGTA-3'), *xbp1-s* (5'-TGTTGCGAGACAAGACGA-3' and 5'-CCTGCACCTGCTGCGGACT-3'),

18S (5’-CACTTGTCCCTCTAAGAAGTTGCA-3’ and 5’-GGTTGATTCCGATAACGAACGA-3’ were previously described [119, 165]). PCR for analysis of *atf6* morpholino efficacy was performed using specific primers for *atf6* (5’-TAGCCTACACTTTTCACCAG-3’ and 5’-ATGTCGTCGAATTTAATGTTAG-3’) and final products visualized on a 3% agarose gel[119].

Morpholino knockdown

Zebrafish embryos at the 1- to 2-cell stage were injected with splice-blocking Morpholinos (MOs; GeneTools LLC) targeting *atf6* (4.6 pmol/embryo, GAGTGGGGTAAGATACACGTTCTAG; generously provided by Dr. Kirsten Sadler Edepli, Mount Sinai School of Medicine); or standard control MO (4.6 pmol/embryo; Gene Tools LLC) using a Drummond Nanoject II microinjector. Efficacy of *atf6* knockdown was measured by PCR.

Cell Culture

Zebrafish Pac-2 cells (passages 20-25, American Type Culture Collection, Manassas, VA) were grown in L15 (Lebovitz) media supplemented with 15% fetal bovine serum (FBS) [216] and pen/strep antibiotic solution. Cells were housed in an incubator kept at 28°C, without humidification or supplemental CO_2. Cells were starved overnight in 1% FBS without the antibiotics before experiments were performed.

Protein isolation and Western blot analysis

Whole 6 dpf zebrafish were euthanized with 0.083% tricaine and homogenized for 15 sec with a polytron (IKA Works Inc., Wilmington, NC) in cold RIPA buffer containing proteinase inhibitors (Complete Mini; Roche Diagnostics GmbH, Penzberg, Germany), phosphatase inhibitor cocktail no. 2 at a 1:100 dilution (Sigma-Aldrich) and 1 mM phenylmethanesulfonyl fluoride (PMSF, Sigma-Aldrich). Afterwards, lysates were diluted 1:1 with 2X Laemmli buffer. Proteins from Pac-2 cells were isolated with direct lysis using 1x Laemmli buffer.

Proteins (30 µg, quantified by Bradford assay) were separated using 10% or 13% (for LC3) SDS-PAGE and transferred to nitrocellulose membranes. Blots were then probed with antibodies to BiP (1:3000) (Sigma-Aldrich), LC3 (1:600) (Novus Biologicals, Littleton, CO), and β-actin (1:1000) (MP Biomedical; Solon, OH). Antibodies were diluted in 5% milk/0.1% TBS-Tween. Blots were then washed 3 times for 5min in 5% milk/TBST and then incubated with an appropriate HRP-conjugated secondary antibody (1:5000) (GE Healthcare, Piscataway, NJ) for 30min. Proteins were detected by chemiluminescence.

Statistical analyses

Statistical analyses were performed using GraphPad PRISM version 5.0 (GraphPad, La Jolla, CA). Assessments between groups of fish were done with a two-way analysis of variance (ANOVA). Histology post-tests and further comparisons made between zebrafish were analyzed using a Mann-Whitney U test at a 95% confidence interval, unless otherwise noted in the figure legend.

Relative fluorescence data and EdU cell counting were compared with Student t-tests, at a 95% confidence interval. All graphs depict mean ± SEM. Experiments were considered statistically significant if $P<.05$. For all figures * denotes $P<.05$, ** denotes $P<0.01$, and *** denotes $P<.001$, unless otherwise noted specifically in the figure legend.

Results

Glafenine administration produces cellular sloughing comprised of apoptotic IECs

NSAIDs induce gastrointestinal damage in both humans and mice through COX blockade [4, 207]. In an effort to develop a zebrafish model of gastrointestinal injury, we exposed zebrafish larvae at 5.5 days post-fertilization (dpf) to a panel of NSAIDs for 12h (Figure 4A). Administration of Sc-560 (COX-1 [217]), Ns-360 (COX-2 [208]), or indomethacin (non-specific [208]) all failed to generate a visible intestinal phenotype, using maximum tolerable dosages that did not result in a rate of death≥50% (data not shown). Furthermore, combined administration of Sc-560 and Ns-360 resulted in 100% death (data not shown). However, administration of the non-specific NSAID glafenine induced the formation of an opaque, impacted intestinal lumen extending from the distal part of segment 1 through segment 3, with the production of a visible “tube” of material extending from the cloaca (Figure 5A, white arrowheads). Dose titration studies revealed that administration of 25 μM glafenine for 12h produced the highest level of “tube” formation with minimal zebrafish death (Figure 4B).

A

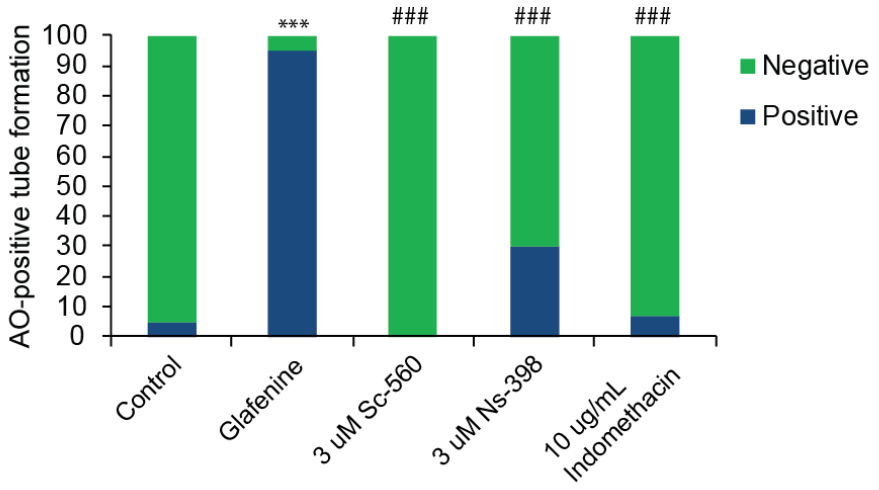

B

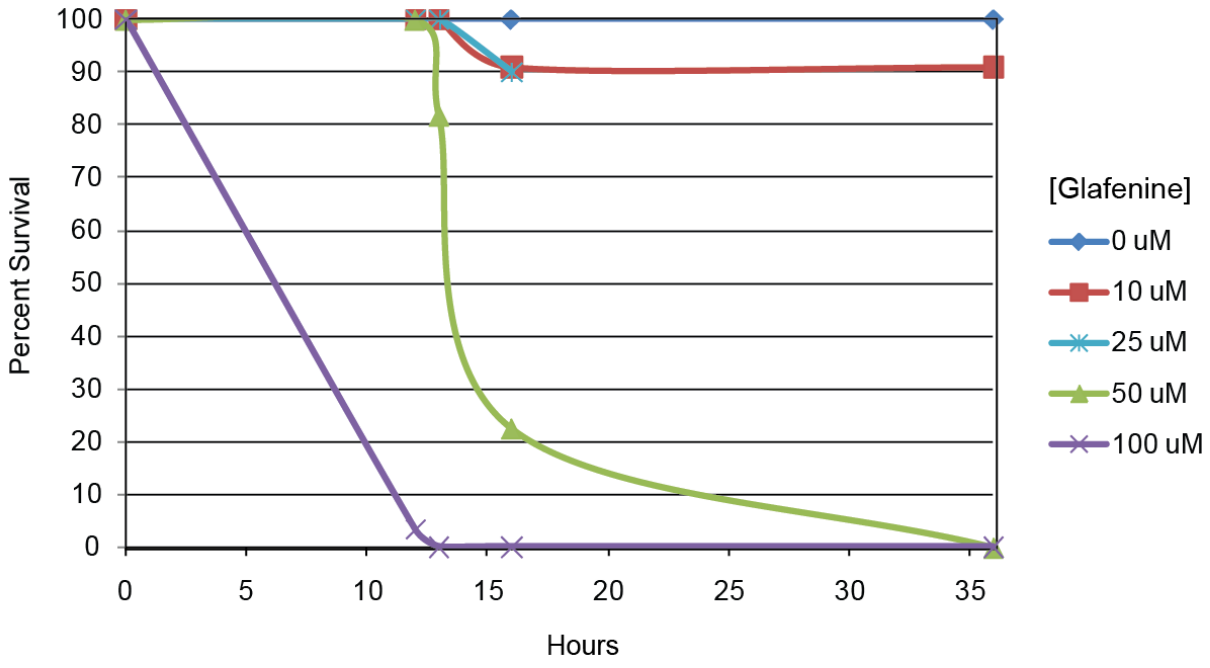

Figure 4: Only the NSAID glafenine induces apoptotic tubes at non-lethal dosages. A) Studies with COX inhibitors demonstrate that the effects of glafenine are specific to the drug. *** denotes *P*<.001 relative to control; ### denotes *P*<.001 relative to glafenine. ⩾10 per condition. B) Dose -dependent survival studies with glafenine. Pooled results of 3 or more independent experiments, N ≥20 for time points through 12h; N ≥10 for longer time points.

Because of the documented role of prostaglandins in IEC survival [4], we speculated that the impacted lumen was composed of expulsed dead IECs. To test whether cells in the lumenal mass were still alive, we exposed untreated and glafenine-treated zebrafish to the apoptosis reporter dye acridine orange (AO) for 30 min and imaged them by fluorescence microscopy. An intense streak of AO positive cells in the lumen of glafenine-exposed fish could be observed by wide-field (Figure 5B, left panel) and by confocal microscopy analysis, suggesting the presence of cellular entities (Figure 5B, right panel). The mass extending from the cloaca observed by brightfield microscopy was also AO-positive (Figure 5B), suggesting that dead cells are expelled from the distal intestine through the cloaca. Analysis of relative AO fluorescence in the intestinal lumen revealed a 2.2-fold increase in glafenine-treated fish compared to untreated controls (Figure 5C). Histological assessment of serial sections revealed marked intestinal sloughing into the lumen in segment 1, while segment 2 was characterized by an impacted lumen with pyknotic epithelial nuclei, cellular hypertrophy/hyperplasia, and apical/sloughing nuclei (Figure 5D and Figure 6B-E). All of these phenotypes are signs of cellular damage and apoptosis. Blinded, histological scoring of segment 2 sections showed a statistically significant increase in cellular damage in glafenine-treated fish compared to control (8.8 vs 2.6, Figure 5E). In addition, an increase in activated caspase-3 positive cells was observed in the epithelium (segment 1) and lumenal debris (segments 1 and 2) of glafenine-treated fish but not untreated fish (Figure 5F). This staining was not seen using IgG control antibody (Figure 6F). In contrast, caspase-3 staining

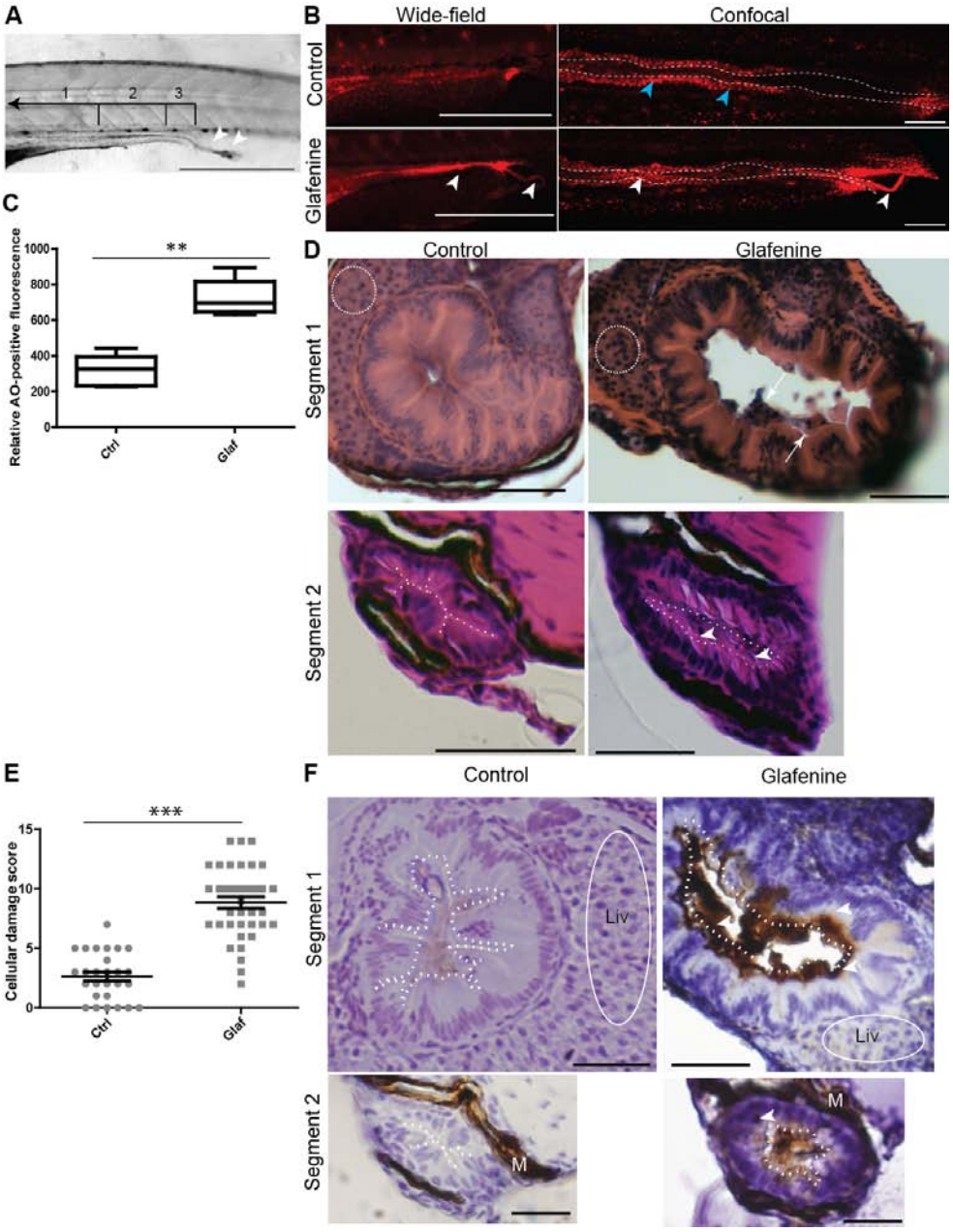

Figure 5: Glafenine results in apoptotic cell death with sloughing and dysmorphic cellular architecture. All studies at 12h glafenine exposure. A) Lumenal sloughing is apparent on bright-field microscopy. Bar represents 1 mm; segments of the intestine are bracketed and labeled. Arrow heads show sloughing from the intestine. B) AO staining shows apoptotic lumenal and sloughing debris. Blue arrowheads point to enterocytes that auto-fluoresce red; white arrowheads point to apoptotic lumenal and extruded debris. Bar represents 1 mm for wide-field images; bar represents 50 μm for confocal images. C) Apoptotic mass can be detected by differences in relative AO fluorescence. Representative of 4 independent experiments, N=4 per experiment. D) H&E sections of glafenine-induced injury. The edge of IECs are

outlined in white in segment 2 images. Arrows point to sloughed cellular debris and nuclei. Regions of liver are encircled with white dashes. Bar represents 50 μm. E) Segment 2 histological scores, pooled from 3 independent experiments. N as portrayed. F) Activated caspase-3 IHC. Lumenal edges are outlined in white. Arrowheads point to positively staining IECs, M denotes staining melanocytes. Regions of liver are encircled by a solid white line (denoted with Liv). Bars represent 50μm for segment 1, 12.5μm for segment 2.

A

Score	Sloughing
0	basal
1	midline
4	apical
6	luminal

Score	Pyknosis
0	none
2	mild
4	moderate
6	severe

Score	Proliferation/hypertrophy
0	none
2	mild
4	moderate
6	severe

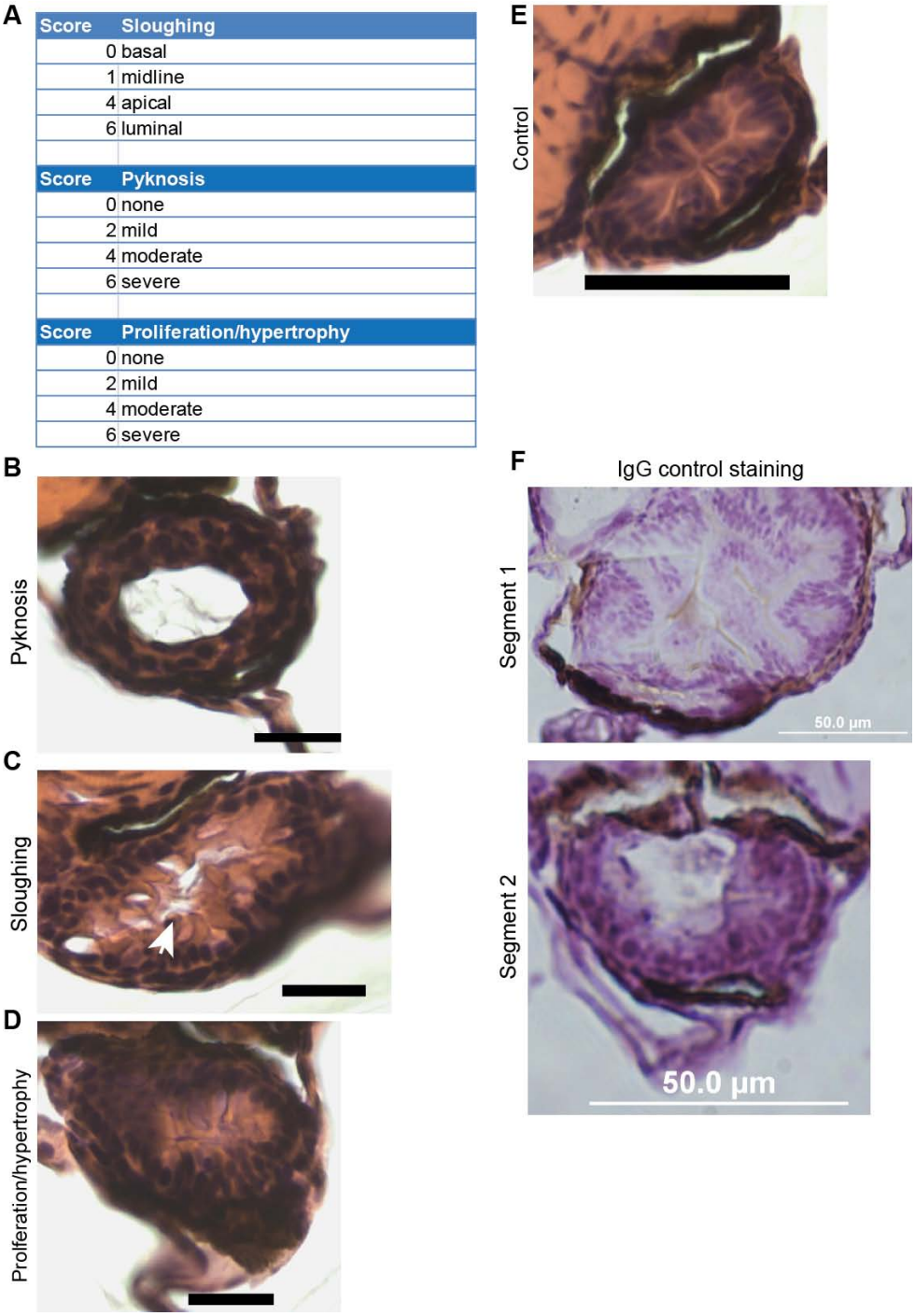

Figure 6: Details of the segment 2 histological scoring system. A) Histological criteria used in the intestinal damage assessment. B-F) Bars represent 50µm. B) Example of pyknotic nuclei. Pyknosis score of 6, total score of 10. C) Example of sloughing, arrow points to an apical nucleus. Sloughing score of 4, total score of 10. D) Example of proliferation/hypertrophy. Proliferation score of 4, total score of 12. E) Control fish, total score of 1. F) IgG (rabbit) control IHC for Caspase-3 studies, which show that the Caspase-3 staining observed is enterocyte and lumenal debris-specific.

was virtually absent in the liver of glafenine-treated zebrafish (Figure 5F, encircled in white). Together, these findings suggest that glafenine treatment induces cellular apoptosis in the intestine.

We next performed kinetic analysis of glafenine-induced intestinal injury. To facilitate this, we developed a rapid apoptosis/injury assay (see Methods) using AO staining. We observed that glafenine induced epithelial injury and apoptotic tubes in about 50% of zebrafish as early as 3h, which increased to ~90% of fish at 12h of exposure (Figure 7A). Histological analysis of segment 2 after 3h of glafenine exposure confirmed the presence of injured epithelial cells (Figure 7B). Additionally, marked intestinal sloughing was found in segment 1 at 3h (Figure 7C) and this feature persisted through 12 h of treatment (Figure 5D). Histological analysis of the liver at 3, 6, and 12h of glafenine exposure showed minimal cellular damage that could be at best described as hydropic changes, maximally seen at 6h (Figure 7D). To determine whether glafenine is still bioactive after long-term treatment (12h), media-swapping studies were performed where a new, untreated cohort of zebrafish were introduced into media in which a different group of zebrafish was exposed to 12h of glafenine. The conditioned media did not lead to AO-positive tubes in the new group of fish (data not shown). These data demonstrate that glafenine-induced injury occurs acutely and that the drug is no longer active after 12h.

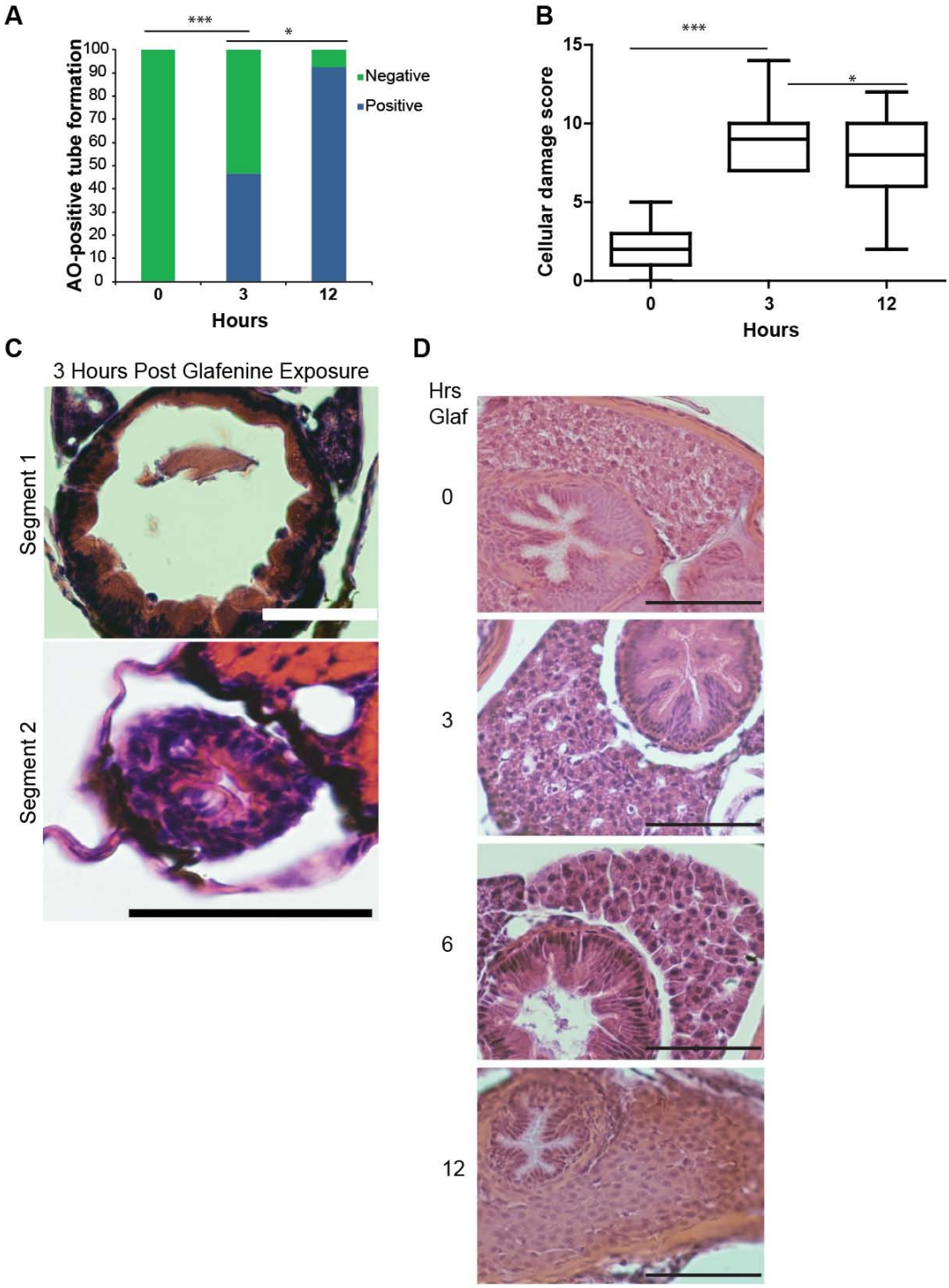

Figure 7: Progressive glafenine-induced injury over 0-12h is centered on the intestine. A) AO-positive tube formation, N≥13. B) Segment 2 histological score, N ≥ 9. 0 & 12h time points recapitulated from Fig 1. C) 3h histology. Bars represent 50µm. D) Scale bars for all images are 50 µm. H&E sections of livers of zebrafish exposed to 0, 3, 6, and 12h of glafenine. Mild hydropic changes are seen at 6h.

To identify the cellular origins of the damaged cells, we performed TEM ultrastructural analysis of glafenine-treated fish. The apoptotic tubes observed macroscopically in glafenine-exposed fish were comprised of cellular debris and multiple, distinctively apoptotic IECs within the epithelium of segments 1 and 2 and in the lumen of segment 2 (Figure 8A), confirming that the Caspase-3 and AO signals described earlier were due to apoptosis. Debris consistent with microvilli vesiculation, a hallmark of apoptotic cell shedding [29], was also observed only in injured zebrafish (Figure 8B). In addition, IECs of glafenine-exposed zebrafish showed features of ER stress with pitted ER in intestinal segments 1 and 2, which was most pronounced at 3h of glafenine exposure (Figure 8C). Further kinetic analysis revealed increasing signs of ER and mitochondrial stress over time, from 1-12h of exposure (Figure 9A&B). Early signs of ER stress peak at 3h, while organelle stress (along with apoptosis) steadily increases up to 12h after initial exposure; however, despite the fact that autophagy is initiated, most organelles are not fully enveloped by ER, indicating the process is in its early stages (Figure 9A&B).

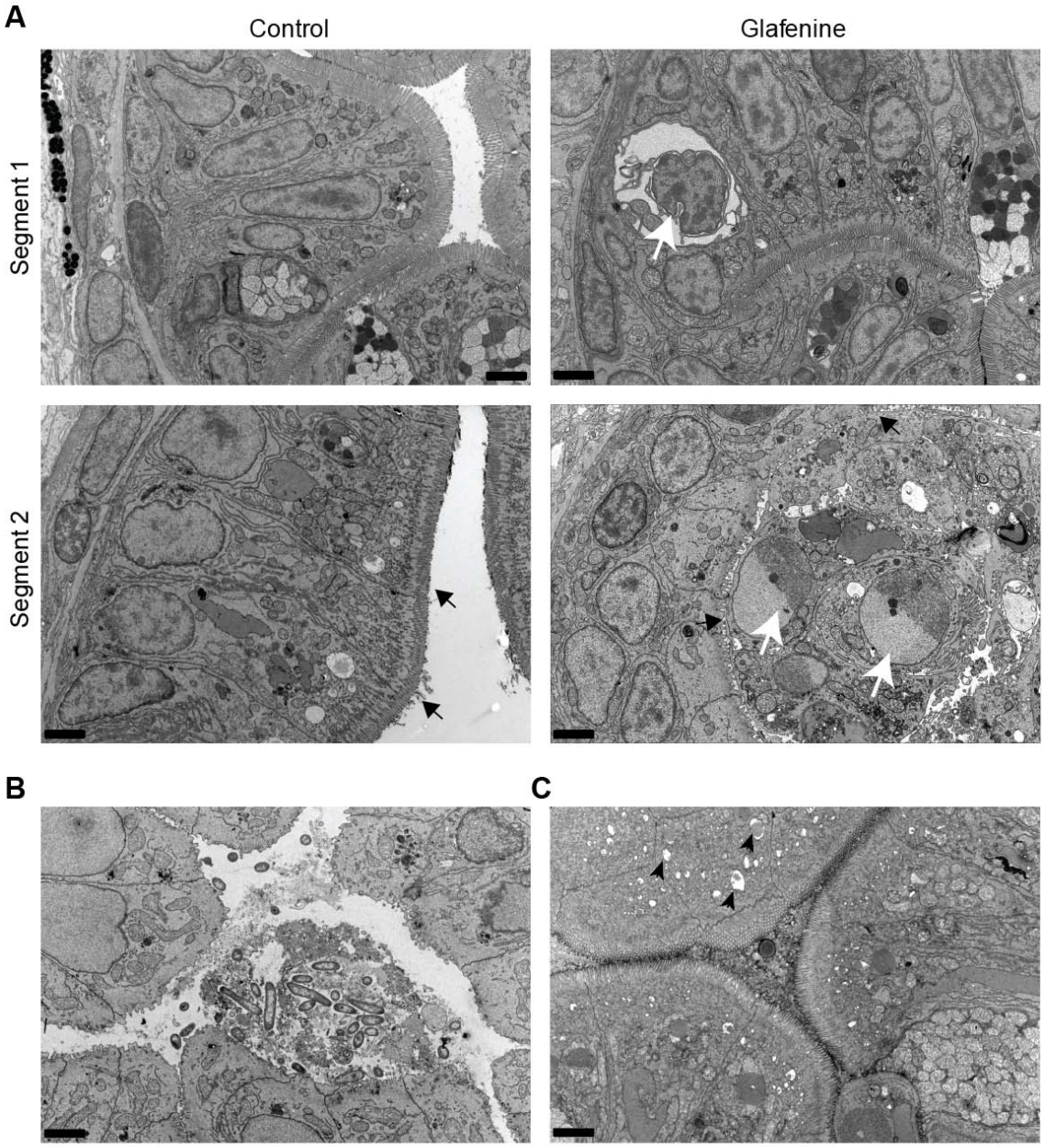

Figure 8: TEM identifies the apoptotic cells as intestinal epithelial in origin. TEM images, representative of 2 separate fish, across multiple sections at 12h glafenine exposure. 5000x magnification, bars represent 2µm. A&B fixed at 12h of exposure; C taken at 3h exposure to glafenine. A) Ultrastructure architecture of control and glafenine-injured fish in segment 1 and segment 2 of the intestinal epithelium. Apoptotic IECs (white arrows) and lumenal cellular debris (seg 2, white arrows) can be observed. Brush border is indicated by black arrows. B) Lumenal debris seen with glafenine injury in segment 1, which is consistent with microvesiculation of intestinal brush border. C) ER stress in segment 2, with characteristic pitting marked by black arrows.

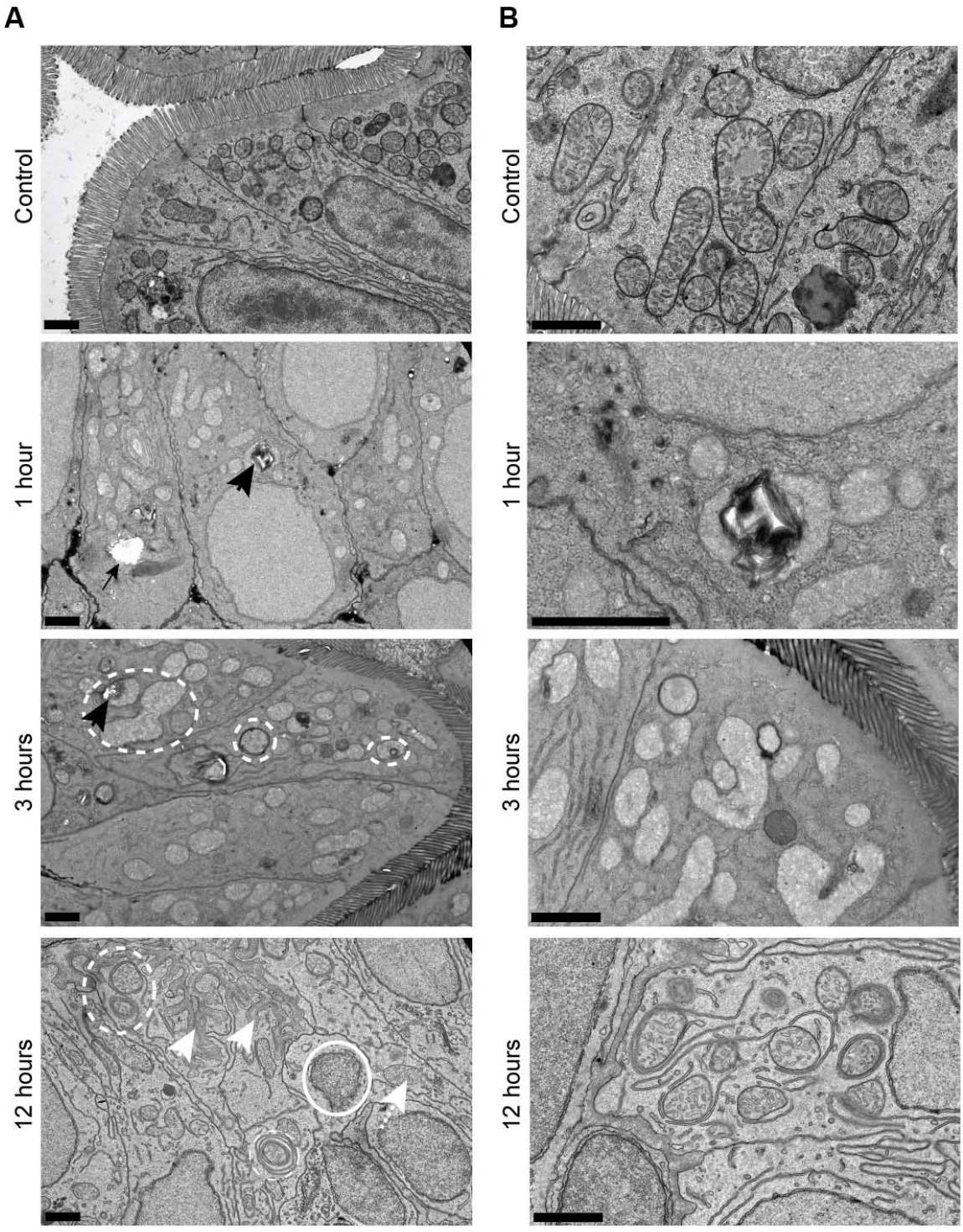

Figure 9: Glafenine leads to ER stress and arrested autophagy. 5.5-6 dpf zebrafish larvae were exposed to glafenine for the indicated times. Black arrows point to ER stress evidenced by pitting. Dashed circles outline stressed organelles being enveloped by ER. Solid circles outline dead organelles. Dashed, white arrows point to stressed mitochondria, while solid, white arrows

point to basement membrane invagination. Scale bars are 1 μm for all images. A) Lower magnification images. B) Higher magnification images.

To determine if glafenine-induced IEC apoptosis was associated with reductions in epithelial barrier function, we gavaged zebrafish with TxR-labeled 10kD dextran and monitored extra-intestinal fluorescence. Strikingly, extra-intestinal fluorescence in zebrafish treated with glafenine for 1 or 3 hours was low and indistinguishable from untreated controls (Figure 10A-B). Conversely, positive control treatment groups co-gavaged with TxR-dextran and 20mM EDTA displayed infiltration of TxR-dextran into intersomitic spaces and circulation (Figure 10A). These results suggest that glafenine treatment alone does not robustly compromise epithelial barrier function during acute damage when the drug is most active. TxR-dextran gavage after 12 h of glafenine exposure exhibited similar results (data not shown).

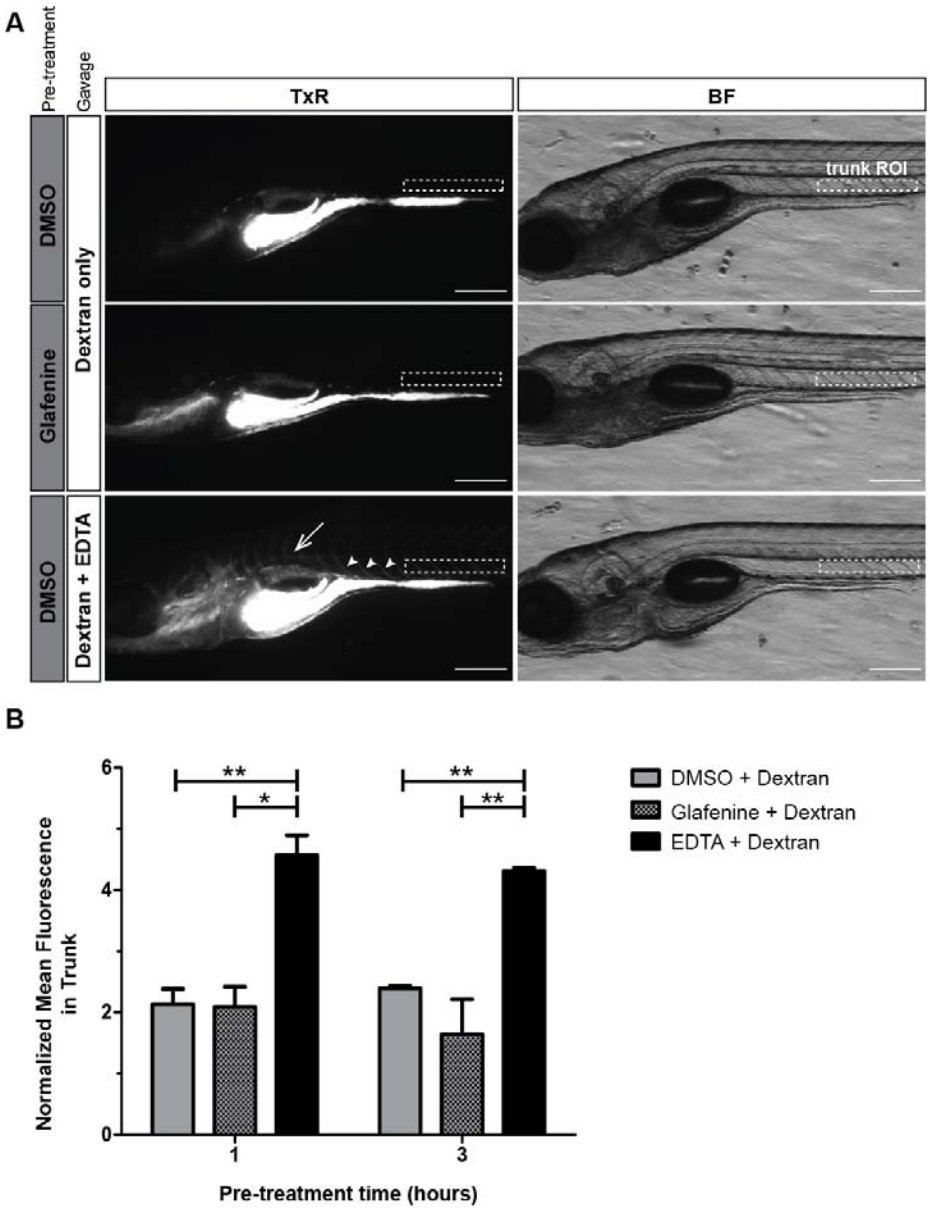

Figure 10: Intestinal epithelial barrier leakage does not occur with acute glafenine treatment. Wild-type TL zebrafish larvae at 6dpf were pre-treated with glafenine or vehicle control for the indicated times, followed by gavage with 1% TxR-dextran or 1% TxR-dextran plus 20mM EDTA (positive control). ImageJ was used to quantitate the relative mean fluorescence in an region of interest (ROI) in the zebrafish larvae trunk above segment 2 and 3 of the intestine (trunk ROI; small white dashed rectangle in A), and normalized to an ROI outside of the fish as an internal control to account for background glare (an ROI outside of the fish was used). A) Dextran leaks into circulation and intersomitic spaces when co-gavaged with EDTA. Representative images of larvae from the 1hr pre-treatment group are shown. In larvae gavaged with dextran only, the dextran remains in the intestinal lumen. When co-gavaged with dextran plus EDTA, fluorescent signal is observed in circulation (dorsal aorta, white arrow) and intersomitic vessels and spaces (white arrowheads). Scale bars equals 200µm.

(TxR= Texas Red; BF=brightfield). B) Treatment with glafenine does not lead to acute intestinal barrier disruption. Mean normalized TxR fluorescence in the trunk was determined following 1h or 3h of pre-treatment with glafenine or control. Graph represents data averaged from 2 experimental replicates taking into account the mean, SD, and N (16-19 larvae/condition/experiment). Two-way ANOVA with Bonferroni post-test was performed to compare each column to all other columns.

Because glafenine has been reported to cause anaphylaxis in humans, as well as liver damage [218, 219], we determined impact of glafenine in extra-intestinal sites. Importantly, no changes were observed in the skin or musculature of glafenine-treated fish, suggesting a predominantly gastrointestinal phenotype (Figure 11). This was confirmed by AO staining which revealed no effects of glafenine treatment, with the exception of the liver (Figure 12). However, histological analysis and caspase 3 staining failed to document evidence of cellular damage/death (Figures1-2). Together, these data suggest that glafenine causes minimal liver damage. Additionally, we noticed no gross bleeding into the intestine in control and glafenine-exposed *Tg(gata1:dsRed)*^{sd2};*(kdr1:EGFP)*^{s843} fish, with all dsRed-labeled red blood cells overlapping the EGFP-labeled vasculature (Figure 13A-B). Altogether, these data suggest a gastroenterological-specific phenotype, with damage most specific to the intestinal track.

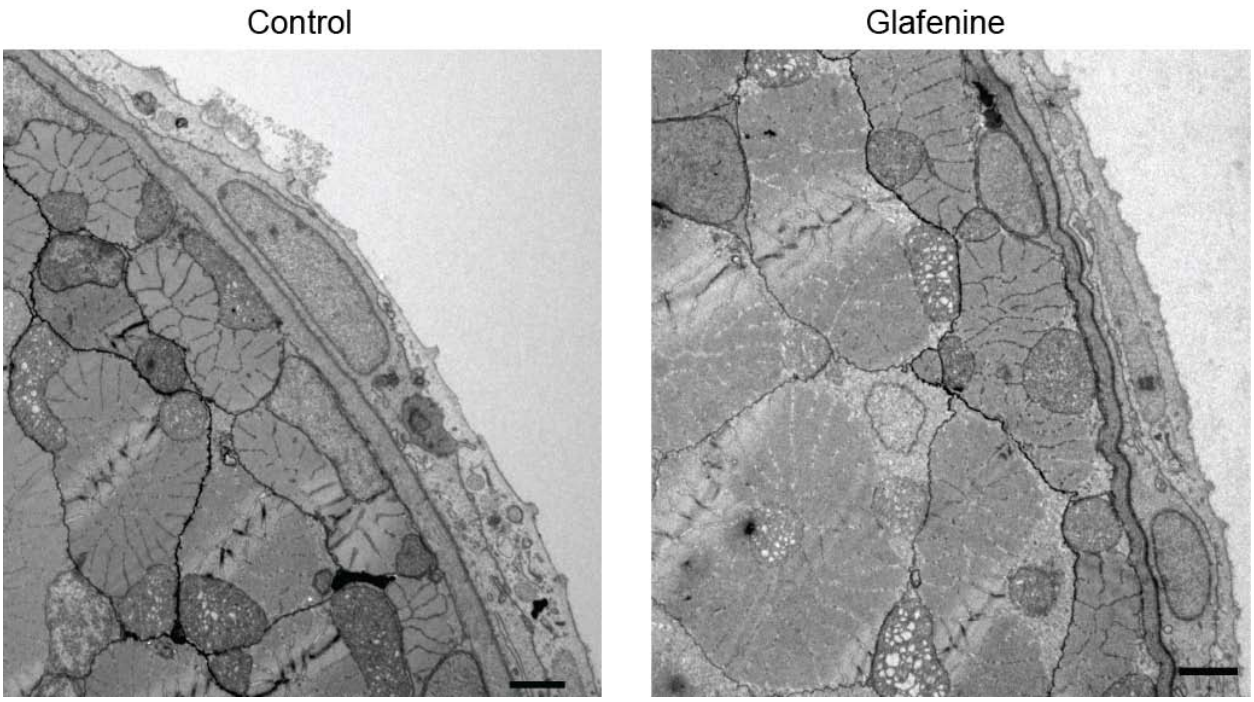

Figure 11: TEM studies show that glafenine-induced injury (12h) keeps the skin and musculature intact. Representative of 3 separate fish per condition.

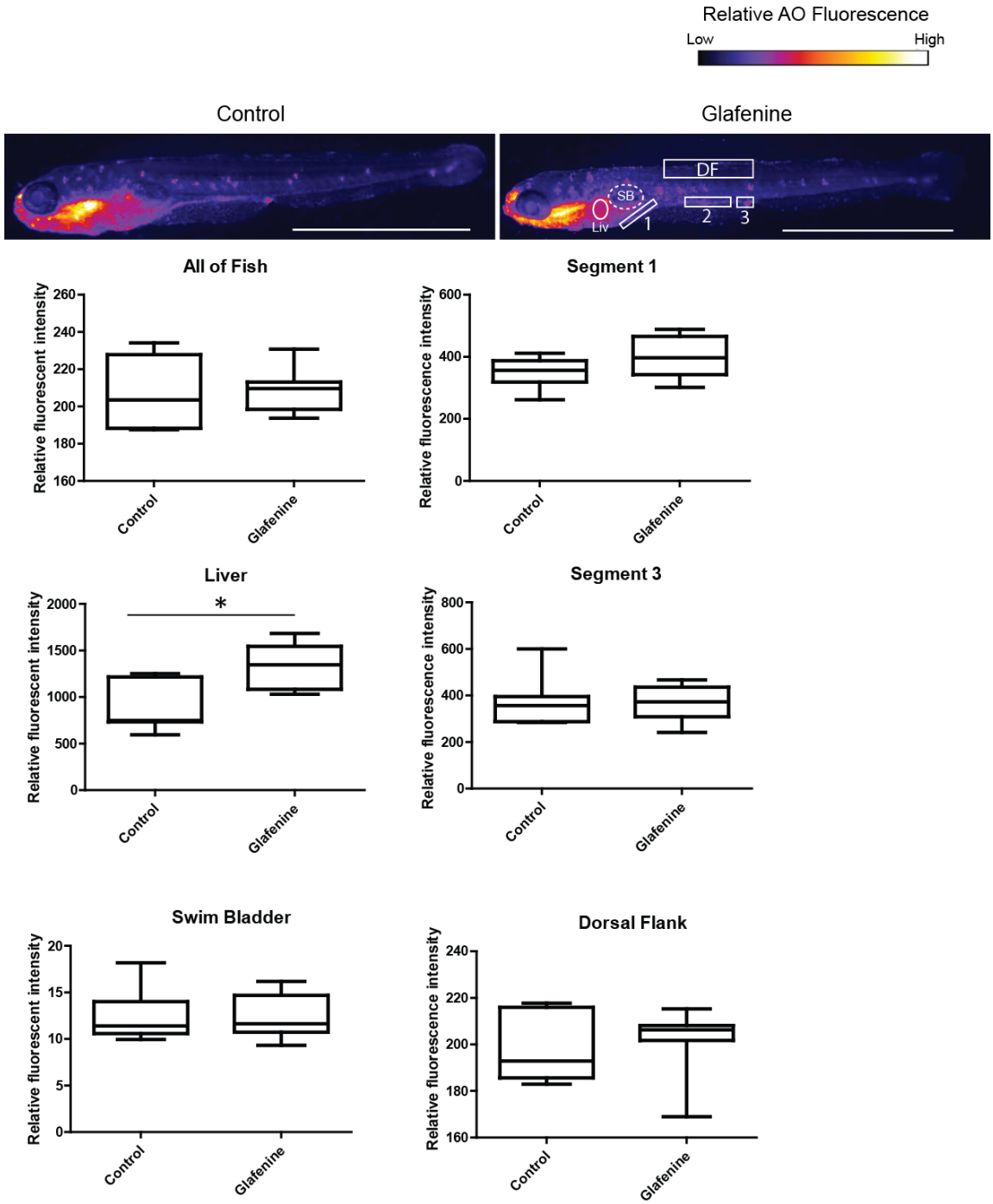

Figure 12: Glafenine-induced injury is specific to the gastroenterological system. Acridine orange staining marks apoptotic cells throughout the fish. Studies were performed at 12h glafenine exposure. Representative control and glafenine-treated fish are shown, with the regions analyzed shown on the glafenine image. Bars equal 1mm. Representative of 3 independent experiments, N≥4. SB = Swim bladder, Liv = Liver, DF = Dorsal fin.

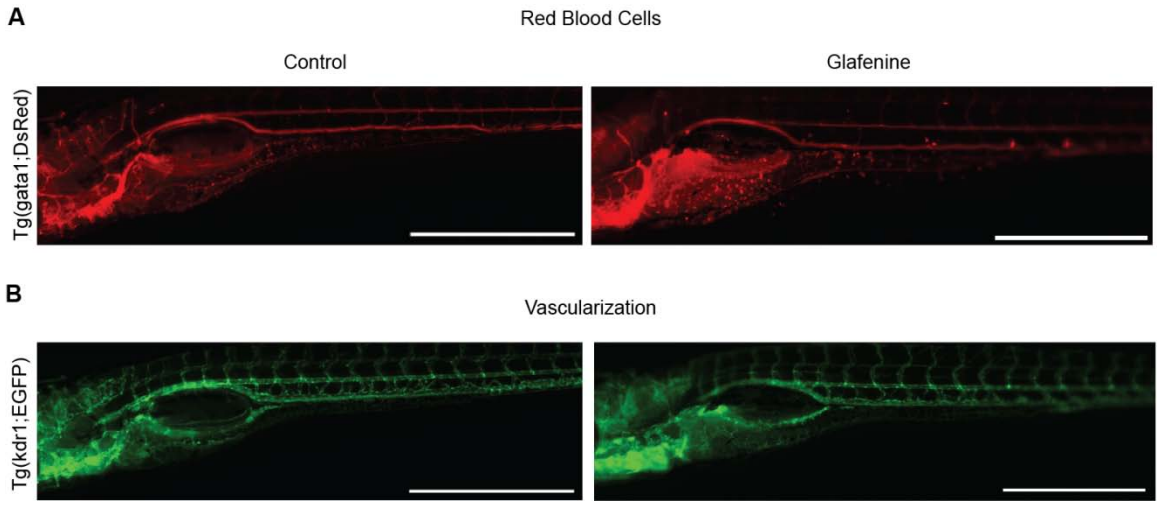

Figure 13: Glafenine-treatment does not result in gross intestinal bleeding. Double-reporter Tg(gata1:dsRed)sd2;(kdr1:EGFP)s843 zebrafish track both blood cells (red channel) and vasculature (green channel). Images representative of 5 individual fish, taken at 12h glafenine exposure. Bars are 1mm in length. A) The zebrafish show no gross bleeding into the intestinal lumen. B) The zebrafish show no gross vascular defects.

The mu-opioid agonist DALDA protects against glafenine-induced injury

Since apoptosis is an important feature of our model, we investigated the impact of anti-apoptotic, pro-proliferative, and/or pro-migratory compounds on glafenine-induced injury using the formation of AO positive tubes as a rapid screening assay. We identified several compounds that conferred protection against glafenine-induced injury when added to the housing media. R-spondin1 (a β-catenin activator), the MOR agonist DALDA, the COX-2 derivative product dmPGE2, and the pan-caspase inhibitor Q-VD-OPh all afforded significant protection (Figure 14A). These compounds all share the characteristic of engaging anti-apoptotic or pro-survival signaling pathways [205, 220-222]. In contrast, the mitogenic factors hIGF1 and mEGF failed to protect against glafenine-induced injury. Together, these data suggests that only a subset of pro-survival, anti-apoptotic signals are protective in this model. We hypothesized that mitigation of ER stress was the common factor of the drugs that reduced glafenine-mediated AO tube formation.

Given the recent discovery of the intestinal-protective effects of mu-opioid signaling [205], we decided to further investigate the effect of this opiate on intestinal injury in this zebrafish model. Co-administration of the opioid inhibitor Naloxone (1mM) alongside DALDA treatment abolished DALDA-mediated protection as determined by the tube assay (data not shown), demonstrating that DALDA-protection was mediated through MOR signaling. Histological assessment of DALDA-treated, glafenine-exposed fish showed a ~45% decrease

in intestinal damage compared to untreated glafenine-exposed animals (Figure 14B). In addition, glafenine-induced zebrafish mortality was improved by ~2-fold by DALDA treatment (Figure 14C). Because apoptosis plays a central role in this injury model, we determined the level of activated caspase-3 staining in the intestinal tissues of zebrafish co-treated with Glafenine and DALDA. In accordance with decreased AO tube formation and improvement of animal survival, DALDA sharply reduced the amount of activated caspase 3 staining in the intestine compared to fish exposed only to glafenine (Figure 14D). Additionally, DALDA treatment enhanced epithelial cell proliferation during glafenine injury ~2-fold as measured by EdU incorporation (Figure 14E).

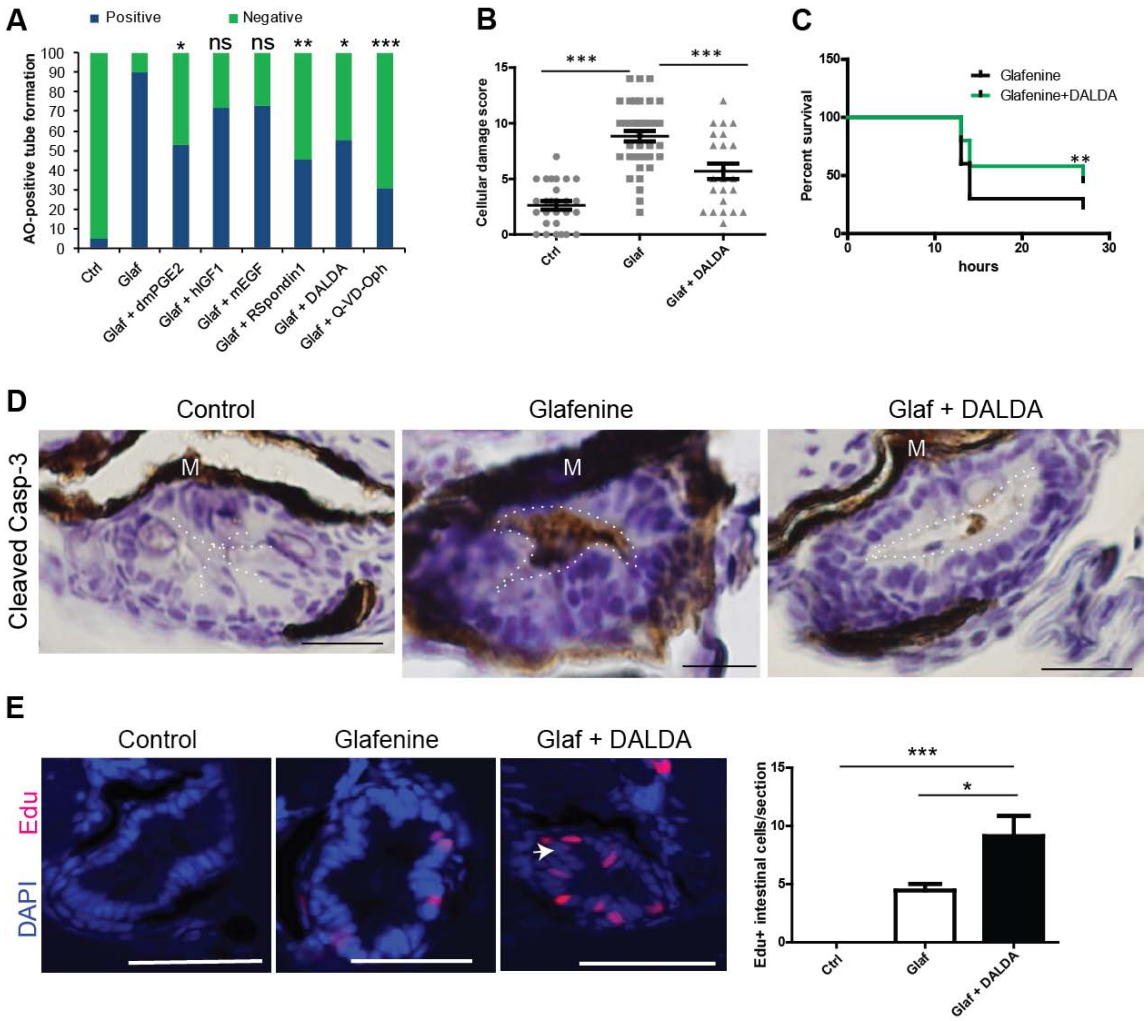

Figure 14: Glafenine-injury can be prevented with a subset of anti-apoptotic/pro-survival drugs, including the MOR agonist DALDA. All studies performed at 12h drug(s) exposure. A) Rapid apoptosis assays show that glafenine-induced injury can be prevented by drugs that engage pro-survival and/or anti-apoptotic signaling, but not solely proliferative signaling. ≥15 per group. Control, glafenine, and glafenine + DALDA results are all representative of 3 or more independent experiments. dmPGE2 representative of 2 independent experiments. Other drugs representative of replicate experiments performed on the same day with different groups of larvae. Significance shown is relative to glafenine treatment alone. *P*<.001 between control and glafenine groups (not shown on graph). Dosages: 10μM dmPGE2, 250ng/mL hIGF1, 10nM mEGF and R-spondin, 50μM Q-VD-Oph. B) Segment 2 histological scores. N for each group is represented on the graph. Control and Glafenine groups recapitulated from Figure 1, for ease of comparison with DALDA treatment. C) DALDA enhances zebrafish survival from glafenine-induced injury. N=50, pooled from 3 independent experiments. Glafenine at 50μM final concentration. D) Activated caspase-3 IHC staining in the intestinal epithelium. Representative of 4 fish per group. Scale bar equals 12.5μm. The lumenal edge is outlined in

white. E) Proliferation in segment 2 in response to drug treatment. EdU staining of zebrafish with 12h of drug exposure for each group. ≥8, except for control group, where N=4. Scale bar equals 50μm.

Opioid signaling overcomes glafenine-induced blockade of ER stress response genes, allowing for cell survival

Since DALDA amelioration of glafenine-induced intestinal injury is associated with decreased apoptotic markers, we speculated that DALDA-protection is mediated by either preventing the observed ER stress and/or by increasing compensatory responses such as autophagy that can ward off apoptosis in the presence of cell stress. Interestingly, ER stress was present (although diminished) and autophagy was enhanced in zebrafish treated with DALDA compared to glafenine-injury alone (Figure 15A). DALDA-treated zebrafish maintained an organized epithelium without basement membrane invagination, and organelles did not appear swollen or lacking in sub-organelle architecture. ER stress, based on pitting white lesions, was not prominent in DALDA-treated fish. Also, increased smooth ER was apparent, presumably the result of resolving autophagy and the re-establishment of subcellular structures consumed during autophagy (Figure 15A). IECs in the DALDA-treated group also displayed enhanced rough ER (Figure 15B), a typical sign of resolving autophagy as resolution requires increased protein synthesis.

Given the presence of ER stress, we investigated downstream protein/genes of the UPR and autophagy cascades. Protein levels of the early UPR mediator BiP were similar in lysates from whole fish exposed to glafenine with or without DALDA (Figure 15C). In contrast, eIF2a phosphorylation, which is downstream of PERK activation, could not be detected (data not shown). Quantitative RT-PCR assays using microdissected digestive tracts demonstrated

that two UPR genes normally up-regulated downstream of BiP accumulation, spliced-*xbp1* (*s-xbp1*) and *atf6* [119, 223], were atypically not up-regulated in glafenine-exposed compared to untreated fish, although these genes were induced in DALDA-treated fish (Figure 15D). These results were recapitulated using whole larvae lysates (Figure 16A), and DALDA was able to drastically induce these genes in the absence of glafenine-injury and inhibition (Figure 16B). Since *atf6* is a key mediator of the ER stress response, leading to the UPR and autophagy, we next determined the functional role of this gene in DALDA-mediated protection from injury. Zebrafish injected with *atf6*-morpholino (MO) displayed abrogation of DALDA-mediated rescue of glafenine-induced injury compared to animals injected with control MO (Figure 15E, knockdown confirmed via PCR), suggesting that enhancement of the UPR and autophagy responses mediates DALDA rescue of glafenine injury.

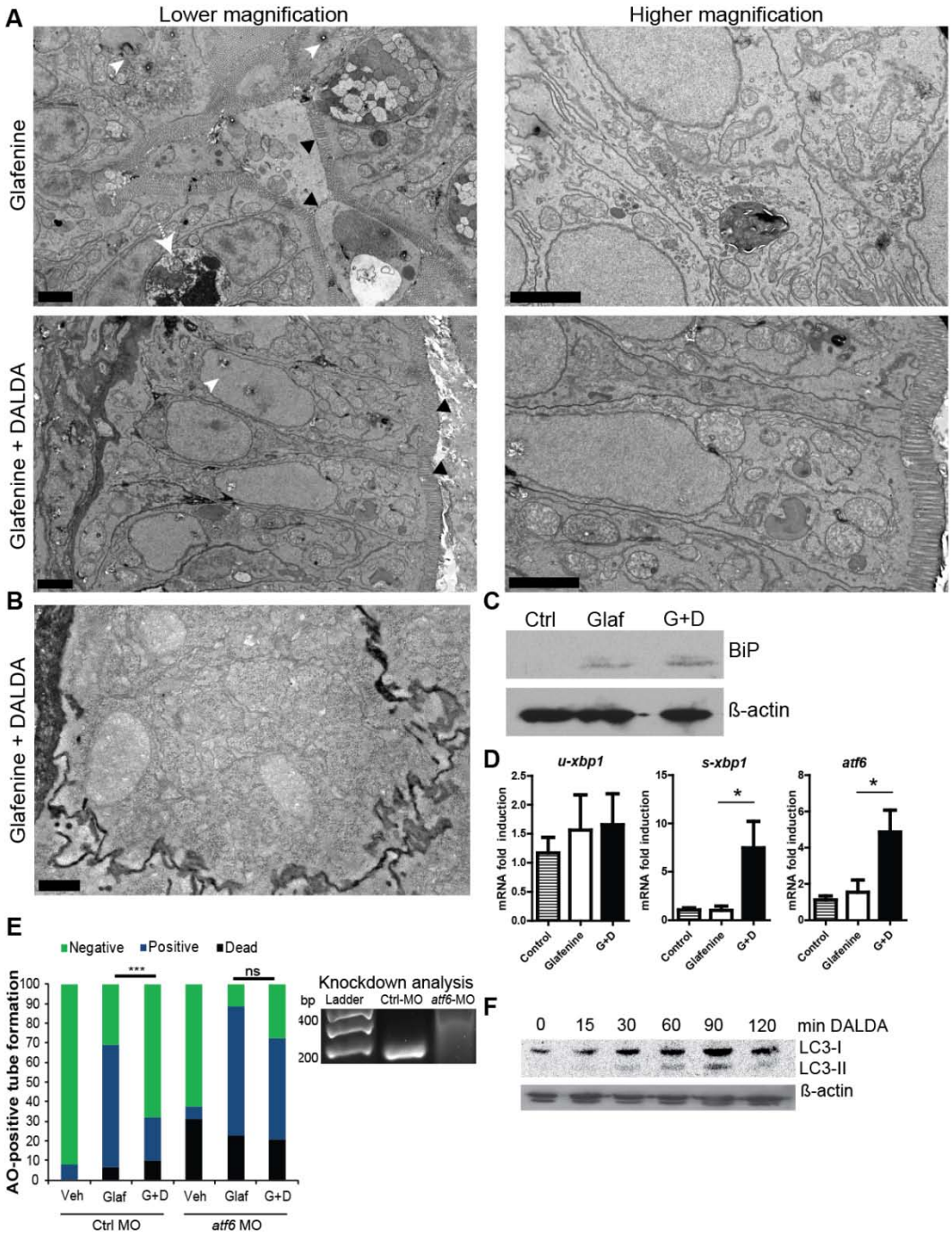

Figure 15: DALDA reverses Glafenine-induced organelle stress, restores proper UPR/autophagy responses. All studies shown at 12h glafenine exposure. A) TEM with and without DALDA treatment demonstrates a lack of ER stress and resolved autophagy. White arrowheads show pitting from ER stress. Black arrows indicate the brush border. Dashed arrows demark apoptotic IEC. Scale bars equal 2 µm. B) Same conditions as in A, showing granularity in the cytoplasm of segment 1 IECs, indicative of rough ER. Scale bar is 0.5 µm. C) Glafenine-injury induces BiP protein accumulation, an early

signal in the UPR and autophagy cascades. Western blot representative of 4 independent experiments, each consisting of protein lysate from ≥10 pooled fish/condition. D) Real-time PCR for UPR/autophagy response genes: *u-xbp1* (unspliced), *s-xbp1*(spliced), and *atf6*. Each replicate for each condition was generated from 10 pooled micro-dissected fish gastrointestinal tracks, ≥N 4/group. E) Fish were injected with 5 pmol of control or *atf6* morpholino in 4.6 nL of water and subjected to our standard AO tube assay. Pooled from 2 independent experiments, N≥29/group. RT-PCR for *atf6* in morpholino-injected fish, at 6 dpf. WT band is at 180 BP, the morphant with an intron-1 inclusion is at 314 BP. Representative of triplicate groups of 2 independent experiments. F) Western blot of lysate from Pac-2 cells exposed to 10 μM DALDA for the indicated time. Representative of 2 independent experiments.

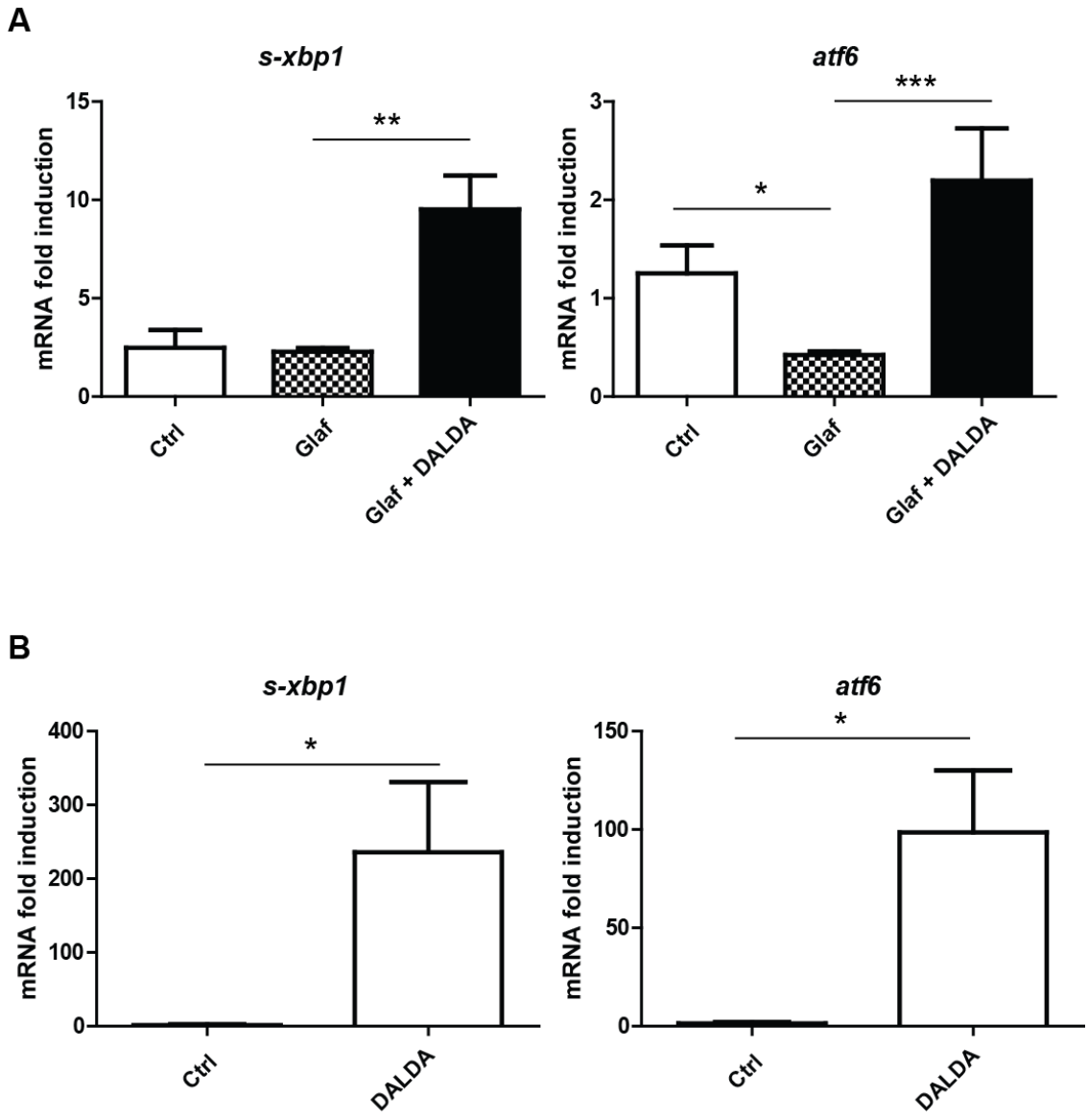

Figure 16: Autophagy response genes spliced *xbp1* (s-*xbp1*), and *atf6* expression following glafenine and/or DALDA exposure. Fish were treated as indicated and RNA extracted from whole animals at 12h glafenine exposure. s-*xbp1* and *atf6* expression was determined using ABI Prism HT7700. Samples are from whole tissue lysates of 10 fish per sample, N ≥ 2 per group.

To determine if DALDA is sufficient to stimulate autophagy in zebrafish cells, we examined the effect of DALDA on the production and processing of the autophagy marker LC3. Zebrafish larvae at 5 dpf showed high baseline levels of LC3-II (data not shown), therefore we tested this question using the zebrafish Pac-2 fibroblast cell line. Cells were treated with DALDA for 0-2 h and LC3 conversion was evaluated by Western blot. DALDA treatment progressively (0-90m) enhanced LC3-I production, as well as processing to generate LC3-II (Figure 15G). Together, these findings demonstrate that glafenine induces cellular organelle stress in the intestine while retarding downstream, pro-survival and autophagic signals *atf6* and *s-xbp1*, resulting in enhanced apoptosis and intestinal injury. Activation of MOR signaling rescues proper autophagy response through induction of *atf6* and allows cellular survival and maintenance of intestinal homeostasis (Figure 17).

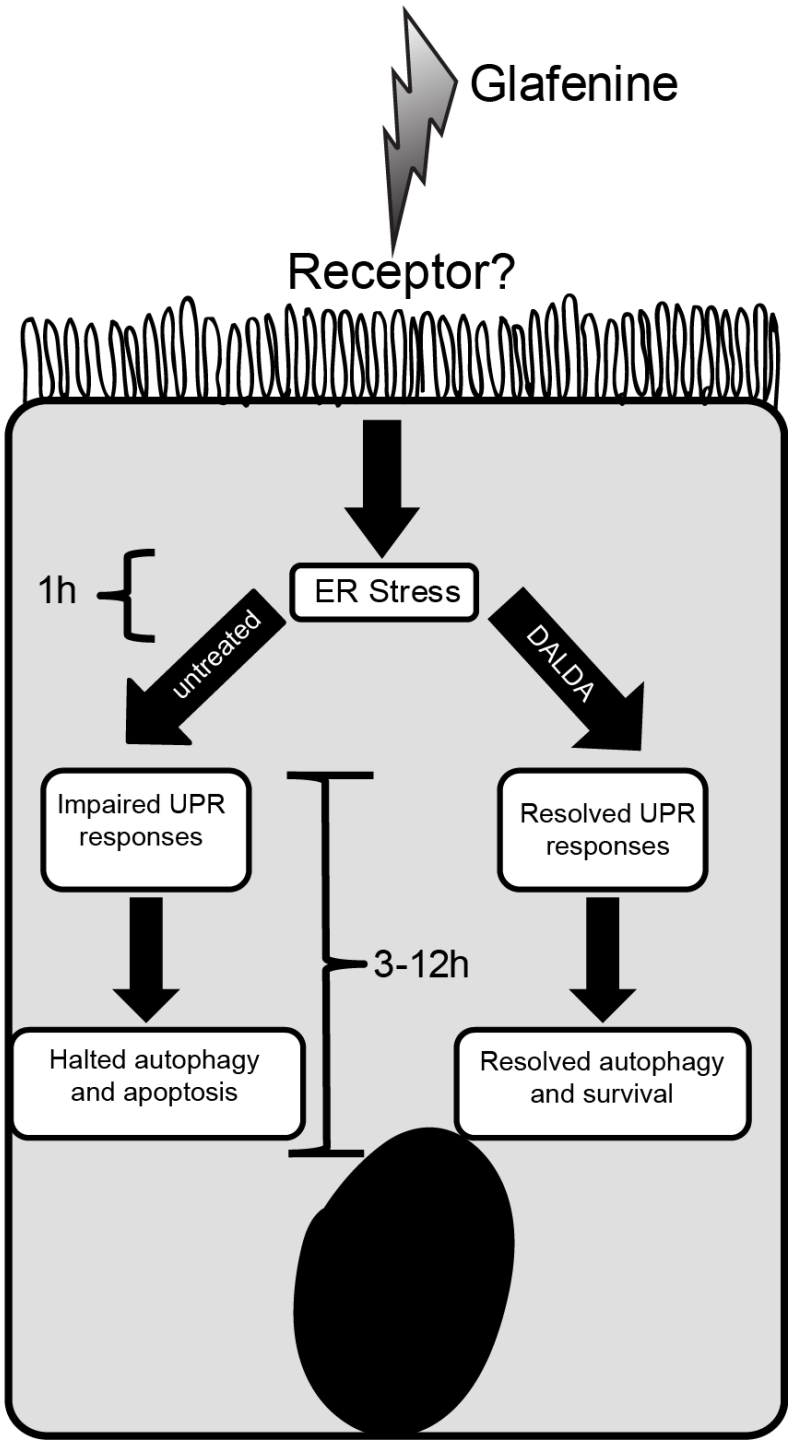

Figure 17: Schematic of glafenine-induced intestinal injury in zebrafish and MOR-mediated protection. Glafenine induces ER stress and UPR response. However, this process is halted with loss of downstream gene induction, leading to inefficient autophagy response and induction of IEC apoptosis. In presence of DALDA, glafenine-mediated blockade of the UPR process is restored and autophagy is successfully completed, resulting in reduced IEC apoptosis and maintenance of epithelial layer.

Discussion

Recent studies in mice and in human patients have implicated improper IEC autophagy and UPR in the face of ER stress as a potential etiology for IBD [17-19]. In this study, we recapitulate this IEC apoptosis in the zebrafish using the NSAID glafenine, an inhibitor of both COX isoforms that was pulled from the market after Phase IV studies showed that the drug results in anaphylaxis and gastrointestinal disturbances in human patients [218]. Current murine models for studying ER-stress induced IEC damage require the production of genetic knockouts. This zebrafish model provides several advantages over those systems, including the use of chemical induction and the ease of live imaging and screening for intestinal damage phenotypes. This is also the first larval zebrafish model to demonstrate marked intestinal pathology, namely IEC apoptosis. Previous reports only presented vague systemic inflammatory infiltration without overt changes in the intestinal epithelium [116, 117].

We present several lines of evidence indicating that the NSAID glafenine induces IEC apoptosis by enhancing ER stress, while interfering with compensatory rescue UPR and autophagic responses (Figure 17). First, TEM revealed ER pitting shortly after glafenine exposure (1-3h), a hallmark of ER stress. After extended glafenine exposure (12h), IECs displayed features which indicated an arrested autophagic response including partially enveloped organelles and numerous swollen, stressed organelles in living epithelial cells alongside many distinctively apoptotic cells. Secondly, induction of UPR-associated genes *atf6* and *s-xbp1* are impaired in glafenine-exposed fish.

Finally, the presence of activated caspase-3-positive apoptotic cells in both intestinal epithelium and the lumenal compartment of glafenine-treated fish are consistent with a failure to adequately respond to cellular stress [17, 19, 224, 225]. These findings suggest that glafenine induces a strong IEC stress phenotype that translates into increased cellular apoptosis and epithelial damage. While some liver damage likely exists, the intestinal-cell phenotype is far more pronounced. Additionally, our TEM analysis and AO staining studies, alongside the use of an NF-κB reporter strain to assess tissue-specific NF-κB activity (Figure 18), showed a gastroenterological-specific phenotype, another strength of this model.

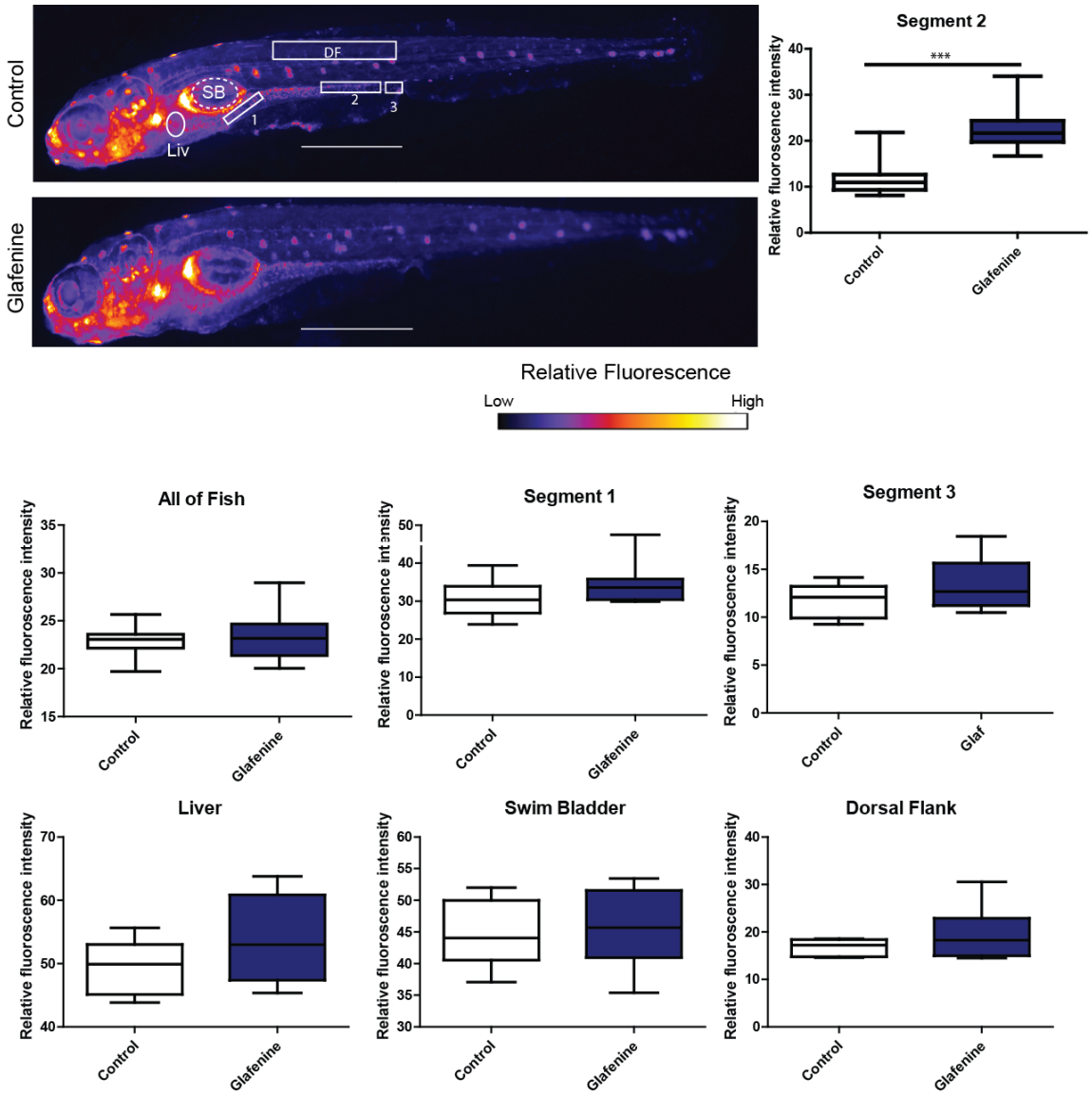

Figure 18: *Tg(NFkB:EGFP)* fish show increased segment 2 NF-κB activation in zebrafish after injury with glafenine. *Tg(NFkB:EGFP)*^{nc1} reporter zebrafish were used to assess NF-κB activation at 12h of glafenine exposure. Representative of 3 independent experiments, N as portrayed. Bar represents 1 mm. The same regions as in Figure 12 were used, as marked on the fish. SB = Swim bladder, Liv = Liver, DF = Dorsal fin.

Interestingly, despite the observed IEC apoptosis, the epithelial barrier remains intact. Using TxR-labeled dextran and oral gavage, we observed that the dextran does not leak out of the intestine in glafenine-treated zebrafish. This suggests that glafenine-induced apoptosis is highly controlled, and results in cell shedding with maintenance of the epithelial barrier. Our TEM results support these findings, demonstrating the presence of shedding apoptotic IECs in the epithelial border with maintenance of the barrier by cells basal to the dying cell—together forming the characteristic Y-pattern of controlled cell shedding [29]. Additionally, glafenine treatment of zebrafish larvae has previously been shown to cause increased activity of digestive enzymes phospholipase and protease within the intestinal lumen [226]. Our results provide a potential physiologic explanation for this observation: that these and other enzymes may be released promiscuously from apoptotic IECs after glafenine exposure.

While our kinetic and media-swapping studies suggest that glafenine-injury is rapid and acute, the mechanism by which glafenine induces epithelial-specific stress responses and damage is uncertain. Intestinal epithelium damage is a well-known effect of COX inhibitors [4, 207]. NSAIDs decouple mitochondrial oxidative phosphorylation within 1h of administration [227], resulting in ER and general cell stress that in the highly energy-dependent enterocyte can lead to cellular death. In our model, TEM showed characteristic mitochondrial vacuolization typical of NSAID-induced mitochondrial injury, suggesting that this may be the mechanism of injury in our model. Previous, *in vitro* only, studies demonstrated that other NSAIDs induce apoptosis through improper ER stress

responses [225], also suggesting that the effects of glafenine observed here are a result of its COX-inhibitory properties. The fact that dmPGE2 rescues zebrafish from IEC apoptosis in this model lends credence to this theory. The observation that other NSAIDs were unable to recapitulate the injury caused by glafenine suggest that these inhibitors, as opposed to glafenine, mainly cause non-intestinal mediated mortality over intestinal injury. This is compatible with our observation that zebrafish treated with other NSAIDs died before development of any intestinal apoptosis. In aggregate, we postulate that IECs are unable to appropriately response to glafenine-induced ER stress and as a result undergo rapid and but orderly apoptosis.

Neuropeptides have attracted interest as a means to modulate intestinal inflammation and to promote epithelial restitution [70]. We recently showed that the MOR agonist DALDA protects against DSS-induced intestinal injury through wound healing and proliferative responses in mice[205]. DALDA promoted intestinal proliferation in glafenine-exposed fish consistent with the previously reported properties of the drug [205]. However, other zebrafish bioactive proliferative factors (mEGF and hIGF1) [228, 229] failed to prevent glafenine-injury, suggesting that proliferation is not the primary protective mechanism of DALDA in this model. Interestingly, our study identifies a novel means by which mu opioid signaling may protect against acute epithelial injury. TEM analysis of DALDA-treated fish showed decreased ER stress and enhanced autophagy, leading to reduce cellular apoptosis and maintenance of epithelial layer integrity. Our studies showed that DALDA enhances *atf6* and *s-xbp1* mRNA expression in

zebrafish both in the presence and absence of glafenine, and that the protective effects of DALDA were lost in zebrafish lacking *atf6* function. Furthermore, we were able to establish that DALDA can induce LC3 accumulation and processing *in vitro*. We therefore conclude that MOR signaling enhances proper UPR responses and autophagy, a previously unknown mechanism of neuropeptide-mediated intestinal protection. At least one important autophagy pathway, the PI3K pathway [224], is directly activated by MOR signaling [54], providing a potential mechanism for DALDA's action in this zebrafish model. To support this hypothesis, addition of the PI3K inhibitor wortmannin resulted in complete loss of DALDA-mediated protection (data not shown). Together, our findings show that the zebrafish represents a powerful model to study cellular and molecular events associated with the intestinal injury response and that human relevant drugs (DALDA, NSAIDs) have bioactive effects in this vertebrate system.

In summary, we established a novel zebrafish larvae model of epithelial damage through chemical induction of ER stress and impairment of autophagic responses. We further demonstrated that the MOR agonist DALDA rescues this intestinal damage by potentiating the appropriate adaptive responses, including the UPR and autophagy. This novel model of intestinal injury in zebrafish can be utilized to explore the burgeoning field of ER stress-induced intestinal inflammation, and identify novel targets applicable to human disease.

Acknowledgements

The authors are grateful to Edward Flynn (UNC-CH) for superb technical support; to the Microscopy Services Laboratory of UNC-CH and Victoria Madden for TEM; to Dr. Kirsten Sadler Edepli (Mount Sinai School of Medicine) for providing *atf6* morpholino; to Dr. Arlin Rogers of the Department of Pathology (UNC-CH) for help developing our histological scoring system.

CHAPTER 4

MU OPIOID SIGNALING PROTECTS AGAINST ACUTE MURINE INTESTINAL INJURY IN A MANNER INVOLVING STAT3 SIGNALING[3]

Introduction

Opiates have long been used as analgesics to relieve pain associated with various medical conditions. Here we evaluated the effect and mechanism of mu-opioid signaling on the intestinal wound healing response, and assessed downstream pathways known to be protective against intestinal injury. Mice (C57BL/6) were exposed to 3% dextran sodium sulfate (DSS) for 7 days or 4% DSS for 5 days followed by 7 days of water. The MOR specific agonist DALDA and the antagonist cyprodime were injected subcutaneously (s.c) daily for *in vivo* studies or used for *in vitro* analysis. We found that MOR activation attenuated DSS-induced histological and gross intestinal injury and weight loss, diminished *Ifng*, *Tnf* and *Il6* mRNA expression and promoted intestinal healing during recovery. DALDA also enhanced colonocyte proliferation (Ki-67 staining) by 350%. MOR activation increased STAT3 phosphorylation in both DALDA-treated mice and the CMT-93 cell line. Importantly, DALDA induced colonocyte migration was completely ablated by sh*Stat3* knockdown. Together, this work

[3] Published in *The American Journal of* Pathology. 2011; 179(2): 673-83. Copyright obtained for use in this dissertation.

shows that MOR activation protects against and enhances recovery from DSS-induced intestinal injury. This is associated with an increase in STAT3 activation. Furthermore, STAT3 is required for DALDA-induced colonocyte migration. Consequently, manipulation of MOR signaling may represent a novel means to promote mucosal healing and maintain intestinal homeostasis following intestinal injury.

Background

A critical component of intestinal homeostasis is the presence of an intestinal mucosal barrier, comprised of a single monolayer of intestinal epithelial cells (IEC) that isolates highly antigenic luminal contents from an immunologically rich and underlying stromal compartment [1]. A wide body of research has shown that loss of intestinal barrier function leads to the development of various gastrointestinal inflammatory disorders, including inflammatory bowel diseases (IBD) [1, 5]. Conditions leading to an impaired mucosal barrier function are diverse and include genetic predisposition, medications (NSAIDS[4], antibiotics), radiation exposure [2] and ischemic episodes [3]. Overt damage to the epithelial barrier caused by these injuries triggers a host response termed restitution/wound-healing [10]. In this response, cells at the edge of the wound undergo a dedifferentiation process and migrate into the wounded area. They then undergo cytoskeletal rearrangement [28], re-differentiate, and finally re-establish tight junction barriers with their neighboring cells [10]. This process does not require epithelial proliferation, but renewal of cells are needed to replenish the decreased enterocyte pool after injury [28]. Numerous proliferative

signals such as epidermal growth factors (EGF) [7], transforming growth factors (TGF-β) [30, 31], and cytokines such as IL-22 [32] are implicated in the maintenance of the mucosal barrier. At the molecular level, these proliferative signals utilize various pathways including NF-κB, MAPK, STAT3 and PI3K/Akt [10] pathways. Identifying factors that engage these signaling pathways and promote wound healing is of great therapeutic interest for diseases such as IBD.

Wound healing promoting factors include the various neuropeptides produced by the enteric nervous system. Of strong relevance to IBD, several neuropeptides modulate immune cell function and could consequently impact the development of intestinal inflammation [230]. Opioids are a class of neuropeptides that have traditionally been used as analgesics; however, an emerging literature associates this class of neuropeptide with intestinal proliferation and inflammation [231]. Vertebrates traditionally express three types of opiods receptors: mu, delta, and kappa, all of which are G-protein coupled receptors that preferentially bind to G_i proteins. Binding of ligand to these receptors leads to the prototypical inactivation of neural pain fibers [54, 232, 233]. Interestingly, recent studies have shown opioids to protect against ischemia-reperfusion (I/R)-induced cardiac injury[86, 89]. Furthermore, the peripheral mu specific-agonist DALDA ([D-Arg2,Lys4]dermorphin-(1,4)-amide) [69] reduces inflammation in two experimental models of murine colitis: 2,4,6-trinitrobenzene sulfonic acid (TNBS) and adoptive transfer of $CD45RB^{hi}CD4^{+}$ T-cells [70]. Conversely, experimental colitis is exacerbated in mu-opioid receptor (MOR) knockout mice, [70] and MOR expression is up-regulated in mucosal samples from human IBD patients

compared to controls [71]. Together, these data implicate an important role for MOR signaling in regulating gut homeostasis. Although these studies have not fully addressed the mechanism by which MOR signaling ameliorates intestinal inflammation, it appears that down-regulation of cytokine production and modulation of T-cell function contributes to MOR's beneficial effect.

Based on its beneficial impact in other models of colitis [70], as well as in ischemia-induced cardiac injury [86, 89], we hypothesized that MOR signaling is cytoprotective in the context of intestinal barrier damage. Using a chemical model of acute injury and wound-healing that is T-cell & B-cell independent[234], we observed that the mu-opioid agonist DALDA protects against DSS-induced intestinal injury and promotes healing through activation of STAT3 and induction of cytoprotective factors regulated in part by STAT3. Our findings suggest that MOR agonists could represent a novel means to modulate tissue injury and enhance intestinal restitution and proliferation.

Materials and Methods

DSS-induced acute injury

Wild-type and transgenic NF-κB^{EGFP} reporter mice (C57BL/6 background) were maintained in standard housing cages in specific pathogen free (SPF) conditions. Mice (n=7), were given 3% DSS (MP Biomedicals; Aurora, OH) in their drinking water for 7 days while control mice received water alone. Water consumption was comparable between the different experimental groups. Throughout DSS administration, vehicle (10% DMSO/90% saline), the peripheral (does not cross the blood-brain barrier) MOR agonist DALDA[69] (100% saline,

50 µg/kg) (US Biological; Swampscott, MA), or the MOR antagonist cyprodime [235] (10% DMSO/ 90% saline, 10 mg/kg) (Tocris Bioscience; Ellisville, MI) was injected (s.c.) daily on the mid-dorsal surface of the mice. Mice were monitored daily for weight loss and visible signs of rectal bleeding. Occult bleeding was evaluated at day 4 of the experiment (Hemoccult, Beckmann Coulter Inc.; Fullerton, CA), in accordance with internal pilot studies that showed occult bleeding to be reliably observable in this model from Day 4 onwards. Clinical score, assessing weight loss, occult blood, and stool consistency was calculated as previously described [236]. All animal experiments were approved by the Institutional Animal Care and Use Committee of the University of North Carolina at Chapel Hill.

DSS recovery studies

C57BL/6 mice (n=6) were administered 4% DSS in their drinking water for 5 days, followed by water for a recovery period for 7 days. DALDA or vehicle was injected s.c. daily during the water recovery phase, as described above. Occult bleeding was evaluated at day 12. Mice were euthanized at days 8 and 12. Colonoscopies were performed as described previously [237], on days 5, 8 and 12.

Sample collection and histological evaluation

Mice were sacrificed at the indicated time points by CO_2 asphyxiation followed by cervical separation. The colon was dissected and flushed with ice-cold PBS, longitudinally splayed, swiss rolled, fixed in 10% formalin for 24 hrs, and then embedded in paraffin. Colitis severity was evaluated using

Hematoxylin-Eosin-stained sections by a blinded investigator on a scale from 0 to 40, as described previously [238-240].

IHC staining for pSTAT3(Y705) (Cell Signaling Technology Inc.; Beverly, MA) was performed according to the manufacturer's specifications, at a 1:50 dilution as previously described [237]. Ki-67 staining performed as previously described [237]. All sections were counterstained with Hematoxylin. Two different sections (per animal), approximately 200 µm apart, were assessed for staining, and representative images are shown.

For protein analysis, distal colons were dissected, flushed with ice-cold PBS and homogenized for 15 s with a polytron (IKA Works Inc; Wilmington, NC) in cold RIPA buffer containing proteinase inhibitors (Complete Mini, Roche Diagnostics GmbH; Penzberg, Germany) and phosphatase inhibitor cocktail #2 at a 1:100 dilution (Sigma-Aldrich). After incubation at 4°C for 30 minutes, samples were sonicated and cleared. Lysates were then diluted 1:1 with 2X laemmli buffer.

Confocal analysis of EGFP expression

Colons were fixed in 4% paraformaldehyde for 40 minutes at room temperature, and permeabilized in 2% Triton X-100 for 18-22 hrs at 4°C. Tissues were rinsed in 1X PBS, counterstained with propidum iodide (PI) (Invitrogen/Molecular Probes; Eugene, OR) for 30 minutes, and then placed in custom imaging chambers and immersed in Focus Clear (Cedar Lane Labs; Burlington, NC). Tissues were imaged with an Olympus Fluoview FV1000MPE microscope, with a 25x long-working distance water immersion objective. EGFP

was excited with a 495 nm laser, and PI was excited with a 559 nm laser. Tissue was imaged from the surface to a depth of 120 µm with a standard scale for laser power, offset, and gain based on depth that was maintained between samples. Images were analyzed using BioImage XD and Imaris (Bitplane AG; Zurich, Switzerland).

CMT-93 cell culture and stimulation

Murine rectal carcinoma cells (passage 33-59) (American Type Culture Collection (ATCC); Manassas, VA) were cultured in DMEM-high-glucose as described previously [241]. Cells were starved for 18-22 hrs in Opti-MEM and then treated with DALDA (10 µM) or naloxone (10 mM, Sigma-Aldrich; St. Louis, MO) for the times indicated. Cells were directly lysed in 1X laemmli buffer and protein concentration was measured using Bio-Rad quantification assay (Bio-Rad Laboratories; Hercules, CA).

Luciferase Assays

CMT-93 cells were infected with Ad5κB-Luc vector[242] for 12 hours in Opti-MEM, and then were stimulated with LPS (10 µg/mL) in presence or absence of 10 µM DALDA. Luciferase assay were performed on a Monolight 2010 luminometer for 20 s (Analytical Luminescence, San Diego),

Western blot analysis

Proteins (30 µg) were separated using 10% SDS-PAGE and transferred to nitrocellulose membranes and then probed with antibodies to pSTAT3(Tyr705) (1:2000), ERK1/2 (1:1000), pERK1/2 (1:2000) (Cell Signaling Technologies), STAT3 (1:1000) (Santa Cruz Biotechnologies; Santa Cruz, CA) and β-actin

(1:1000) (MP Biomedical; Solon, OH), were used with 5% milk in TBS-Tween (0.1%) or 5% BSA in TBS-Tween (0.1%) (for Cell Signaling Technologies antibodies), followed by the appropriate HRP-conjugated secondary antibody (GE Healthcare, Piscataway, NJ) and detected by chemiluminescence. Densitometry analysis for pSTAT3 was performed with NIH ImageJ software (http://rsbweb.nih.gov/ij/), to determine the ratio of pSTAT3 to STAT3, where indicated.

Immunofluorescence

CMT-93 cells were grown to 50% confluence in Opti-MEM media on glass cover slides. Cells were fixed in ice cold methanol, blocked with normal goat serum, and incubated with 1:100 anti-pSTAT3(Y705) (Cell Signaling Technologies) followed by anti-rabbit TRITC (1:100) (Jackson Immunoresearch Laboratories; West Grove, PA) for 30 minutes. Cells were then counterstained with Hoechst dye and mounted with Fluoromount-G (Southern Biotech, Birmingham, AL). Images were captured with a Zeiss LSM 710 confocal microscope (Zeiss; Jena, Germany).

RNA isolation and real-time PCR

RNA isolation from colonic tissues and CMT-93 cells and subsequent mRNA analysis was performed as previously described[237], using a ABI Prism HT7700. Specificity and linearity of amplification for each primer set was determined by melting curve analysis and calculation of the slope from serial diluted samples. Relative fold-changes were determined using the ΔΔCT calculation method. Values were normalized to the internal control GAPDH.

Primers: *Tnf* (5'-ATGAGCACAGAAAGCATGATC-3' and 5'-TACAGGCTTGTCACTCGAATT-3')[237], *Il6* (5'-CGGAGGCTTAATTACACATGTT-3' and 5'- CTGGCTTTGTCTTTCTTGTTATC-3')[243], *Il1b* (5'- GCCCATCCTCTGTGACTCAT-3' and 5'-AGGCCACAGGTATTTTGTCG-3'), *GAPDH* (5'-GGTGAAGGTCGGAGTCAACGGA-3' and 5'-GAGGGATCTCGCTCCTGGAAGA-3')[243], *Cox2 (Ptgs2)* (5'-TGAGTACCGCAAACGCTTCTC-3' and 5'- TGCAGCCATTTCCTTCTCTCCT-3')[244]. Cyclin D *(Ccnd1)*, *Ifng, Myc*, and *Reg3b* are QuantiTect primers (Qiagen; Valencia, CA).

Migration and proliferation assays

Migration assays were performed as described previously[245]. Briefly, CMT-93 cells were plated to confluency in Opti-MEM and then were scratched with a P1000 pipette tip. 10 μM DALDA in PBS or PBS alone was then immediately added. 4 different regions per plate were demarked and images were taken at the specified time points using an Olympus IX7 microscope. Images were analyzed with NIH ImageJ software. Each experiment was measured at 4 individual points, and was repeated independently at least 2 times.

Reproductive proliferation assays [246] were performed by plating CMT-93 cells at a known cellular density, and 2 hours after plating, cells were switched to 1% serum media and stimulated for 8 hours with 10 μM DALDA in PBS or PBS alone. Cells were then trypsinized and counted using trypan blue. Each plate

was counted 4 different times, and the experiment was repeated independently at least 2 times.

shRNA knockdown

A stable sh*Stat3* knockdown CMT-93 cell line was created using a lentivirus provided by the UNC-CH Lentiviral shRNA Core with a mixture of 4 different sh*Stat3* constructs. Open Biosystems TC1 library numbers TCRN0000071453-7 were employed (pLKO.1 vector) [247]. Control shRNA virus SHC-002 (Sigma-Aldrich) was used to create a stable control knockdown line. Cells were maintained in selection media containing 2 µg/mL puromycin, to which the lentiviral vectors conferred resistance but completely killed uninfected cells.

Statistical Analyses

Statistical analyses were performed using GraphPad Prism version 5.0a (GraphPad, La Jolla, CA). Comparisons of weight between mouse groups and over time were done with a two-way analysis of variance (ANOVA). Weight post-tests and further comparisons made between mice were analyzed using a Mann-Whitney U test at a 95% confidence interval. *In vitro* data and Ki-67 and pSTAT3 cell counting were compared with student t-tests, at a 95% confidence interval. All graphs depict mean ± S.E.M. Experiments were considered statistically significant if $P<.05$.

Results

DALDA ameliorates DSS-induced intestinal injury

To investigate the impact of MOR signaling in intestinal injury response, we employed the mu-specific agonist DALDA in a DSS model of acute intestinal injury. Mice were administered 3% DSS for 7 days, along with sterile s.c. injections of saline (vehicle), mu-specific agonist DALDA (50 μg/kg) [69], or the mu-specific antagonist cyprodime (10 mg/kg) [235]. We found that DALDA significantly attenuated DSS-induced weight loss (Figure 19A). Clinical scores, which factors in weight loss, diarrhea and bloody stool, showed that DALDA-treated mice displayed a significant reduction in disease compared to untreated mice (mean of 5.92 vs 3.93, $P< .01$), while MOR antagonism exacerbated disease (mean of 5.92 vs 7.92, $P<.01$) (Figure 19B). Histological scores (Figure 19C) showed that DALDA significantly reduced intestinal inflammation as compared to vehicle-treated (mean of 24.2 to 10.8, $P<.01$), while cyprodime worsened inflammation (mean of 24.2 to 33.5, $P<.05$). In addition, DSS-induced histological crypt damage was attenuated by DALDA treatment, while cyprodime exacerbated damage (Figure 19D). The extent of the pathological changes of DALDA and cyprodime on DSS-induced intestinal injury are shown in Figure 19E.

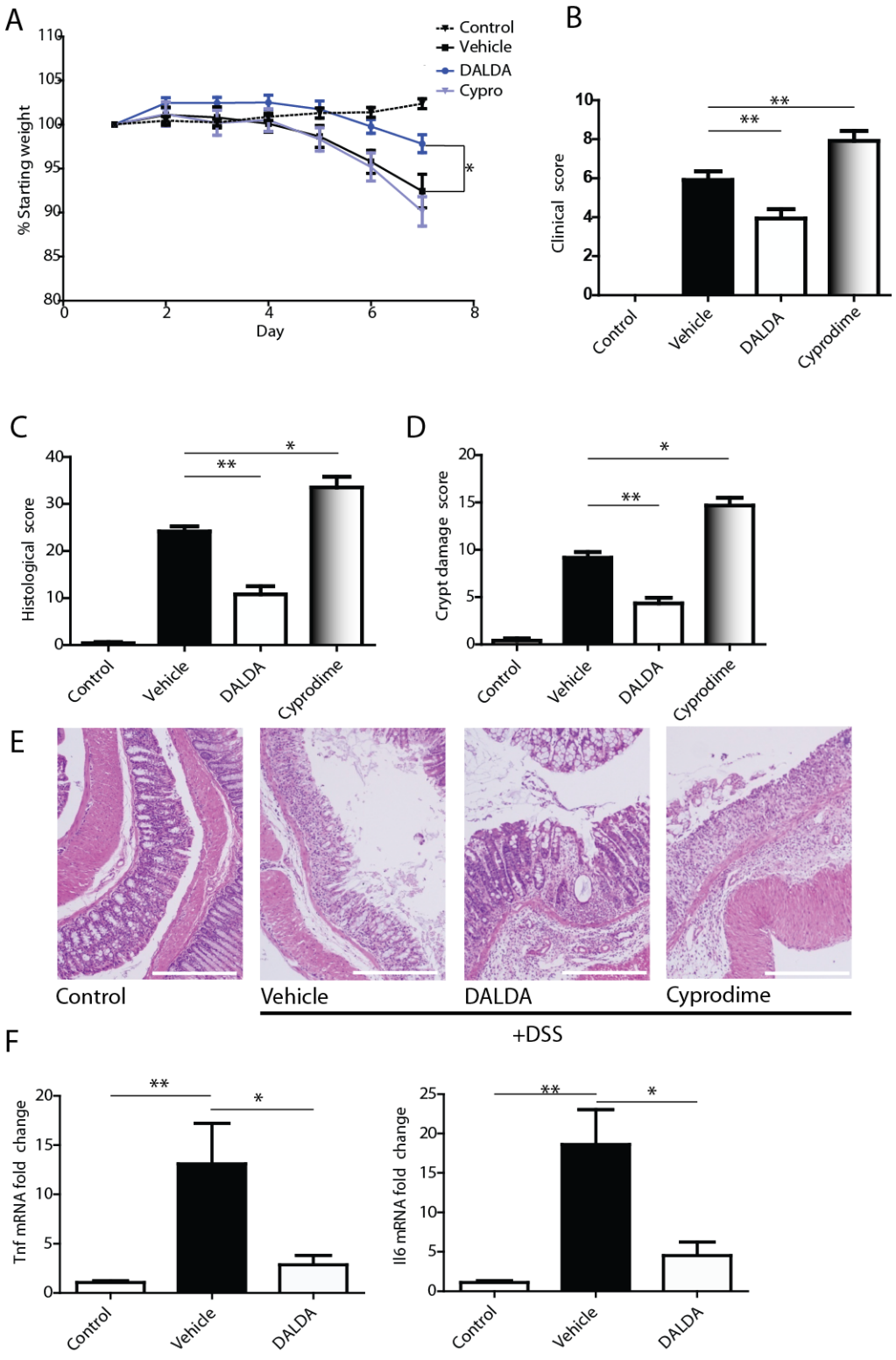

Figure 19: MOR activation protects against DSS-induced intestinal injury. Mice were given 3% DSS for 7 days concurrent with opioid treatment. DALDA (50 µg/kg), cyprodime (10 mg/kg) or vehicle were injected s.c. daily. All graphs

depict mean ± SEM. A) Percent weight loss from starting weight. N=7 for all groups. P<.001 by 2-way ANOVA between treatment groups and over time. P<.05 for DALDA-treated vs. vehicle-treated at day 7. B) Clinical score. N=7 for all groups. P<.01 for DALDA-treated vs. vehicle-treated. C) Histological score. N≥5 for all groups. D) Crypt damage score. N>4 for all groups. E) Representative H&E photomicrographs. Bar = 100 μm for all sections. F) Fold change Tnf and Il6 distal colonic mRNA expression. N≥4 for all groups.

After establishing that MOR activation protected against DSS-induced injury, we assessed the effects of DALDA on inflammatory cytokines. We found that DALDA significantly reduced colonic *Tnf* and *Il6* mRNA expression (Figure 19F). As these cytokines are induced in part through immune-derived NF-κB signaling during experimental colitis [248], we next explored the impact of daily s.c. injections of DALDA on NF-κB activity using fresh-fixed tissues sections obtained from NF-κB^{EGFP} reporter mice and confocal microscopy imaging. As previously reported, EGFP expression in the lamina propria increased in DSS-exposed NF-κB^{EGFP} reporter mice [243, 249]. Interestingly, lamina propria-derived EGFP expression (NF-κB activity) was strongly reduced in DALDA-treated mice (Figure 20A). Moreover, DALDA failed to block LPS-induced NF-κB transcriptional activity in CMT-93 cells (Figure 20B). These findings indicate that DALDA protects against DSS-induced acute intestinal injury in mice, and is associated with reduced immune cell-derived NF-κB activation and pro-inflammatory gene expression without directly inhibiting NF-κB signaling.

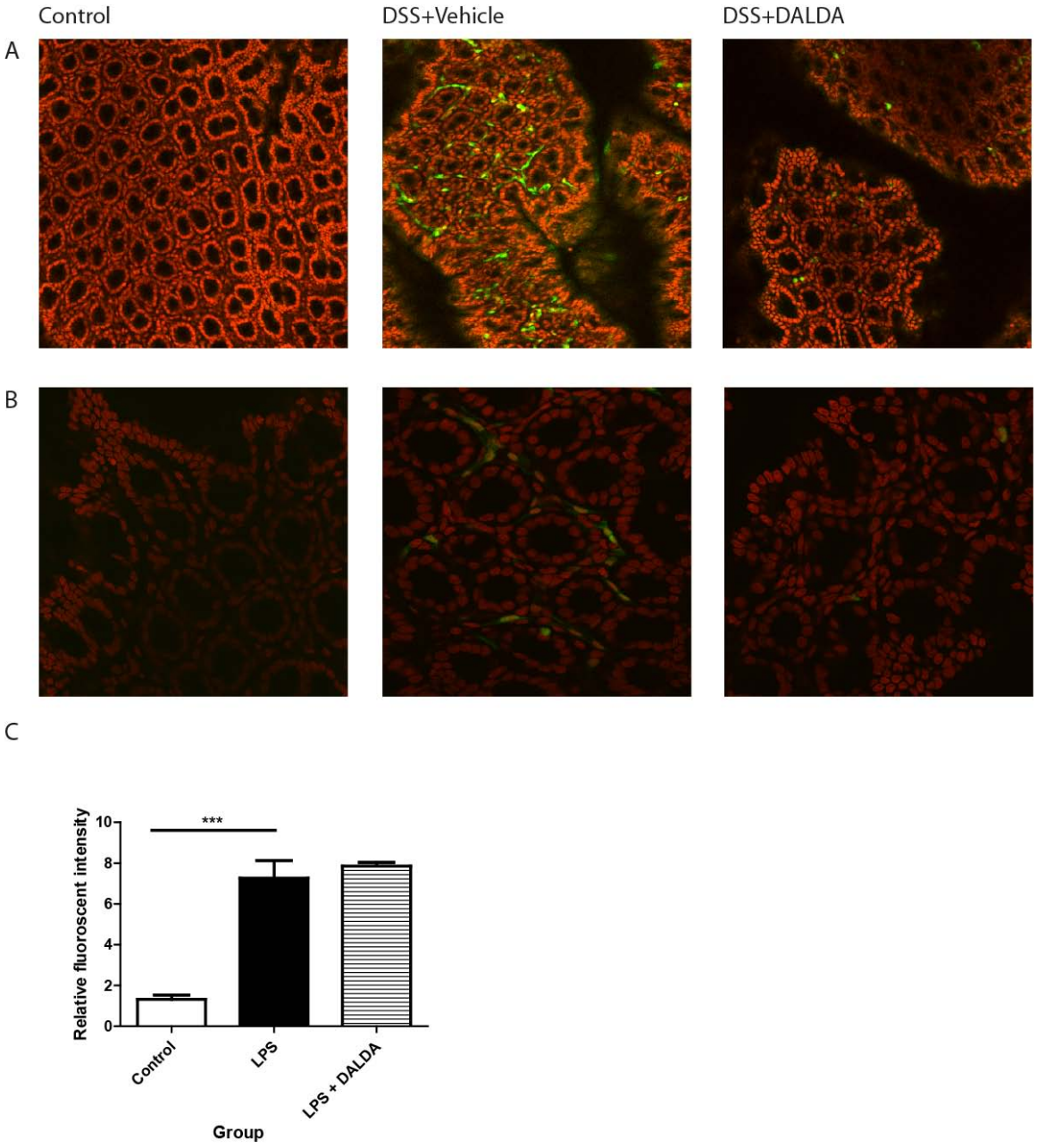

Figure 20: DALDA prevents DSS-induced EGFP expression in DSS-exposed NF-κB^{EGFP} mice. NF-κB^{EGFP} mice were administered 3% DSS for 7 days, concurrent with DALDA (50 µg/kg), cyprodime (10 mg/kg) or vehicle treatment. Colonic EGFP expression was assessed in whole tissue mounts using confocal microscopy. Propidium iodide (red) was used to visualize nuclei. 4 mice per condition were visualized macroscopically (data not shown), and 2 per condition were visualized further by confocal microscopy. A) 25x magnification. B) 60x magnification of the same tissues as shown in A. C) LPS induced NF-κB transcriptional activity is not blocked by DALDA. CMT-93 were infected with Ad5κB-Luc for 12 hours, and then stimulated with 10 µg/mL LPS in the presence or absence of 10 µM DALDA for 12 additional hours.

MOR activation enhances recovery from DSS-induced intestinal injury

As wound-healing is a critical process during tissue repair, we evaluated the impact of DALDA on recovery from DSS-induced intestinal injury. Mice were administered 4% DSS for 5 days, followed by 7 days of s.c. injections of saline or 50 μg/kg DALDA. Gross mucosal damage visualized by colonoscopy showed attenuation of macroscopic lesions by day 7 in DALDA-treated mice (Figure 21B). Furthermore, DALDA enhanced weight loss recovery and DALDA-treated mice returned to near-normal weight by day 7 of the recovery phase (Figure 21A). DALDA similarly reduced clinical scores after 7 days of recovery (mean of 5.3 vs 2.3, $P<.05$, Figure 21C), while histological scores were noticeably lower after only 3 days of therapy (mean 29.2 vs. 15.6, $P<.01$ at day 3, 23.2 vs. 11.3, $P<.01$ at day 7, Figure 21D), with initial improvements associated with decreased crypt damage (mean 9.7 vs. 3.7, $P< .05$ at day 3, Figure 21E). In accordance with histological and clinical decreases in disease, *Tnf*, *Il6*, *Il1b* and *Ifng* mRNA levels were significantly reduced in DALDA-treated compared to vehicle-treated mice (Figure 21F). These findings indicate that DALDA protects against DSS-induced intestinal injury and promotes wound healing.

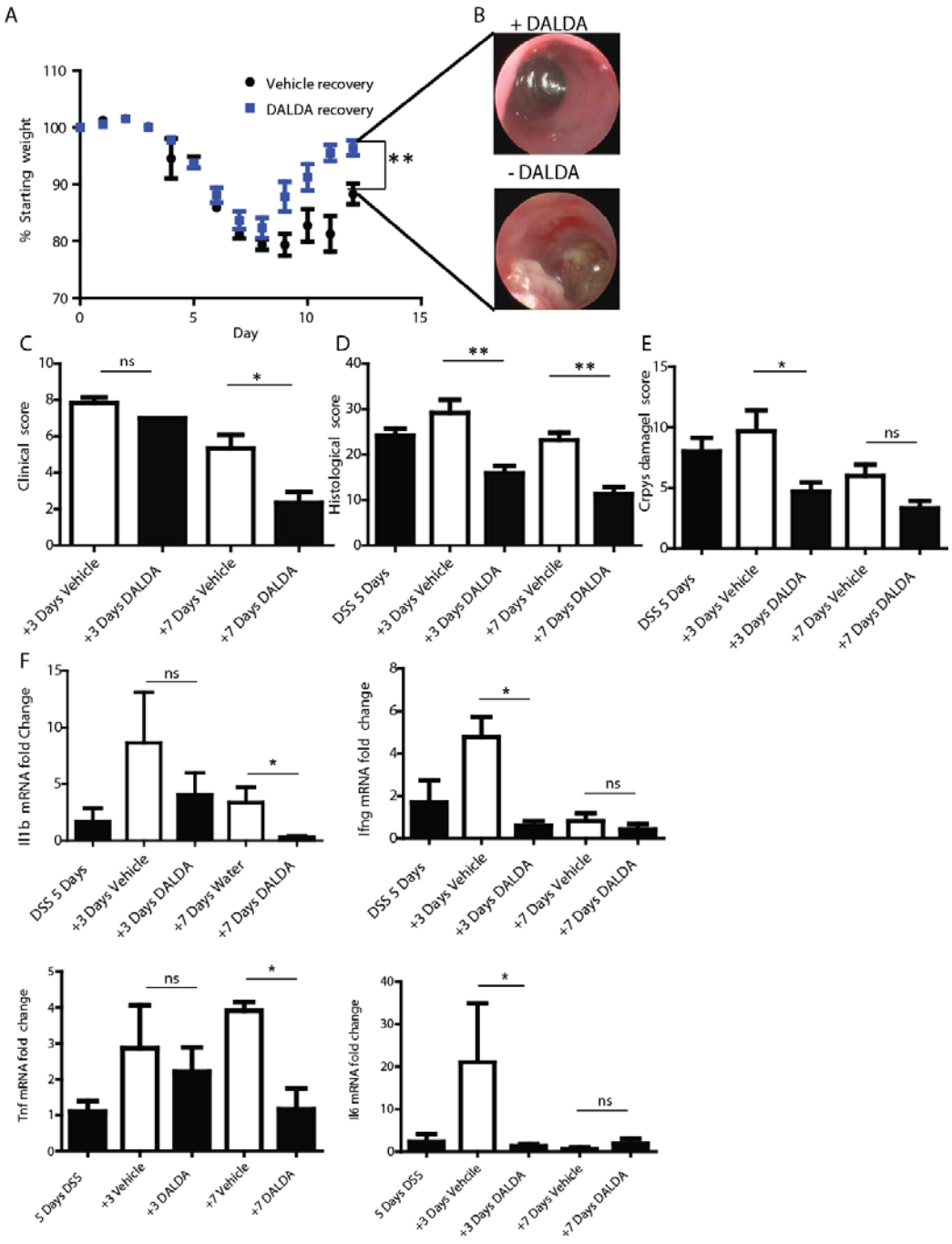

Figure 21: MOR activation enhances recovery from DSS-induced intestinal injury. Mice were administered 4% DSS for 5 days, followed by 7 days of water recovery concurrent with treatment: 50 µg/kg DALDA or vehicle were injected s.c. daily. All graphs depict mean ± SEM. A) Percent weight loss from starting weight. N>6 for all groups. B) Representative colonoscopies for each group on the final day of the experiment. C) Clinical score. N=6 for all groups. D) Histological score. N>4 for all groups. E) Crypt damage score. N>4 for all groups. F) Fold change *Tnf*, *Il6*, *Il1b*, and *Ifng* mRNA accumulation was determined by RT-PCR. N≥4 for all groups.

DALDA enhances colonocyte proliferation and STAT3 activation *in vivo*

As proliferation is an important feature of the healing response that occurs after migration/restitution, we measured proliferation in DALDA-treated mice by Ki-67 staining. We observed a modest 38% increase in proliferative activity ($P<.01$) in DALDA-treated mice compared to control (Figure 22). Importantly, proliferation index increased by almost 2-fold ($P<.05$) in DSS-exposed, DALDA-treated mice compared to DSS alone (Figure 22).

Because STAT3 signaling is also a critical proliferative response in the DSS acute model of intestinal injury[32], we next determined the impact of MOR agonism on STAT3 activation. Compared to untreated controls, DSS-exposed mice showed a 5-fold increase in colonic pSTAT3. DALDA therapy alongside DSS injury increased pSTAT3 10-fold ($P<0.001$) over that of untreated controls (Figure 23A); surprisingly, mice given DALDA alone without DSS-injury did not have increased levels of pSTAT3 over control (N=4, data not shown), suggesting that STAT3 activation by MOR is tightly regulated, and that MOR-mediated activation occurs only in the presence of injury. IHC indicated that DALDA-induced STAT3 phosphorylation appears predominately in colonocytes (Figure 23B-C), resulting in a 2.7-fold increase in pSTAT3-positive colonocytes per 20 crypts ($P<0.05$) in DALDA-treated vs. vehicle-treated mice exposed to DSS. We next assessed expression of cytoprotective genes regulated in part by STAT3, using real-time PCR. As anticipated, DALDA significantly enhanced expression of Cox2 *(Ptgs2)*, *Myc*, *Reg3b*, and Cyclin D *(Ccnd1)* mRNA levels in DSS-exposed mice compared to vehicle-treated mice (Figure 23C). These specific

cyto-protective genes were selected because their expression decreased in DSS-exposed STAT3ΔIEC mice compared to wild-type [32], demonstrating that they are regulated by STAT3 in colonocytes.

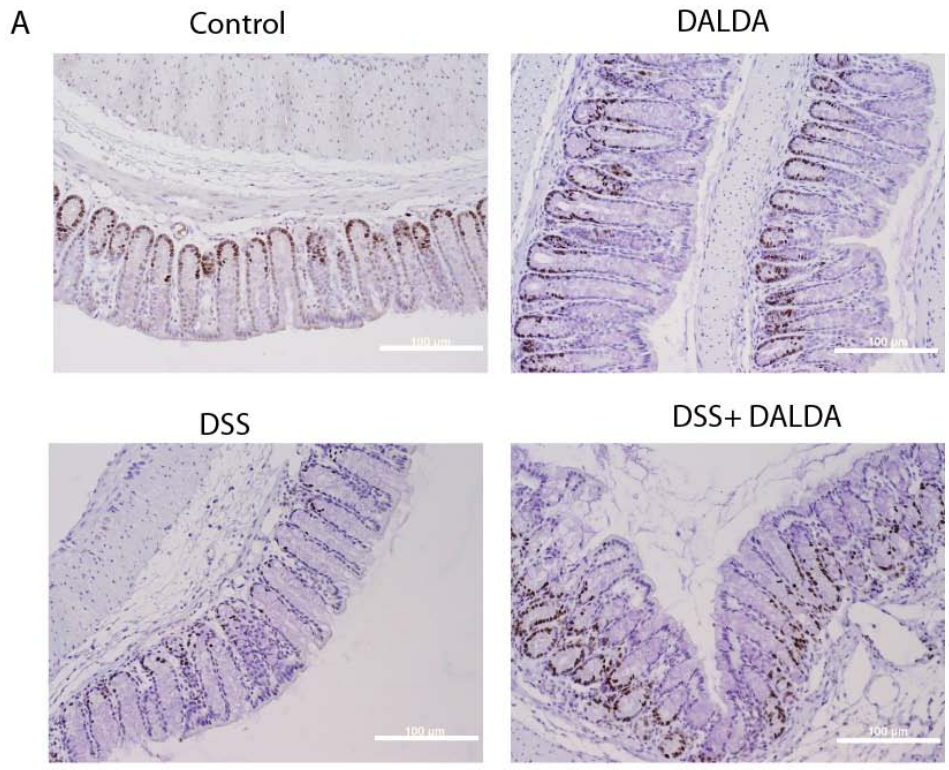

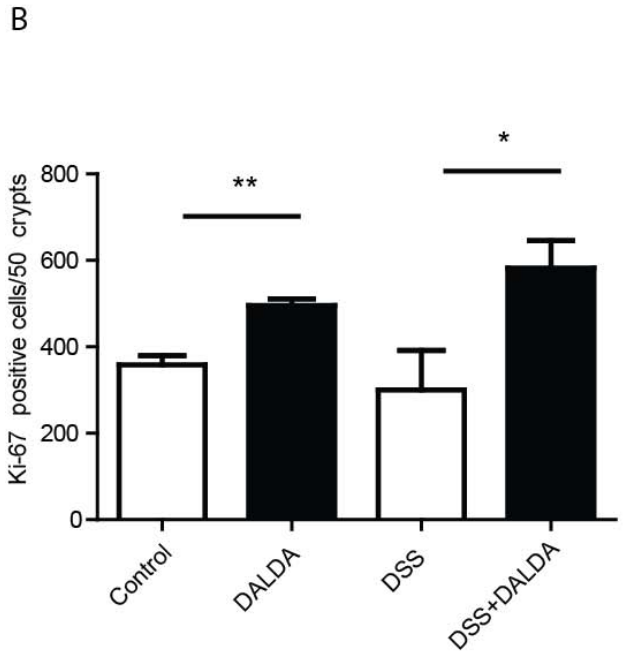

Figure 22: Enhanced colonocyte proliferation in DALDA-treated mice. All graphs depict mean ± SEM. A) Representative photomicrographs. Bar = 100 µm. B) Ki-67 positive cells were counted in 50 crypts across multiple fields of view. N≥4 for all groups except DALDA alone, for which N=3.

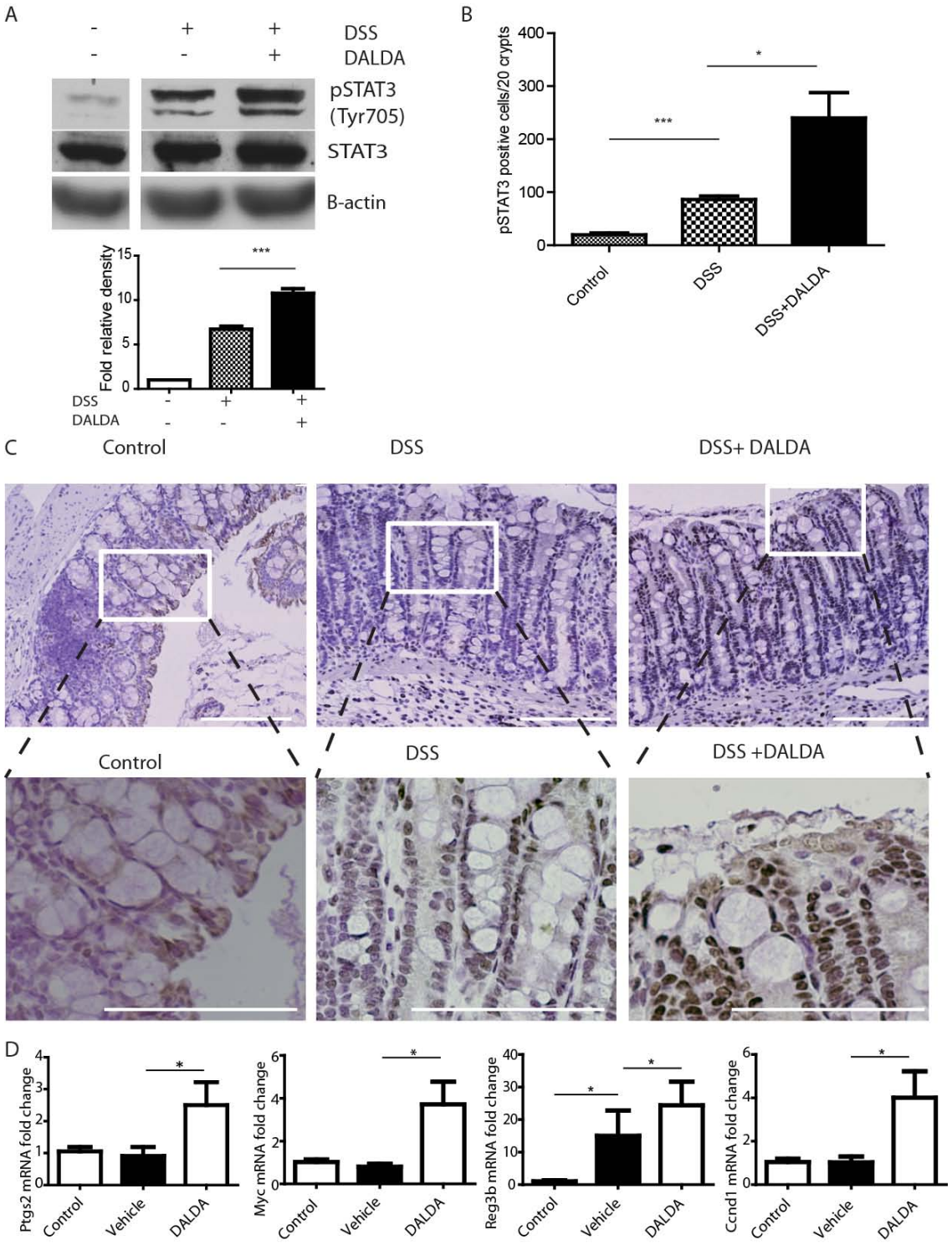

Figure 23: DALDA enhances STAT3 activation in DSS-induced intestinal injury. Mice were administered 3% DSS + vehicle or 3 % DSS + DALDA (50 µg/kg, injected s.c. daily) for 7 days. All graphs depict mean ± SEM. A) Levels of STAT3 phosphorylation (Y705) in distal colonic tissue measured by Western blot.. Relative level of pSTAT3 over total STAT3 was determined by densitometry. Representative of 4 individual mice. B&C) pSTAT3

immunohistochemistry analysis. Representative images of 4 mice per group. Bars represent 100 μm in all images. White boxes outline higher magnification images of each section. Bar graph shows pSTAT3 positive colonocytes per 20 crypts. D) Expression of STAT3-dependent genes (*Ptgs2, Myc*, *Reg3b, Ccnd1*) in distal colonic tissue. N≥3 per group.

DALDA enhances STAT3 phosphorylation *in vitro*

To gain more insight into the role of STAT3 in MOR-mediated protective effect, we utilized an *in vitro* cell system. CMT-93 cells were exposed to DALDA (10 μM) for 1 hour after which STAT3 phosphorylation was measured by Western blot. Densitometric analysis showed that pSTAT3 levels increased by ~3-fold in DALDA-treated cells compared to unstimulated cells ($P<0.05$ compared to an assumption of a 0-fold change, Figure 24A). In addition, immunofluorescence assays showed an increased level of pSTAT3 in DALDA-treated cells compared to unstimulated cells (Figure 24B). We determined whether the general opioid antagonist naloxone could inhibit DALDA-induced pSTAT3 activation, and indeed we see that 30 minute pretreatment with naloxone (Figure 25C) blockades STAT3 phosphorlyation. We then investigated the impact of DALDA on cyto-protective genes regulated in part by STAT3 using real-time PCR. Expression of *Myc*, Cox2 *(Ptgs2)*, Cyclin D (*Ccnd1)* and *Reg3b* mRNA were significantly induced in DALDA-stimulated CMT-93 cells (Figure 24C). These studies indicate that colonocytes respond to a mu-opioid receptor agonist by activating STAT3 signaling and downstream cyto-protective mediators.

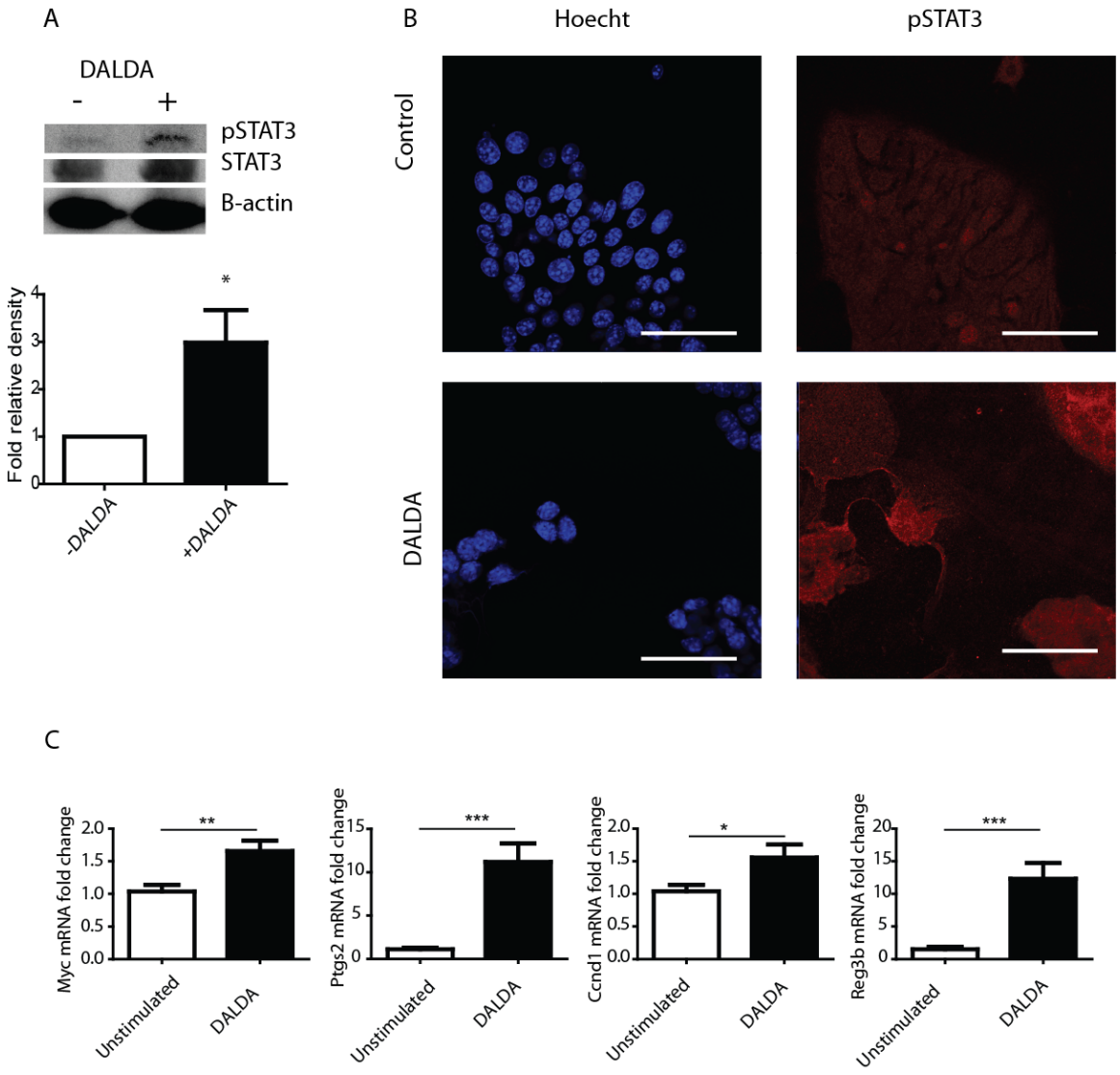

Figure 24: DALDA induces STAT3 phosphorylation in CMT-93 cells. A-C) CMT-93 cells were treated for 1 hour with 10 µM DALDA or vehicle. A) Western blot and densitometry comparing pSTAT3 to STAT3 within the same sample. Representative of 8 independent experiments. B) pSTAT3 immunofluorescence staining, representative of triplicate samples, from 2 independent experiments. C) Activation of STAT3 dependent genes (*Ptgs2, Myc*, *Ccnd1*, *Reg3b*). N≥4 for both groups, in two independent experiments.

ERK phosphorylation is a well established downstream consequence of G_i-coupled GPCR activation and a classic effector of MOR activation [250]. We detected ERK1/2 phosphorylation in the distal colonic tissue of DALDA-treated mice and in DALDA stimulated CMT-93 cells (Figure 25A and C). To confirm the specificity of DALDA-induced ERK1/2 phosphorylation, CMT93 cells were pretreated (30 min) with the mu-opioid receptor competitive antagonist naloxone (10 mM) and then stimulated with DALDA. Interestingly, levels of pERK1/2 are slightly augmented in naloxone treated cells, a phenomenon previously reported [251, 252]. Importantly, naloxone attenuated DALDA-induced pERK1/2 in CMT93 cells (Figure 25B).

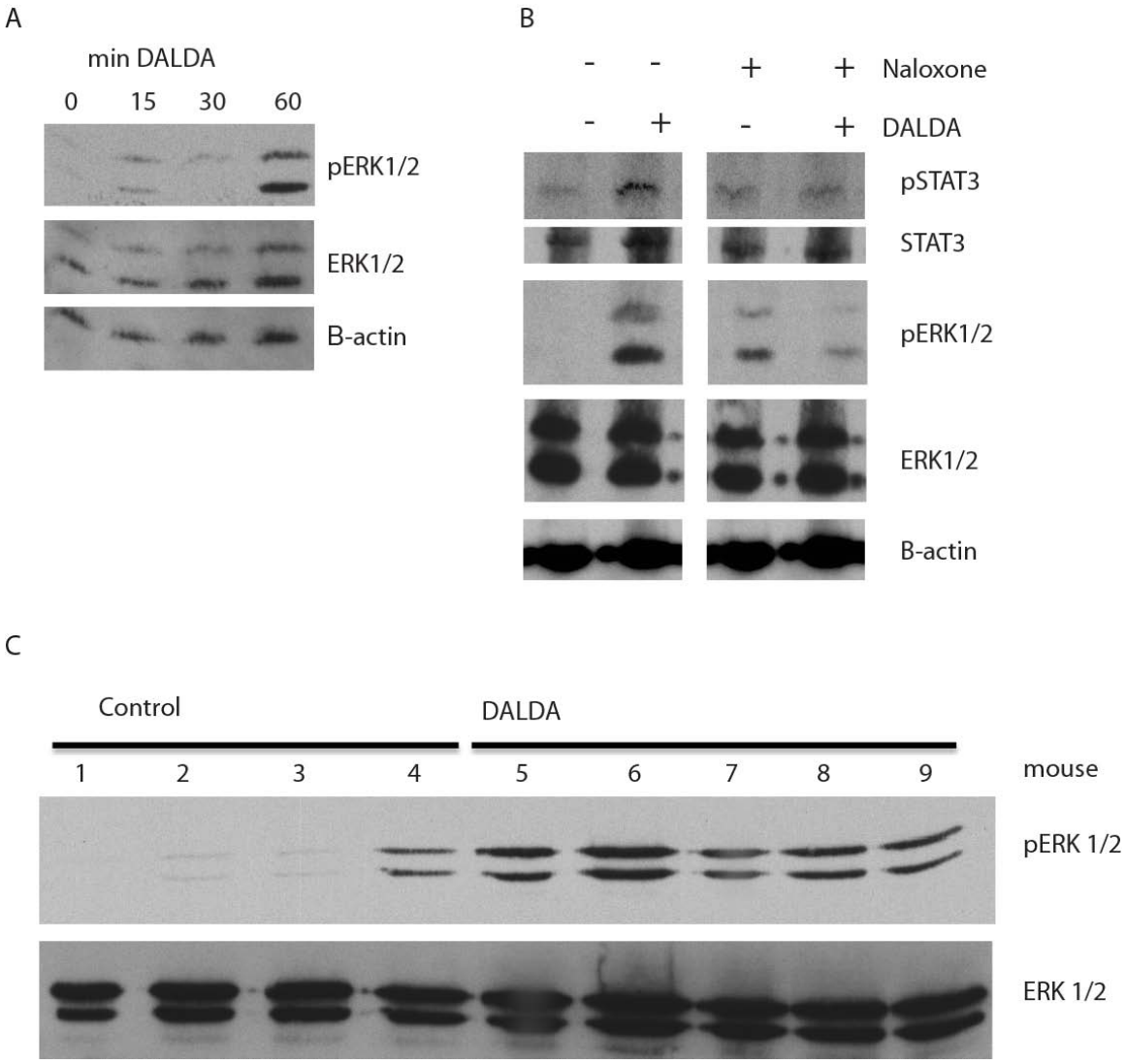

Figure 25: DALDA induces ERK1/2 phosphorylation by an opioid-dependent pathway. A) Western blot for pERK1/2 in CMT-93 cells stimulated with 10 µM DALDA for 0-60 minutes. Representative of 3 individual experiments. B) Western blot for pSTAT3 and pERK1/2 in CMT-93 cells stimulated with DALDA for 1 hr with or without 30 minute pre-treatment with 1 mM of the opioid antagonist Naloxone. Representative of 3 individual experiments. C) DALDA induces colonic ERK1/2 phosphorylation *in vivo.* Western blot for pERK1/2 from distal colonic protein extracts from individual control mice or mice injected with 50 µg/kg DALDA daily s.c. for 7 days.

DALDA enhances colonocyte migration in a STAT3-dependent manner

Since DALDA promoted proliferation *in vivo* and activated protective/proliferative signaling *in vitro*, we next explored the effect of MOR activation on cellular restitution/migration using an *in vitro* wound healing/scratch-assay model. Immediately following wounding, cells were incubated with DALDA (10 μM) and 8 hours later the distance migrated into the scratch was measured with ImageJ. Migration increased by 67% ($P<.001$) in DALDA-treated compared to untreated cells (Figure 26A-B). Furthermore, reproductive cellular proliferation assays showed that DALDA enhanced CMT-93 proliferation by 45% over the same time period (Figure 26C; $P<0.05$). Since DALDA enhanced STAT3 phosphorylation *in vivo* and *in vitro*, we determined the functional impact of this signaling event on CMT-93 migration using an shRNA knockdown approach. CMT-93 cells were infected with a lentiviral vector containing sh*Stat3* and a puromycin resistance gene, allowing for the selection and maintenance of a stable knockdown line. STAT3 expression was efficiently inhibited in sh*Stat3* infected cells compared to scramble controls (Figure 26D). Moreover, DALDA-induced pSTAT3 was strongly blocked in sh*Stat3* infected cells compared to sh control (Figure 26E). Most importantly, DALDA-induced cellular migration was completely abrogated in sh*Stat3* infected cells compared to control-infected cells (Figure 26F). These findings demonstrate that DALDA drives colonocyte migration in a STAT3-dependent manner, and combined with our *in vivo* studies shows that MOR activation enhances intestinal wound healing by both enhancing

restitution/migration and cellular proliferation, in a manner involving STAT3 signaling.

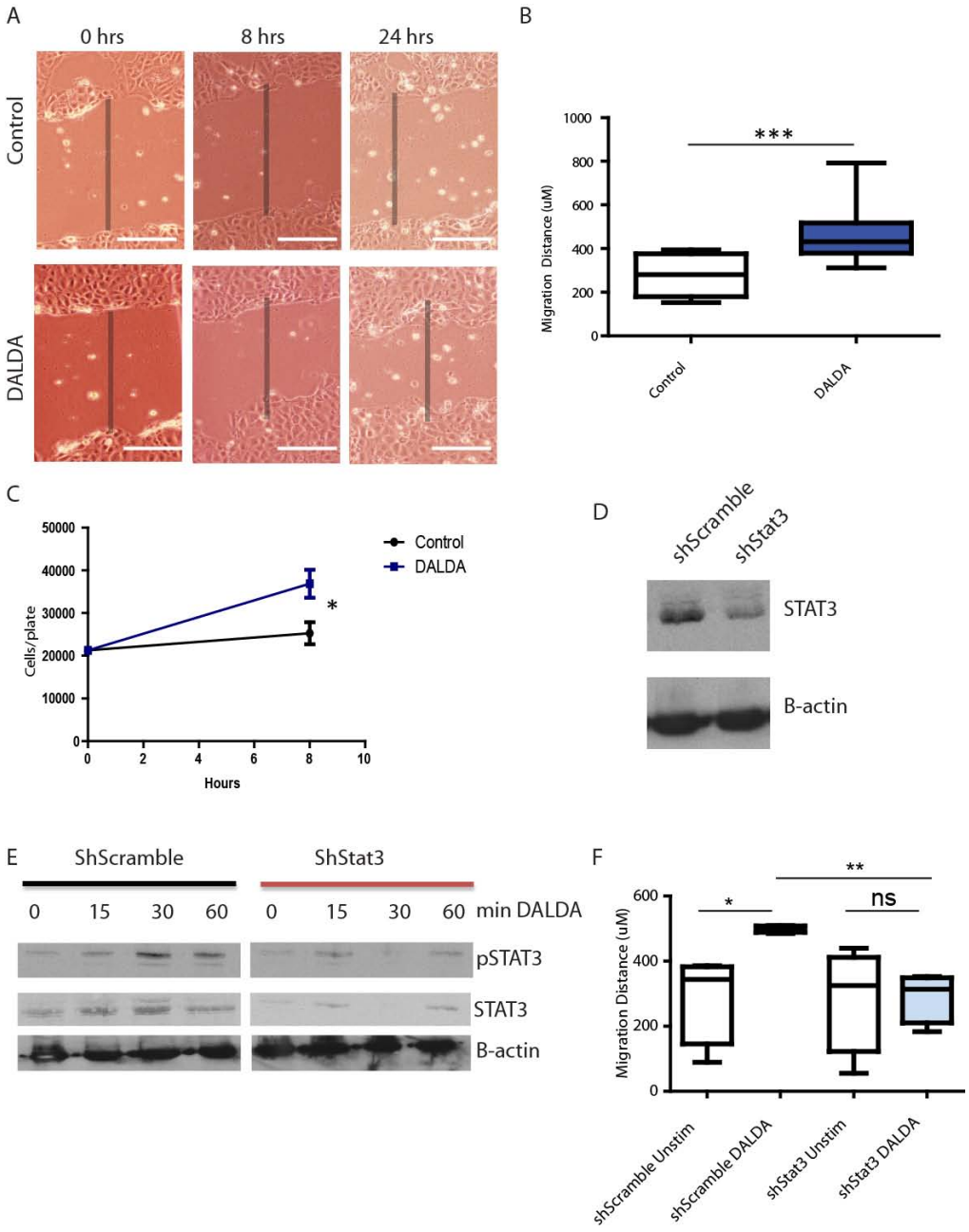

Figure 26: DALDA enhances colonocyte migration in a STAT3-dependent manner. A) CMT-93 monolayers were scratched and treated with 10 µM DALDA or vehicle. Migration was observed over a 24h period. A) Representative photomicrographs of cell migration. Shaded area shows initial wound area. Bars represent 100 µm in all images. B) Quantification of migration distance after 8 hours. Mean results of 3 independent experiments, N=4 for each experiment. C) Reproductive cellular proliferation assays. CMT-93 cells were treated with 10 µM DALDA or vehicle for 8 hours and direct cell quantification was performed. Mean results of 2 independent experiments, N=4 for each experiment. D-F) Cells were infected with a sh*Stat3* lentivirus to reduce *Stat3* expression or control

scrambled shRNA (shScramble) D) Western blot representative of 3 independent experiments illustrate *Stat3* knockdown in sh*Stat3* cells. E) Western blots show reduced DALDA-induced STAT3 phosphorylation in sh*STAT3* infected CMT-93 cells. Representative of 2 individual experiments. F) Quantification of migration over an 8-hour period. Representative of 2 separate experiments, N=4 per experiment.

Discussion

As a result of their ability to promote intestinal repair, increasing clinical interest has focused upon the use of trophic factors to treat diseases associated with chronic epithelial injury such as IBD [5, 25, 253]. Here we have demonstrated that peripheral activation of the mu-opioid pathway protects against DSS-induced intestinal injury and enhances wound healing. We have shown that the MOR-specific agonist DALDA activates proliferative signaling in the intestine, a response associated with enhanced colonocyte-derived STAT3 activation and induction of cytoprotective genes. In contrast, the MOR-specific antagonist cyprodime worsens DSS-induced intestinal injury, suggesting that this opioid pathway plays an essential role in the intestinal wound-healing response. Interestingly, previous reports have shown that low-dose therapy of the non-specific opioid antagonist naltrexone protects against both DSS-induced injury in mice and ameliorates Crohn's disease in a small, open label patient study [72, 73]. In these studies, naltrexone was deliberately administered at levels below the dose needed to pharmacologically blockade receptor function. Because the MOR-specific antagonist cyprodime exacerbates DSS-induced colitis, it is likely that low-dose naltrexone therapy acts to potentiate endogenous opiate signaling [58, 72, 73]. However, such a mechanism remains controversial and has never been truly established.

Our work provides significant new insights into the mechanisms behind DALDA- mediated amelioration of intestinal injury and inflammation. Chronic opiate administration is known to be immunosuppressive clinically, and

specifically inhibits T-cell, B-cell, and natural killer cell function [230, 254, 255]. Moreover, DALDA has been shown to be protective in two T-cell driven models of murine colitis: the TNBS and adoptive transfer of $CD45RB^{hi}CD4^{+}$ T-cell models [70]. This implies that MOR-mediated immunosuppression may provide a potential mechanism for MOR-mediated protection from intestinal injury. However, DSS-induced acute colitis has been shown to be T-cell, B-cell, and NK-cell independent [234], and hence DALDA cannot be solely operating through inhibition of adaptive immune responses. While we observed decreased activation of NF-κB (EGFP expression) and inflammatory gene expression in DALDA-treated mice, these observations are likely a secondary effect of the drug since genetic ablation of IEC-derived NF-κB signaling [23, 40, 256-258] and blockade of the pathway [243, 249, 259] are both known to exacerbate injury response in the intestine. In addition, in vitro NF-κB transcriptional activity in IEC was not inhibited by DALDA treatment.

We show that DALDA operates in part through the enhancement of wound healing and cellular proliferation in response to DSS-induced epithelial damage. Indeed, an early effect of DALDA therapy is improvement of crypt damage score and enhanced epithelial proliferative responses (Ki-67 staining). These observations suggest that DALDA acts by enhancing both epithelial proliferation and damage repair responses. This concurs with our *in vitro* data showing that DALDA enhanced IEC proliferation/migration following wounding,. We postulate that the enhanced wound-healing afforded by DALDA limits luminal antigenic activation of lamina propria immune cells (NF-κB activation, cytokine expression)

and inflammation through epithelial restitution/migration and enhanced colonocyte proliferation.

The novel finding that DALDA induced IEC STAT3 phosphorylation both *in vivo* and *in vitro* is particularly relevant to the wound healing response. IEC-derived STAT3 signaling has been shown to confer protective responses against DSS-induced intestinal injury through the promotion of wound healing responses [32, 260], and furthermore, STAT3 signaling is a known driver of enterocyte proliferation [261, 262]. IHC staining demonstrated that colonocytes are the predominant cells exhibiting pSTAT3 in DALDA-treated, DSS-exposed mice. DALDA enhanced expression of cyto-protective genes (*Reg3b*, *Ccnd1*, *Cox2*, *myc*) that are lost in STAT3ΔIEC mice known to be sensitive to DSS injury [32]. The up-regulation of these genes only in the presence of DALDA suggests that while DSS alone can up-regulate colonocyte STAT3 activation to an extent, only the presence of DALDA and subsequent exogenous MOR signaling is sufficient to generate protective responses, through higher elevated pSTAT3 levels, increased cyto-protective gene expression and proliferation (Ki-67 staining).

Our gene expression observations could also be recapitulated *in vitro* with CMT-93 colonocytes, where we also saw DALDA increase pSTAT3 levels in CMT-93 cells and enhance cellular migration in response to a wound, as well as enhance cellular proliferation. Knockdown of STAT3 demonstrated the importance of STAT3 signaling in DALDA-mediated enhanced migration, as this response was abrogated in sh*Stat3*-infected CMT-93 cells compared to control.

These observations strongly suggest that DALDA promotes protective function in the intestine through a mechanism involving STAT3 activation. Although IECs are the predominant cells exhibiting pSTAT3 in response to DALDA treatment, it is unclear whether these cells are the main target of the opioid. Tissue-specific MOR gene deletion will be necessary to evaluate the cellular compartment implicated in DALDA-induced protective response. Additionally, while STAT3ΔIEC mice are available, previous work has shown that these mice are extremely sensitive to DSS-colitis and have severe defects in epithelial restitution[32], making exploring the role of DALDA on such a sensitive background untenable.

ERK1/2 is a canonical downstream effector of G_i-coupled signaling and represents a classical read-out of opioid signaling. Interestingly, while we observed persistent *in vivo* activation of ERK1/2 in DALDA-injected mice, STAT3 phosphorylation was observed only in the context of DALDA administration during an injury response. This suggests that MOR-mediated STAT3-driven proliferation *in vivo* is tightly regulated and activation depends on the injury status of the epithelium. A previous study has identified IL-22 as a key cytokine involved in DSS-induced pSTAT3 and injury response [32]. Interestingly, we observed enhanced colonic IL-22 mRNA expression in DALDA-treated, DSS-exposed mice (Goldsmith and Jobin, unpublished observation). Further studies will be required before establishing the functional role of IL-22 in DALDA-mediated cytoprotective effect in the intestine.

Our work highlights a potential new therapeutic class of compounds for the treatment of diseases involving intestinal barrier damage, including ischemic injury, radiation-induced damage, and IBD. One could envision the use of opioids as an adjunct therapy in IBD by helping to induce or maintain remission through promoting re-epithelialization of the intestine. In particular, opioids could be used as an adjunct in helping to induce remission in IBD by lowering the amount of prednisone needed, or as a mainline therapy in steroid-refractory patients. Use of opioids for IBD therapy needs to be pursued cautiously, however, as our work shows that opioids likely act through increased colonocyte proliferation and IBD patients already have an increased risk of malignant transformation. Consequently, MOR-targeted therapy would likely be best suited towards short-term use for remission induction, similar to prednisone. Other, non-IBD, applications could include enhancing recovery from radiotherapy-induced injury and use as a gut-saving agent in cases of ischemic injury.

In summary, this report establishes mu-specific opioids as promoters of colonocyte migration/restitution and proliferation in the intestine involving the activation of STAT3-dependent pathways. Since opioids are already available on the market and have well-known safety profiles, this class of compounds could represent a novel therapeutic approach to gastrointestinal therapy, once clinical trials validate their beneficial impact in patients.

Acknowledgements

The authors would like to thank Dr. Joseph Galenko in the CGIBD at UNC-CH for his assistance with statistical analysis. The authors would also like to thank the Dr. Scott Plevy of UNC-CH for his generous donation of the lentiviral constructs generated by the UNC Lenti-shRNA core and Dr. Taku Kobayashi of UNC-CH for his help generating the knockdown lines. We would also like to thank Mr. Greg Gipson for technical assistance with mouse experiments, as well as Dr. Janelle C. Arthur and Dr. Javier Rivera-Guzman of UNC-CH for critical reading of the manuscript. We would also like to thank Dr. Robert Bagnell (Director, Microscopy Services Laboratory) and Mr. Robert Currin (Manager, Cell & Molecular Imaging Facility and UNC-Olympus Center), both of UNC-CH, for their assistance with the fluorescent microscopy experiments. Finally we would like to thank Dr. Arlin Rogers (UNC-CH, Department of Pathology) for his blinded confirmation of our histological assessment of intestinal injury.

CHAPTER 5

INTESTINAL EPITHELIAL CELL (IEC)-DERIVED MU-OPIOID SIGNALING PROTECTS AGAINST ISCHEMIA REPERFUSION (I/R) INDUCED INJURY THROUGH PI3K SIGNALING[4]

Introduction

Intestinal ischemia has a wide variety of etiologies, including but not limited to atherosclerosis, blood clots, hypotension, and chronic inflammation. Here we evaluated the role of intestinal epithelial cell (IEC)-derived mu-opioid receptor (MOR) signaling in host response to ischemia/reperfusion injury. Ileal ischemia was accomplished through obstruction of the distal branches of the superior mesenteric artery (60min) and reperfusion for 90min (ischemia-reperfusion, I/R). Surgery was performed under isofluorane/ketamine combined anesthesia. Floxed-MOR mice were crossed to villin-cre transgenic mice to selectively delete the MOR gene in IECs ($MOR^{IEC-/-}$). Radio-ligand binding assays demonstrated selective functional loss of MOR signaling in IECs of $MOR^{IEC-/-}$ mice, while brain cortex control tissue retained signaling capacity. Administration of the MOR agonist DALDA significantly protected against both ischemia and reperfusion phases of intestinal I/R injury, an effect completely ablated in $MOR^{IEC-/-}$ mice. This cyto-protective effect was associated with activation of enterocyte-mediated

[4] Under review at *The American Journal of Pathology*

PI3K/GSK3β signaling and decreased cellular apoptosis. Pharmacological blockade of PI3K activation resulted in loss of MOR-mediated cyto-protective function. *In vitro* experiments showed that DALDA-mediated IEC migration was dependent upon PI3K signaling. Together, these data shows that IEC-derived mu-opioid signaling utilizes PI3K pathway to protect cells against the damaging effect of I/R. Targeting MOR signaling may represent a novel mean to alleviate intestinal injury and promote the wound healing response.

Background

The gastrointestinal epithelium performs a wide array of functions for the host including secretion/absorption of nutrients, innate immune surveillance, and physical barrier against the rich, diverse and potentially immunogenic luminal contents. Therefore, preserving the integrity and maintaining intestinal barrier function is critical for host homeostasis. At the forefront of the intestinal barrier lies a single monolayer of intestinal epithelial cells (IECs) [1], which form a tight network of cells through the formation of tight junctions between IECs. These tight junctions are a critical component of the epithelium, and are necessary for the maintenance of the barrier during epithelial injury [27, 29]. The epithelium is a very dynamic system with highly migratory and proliferative IECs that help maintain and replace the barrier [27]. These active cells require constant high levels of blood flow to maintain their function, which is supplied by the superior mesenteric artery for the small intestine and proximal two thirds of large bowel, and the inferior mesenteric artery for the last third of the colon [8, 9, 21]. These arteries are supplemented by significant collateral blood flow to ensure proper intestinal function [8, 9, 21].

Various events such as chronic inflammation [263], infection [1], medications [207, 264], and ischemia can all result in the loss of the intestinal barrier [3, 8], with deleterious consequences for the host. Among these various conditions, intestinal ischemia has been associated with severe disruption of small intestinal function and integrity. Intestinal ischemia results in tissue hypoxia, which can cause induction of cellular apoptosis and loss of the

protective epithelial layer. Beside ischemia, the intestine can experience various level of hypoxia due to atherosclerotic blockade, hemorrhage, veinous emboli, surgical clamping, and cardiac tamponade [3]. In all of these cases, enteric blood supply must be reduced by at least 50% to overcome compensatory mechanisms [8]. Ischemia represents one of the driving factors in the pathogenesis of the newborn disease necrotizing enterocolitis (NEC) [21]. Paradoxically, the restoration of blood flood (reperfusion) enhances the damage to the intestine through the introduction of oxygen free-radicals and increased immune cell activation [3]. In severe cases, ischemia/reperfusion (I/R) injury can result in multiple organ dysfunction syndrome (MODS), with a mortality rate of approximately 30% [6].

I/R induced injury occurs in a multistep fashion. In the first phase, the impaired blood flow to the epithelium generates an adaptive response involving the activation of protective signaling events that induce activity of different transcription factors such as hypoxia-inducible factor (HIF) [22] and nuclear factor kappa-light-chain-enhancer of activated B cells (NF-κB) [23]. In the second phase, the adaptive response is generally overwhelmed by the rapid re-introduction of blood flow/oxygen (reperfusion), which enhances and sustains the inflammatory response [3]. Finally, the sustained intestinal immune response compromises the intestinal barrier function of the epithelium—allowing bacterial translocation across the mucosa, leading to bacteremia and sepsis, and creating a positive feedback loop of inflammation and intestinal damage [3]. In I/R injury, the consequences of this positive feedback loop are typified by NEC [21], where

this sustained response results in progressive loss of a newborn's intestinal track, resulting the death of 2-4% of all very low birth weight infants [24].

Unfortunately, current treatment of I/R injury is completely supportive, and no treatments focus on restoring the epithelial barrier defects that can lead to MODS. Recently, we have found that mu-opioid receptor (MOR) signaling is protective against chemical-induced acute intestinal injury [205]. Rodent studies have demonstrated that opioid signaling is cardio-protective during ischemic episodes [86, 89], and these observations have been successfully extended to a randomized, double-blind clinical trial [265]. MOR is a G protein-coupled receptor, and the cardio-protective effects of MOR signaling are believed to act through the $G_{\beta\gamma}$-subunit of the G_i protein coupled to MOR. Specifically, the $G_{\beta\gamma}$ subunit activates phosphoinositide 3-kinase (PI3K) [54], which can result in numerous pro-survival downstream signaling events, predominately mediated through Akt activation [266]. Additionally, studies have shown that opioid-mediated cardio-protection involves integrated signaling between the PI3K/Akt/GSK3β pathway and the JAK2/STAT3 pathway [89]. However, the role and cellular source of MOR signaling during I/R mediated intestinal injury remain to be defined.

In these studies, we establish that MOR signaling is protective against both the ischemic and reperfusion phase of intestinal I/R injury. Genetically deficient MOR-derived IEC signaling demonstrated that IEC cells are the source of the cyto-protective responses. The MOR-mediated protective effect was in part

attributed to PI3K signaling as pharmacological inhibition of the pathway abrogated DALDA-induced beneficial impact.

Materials and methods

Generation of $MOR^{IEC-/-}$ mice

All mice were on the C57BL/6 background. Villin-Cre mice were crossed to $MOR^{f/f}$ mice which contain loxP sites in introns 1 and 3, to generate mice lacking exons 2 and 3 of the mu opioid receptor (Figure 27A). $MOR^{f/f}$ mice were generated by Xenogen Biosciences (Hopkinton, MA) using homologous recombination. Tail snips were collected from all pups generated from crosses, and genomic DNA was isolated using a Qiagen Blood and Tissue Kit (Qiagen; Valencia, CA). Mice were bred to generate homozygote $MOR^{f/f}$ allele and *Villin*-Cre gene. Primers used for genotyping: *Villin*-Cre promoter (5'-TAAGAAAGGATCATCATCAAAGCCGG-3', and 5'-GTGAAACAGCATTGCTGTCACTT-3') Flox-*Oprm1* (5'-GTGTTTAAACATAGGTACAAGATATTCCCAAGCGAGA-3' and 5'-GTCTCGAGCTGAGATTTAGGAAAGGTGTCGAATTATTG-3').

For phenotypic analysis, RNA was isolated from enterocytes and splenocytes as previously described [237], and expression of MOR, *Oprm1 and Gapdh* was determined by RT-PCR. Amplicons were resolved on a 2% agarose gel and visualized using a Kodak Gel Logic Imager 200 series (Kodak; Rochester, NY). Primers used: *Oprm1* (amplicon 569 bp, 5'-ACCTGGCTCCTGGCTCAACT-3' and 5'- TGGACCCCTGCCTGTATTTTG-3'), *Villin1* (amplicon 330 bp, 5'-CCCCCATCTTCCA-3' and 5'-

TGCCCTGCCAGATATATAACA-3'), CD45 (*Ptprc*) (amplicon 70 bp,5'-ATGGTCCTCTGAATAAAGCCCA-3' and 5'-TCAGCACTATTGGTAGGCTCC-3'), *Gapdh* (amplicon 240 bp, 5'-GGTGAAGGTCGGAGTCAACGGA-3' and 5'-GAGGGATCTCGCTCCTGGAAGA-3') [243].

Ischemia/reperfusion induced injury

$MOR^{f/f}$ and $MOR^{IEC-/-}$ mice (C57BL/6 background) were maintained in standard housing cages in specific pathogen free (SPF) conditions. Mice (n=4-6) were anesthetized under 1% isofluorane, supplemented by 10 mg/kg ketamine injected subcutaneously (s.c.). Vehicle (saline) or the MOR agonist DALDA [69] (100% saline, 50 µg/kg) (US Biological; Swampscott, MA), was injected s.c. ten minutes prior to surgery. The PI3K inhibitor Ly294002 (0.25 mg/kg) (Calbiochem; Darmstadt, Germany), was injected i.p. 10 minutes before administration of DALDA. A mid-line laparotomy was made and peripheral branches of superior mesenteric artery were occluded with aneurysm clips (Kent Scientific; Torrington, CN), to create a 2-3 cm region of ischemic ileum adjacent to the cecum. Collateral blood flow through the intestine was blocked using aneurysm clips across the intestine and collateral vessels, demarking the region of ischemic intestine. Haematoxylin was administered to the edges of ischemic tissue to mark them, and then the incision was closed with surgical staples. Ischemia was maintained for 60 minutes, and then the incision was re-opened and the clamps were removed and the incision was re-closed. The mice were maintained in a heated room for a variable amount of time (0, 1.5, or 4 hours) without anesthesia for the reperfusion phase of injury. All animal experiments were approved by the

Institutional Animal Care and Use Committee of the University of North Carolina at Chapel Hill.

Murine sample collection and histological evaluation

Mice were anesthetized using isoflurane, and then sacrificed by cervical dislocation. The colon was dissected and flushed with ice-cold PBS, longitudinally splayed, swiss rolled, fixed in 10% formalin for 24 hrs, and then embedded in paraffin. Damage severity was evaluated using Haematoxylin and Eosin (H&E)-stained sections by a blinded investigator. The scoring system is based on an IEC apoptosis/necrosis system [267], where a score of 1 signified a loss of only the villus tips; a score of 2 corresponded to loss of 50% of the villus; a score of 3 indicated a loss of the entire villus, but with maintenance of the crypt; and a score of 4 signified complete loss of the epithelial layer. Fractional (to the nearest 0.5) scores were given, and the score was based on the average damage of the entire tissue section.

Cell membrane fraction isolations

Primary intestinal epithelial cells were isolated as described previously [268]. Briefly, small intestines and colons were opened longitudinally, washed, and intestinal epithelial cells were separated from the underlining tissue by shaking the intestines in a solution containing 1.5mM EDTA (with 0.5mM DTT for colon sections) and proteinase inhibitors (Complete Mini, Roche Diagnostics GmbH; Penzberg, Germany) for 30min at 37°C. The remaining tissue was filtered with a 0.45 μm cell culture filter to remove the underlying stroma and samples from three mice were pooled and spun at 1300 rpm for 5 minutes. Cells were

lysed in chilled, hypotonic 50 mM Tric-HCl, pH 7.4 solution for 30 minutes. Cell membrane isolates were then prepared by washing the lysate 3 times in standard binding buffer (50 mM Tris-HCl, 10 mM MgCl2, 0.1 mM EDTA, pH 7.4) followed by centrifugation at 20,000 rpm. The lysate was then resuspended in the binding buffer and passaged through a 26 gauge needle to ensure homogenization; forming the final membrane suspensions used in the radioligand binding assays. Brain membrane homogenates were made using cortex tissue. Brains were harvested from mice and their cortexes were dissected. The tissues were homogenized in standard binding buffer with proteinase inhibitors using a polytron (IKA Works Inc; Wilmington, NC), and then prepared in the same manner as the IECs in standard binding buffer. Protein concentration of each membrane suspension was determined by Bio-Rad quantification assay (Bio-Rad Laboratories; Hercules, CA).

Radioligand binding assay

Radioligand binding assays were performed by the Psychoactive Drug Screening Program at UNC-CH, using a modification of previously described procedures [269]. 50 µL of membrane suspensions were incubated with 0.3, 0.6, 1.25 2.5, 5, or 10 nM H^3-DAMGO (GE Healthcare; Piscataway, NJ) with or without 10 µM naltrexone (Sigma-Aldrich; St. Louis, MO) for 1 hour at room temperature, shielded from light. Samples were then harvested by rapid filtration onto Whatman GF/B glass fiber filters pre-soaked with 0.3% polyethyleneimine using a 96-well Brandel harverster. Four rapid 500-µl washes were performed with chilled standard binding buffer to reduce non-specific binding. The filter

mats were dried and scintillant was melted onto the filters and the radioactivity was counted using a Microbeta scintillation counter. Radioactivity of H^3-DAMGO was quantified by liquid scintillation counting, using EcoScint scintillation cocktail (National Diagnostics; Atlanta, GA). Raw data (decays per minute) was converted to fmols of ligand binding per mg of total tissue, using a detection efficiency of 0.5 to convert from decays per minute to counts per minute.

Immunohistochemistry and immunofluorescence

IHC staining was performed according to the manufacturer's specifications, as previously described [237]. Primary antibodies and dilutions were: pGSK3β(Ser9), 1:400 (Cell Signaling), and pAKT(Ser473), 1:50 (Cell Signaling Technology Inc.; Beverly, MA). IHC for activated caspase 3, 1:400 (R&D Systems; Minneapolis, MN) was performed as described [213]. All sections were counterstained with Hematoxylin. During analysis of IHC, only crypts that had two or more positively staining cells per 10 total crypts in a field of view were counted for IHC analysis.

Fluorometric TUNEL (terminal deoxynucleotidyl transferase dUTP nick labeling) assay was performed using a DeadEnd Kit (Promega; Madison, WI) according to manufacturer protocols. Images were acquired using a Zeiss 710 microscope with a 20X, 1.4 NA objective (Carl Zeiss; Thornwood, NY). Zeiss Zen 2009 software was used for image acquisition. All images were acquired at room temperature.

RNA isolation and real-time PCR

RNA isolation from ileal tissues and subsequent subsequent cDNA amplification was performed as previously described [237], using a ABI Prism HT7700. Specificity and linearity of amplification for each primer set was determined by melting curve analysis and calculation of the slope from serial diluted samples. Relative fold-changes were determined using the ΔΔCT calculation method. Values were normalized to the internal control GAPDH or β-actin. Primers: *Il6* (5'-CGGAGGCTTAATTACACATGTT-3' and 5'-CTGGCTTTGTCTTTCTTGTTATC-3') [243], *Il1b* (5'-GCCCATCCTCTGTGACTCAT-3' and 5'- AGGCCACAGGTATTTTGTCG-3') [205],*Gapdh* (5'-GGTGAAGGTCGGAGTCAACGGA-3' and 5'-GAGGGATCTCGCTCCTGGAAGA-3') [243], *b-actin* (5'-TTACCAACTGGGACGACATG-3' and 5'CTGGGGTGTTGAAGGTCTC-3')

Bacterial ribosomal 16S DNA and cultures

For all bacterial translocation assays, mice were subjected to 60 minutes of ischemia followed by 4 hours of reperfusion in the presence or absence of DALDA as described above. Mice were sacrifice and their livers harvested and weighed. To determine bacterial 16S rDNA loads, livers were incubated in lysis buffer (200 mM NaCl, 100 mM Tris-HCl pH 8, 20 mM EDTA, 20 mg/ml lysozyme) for 30 minutes at 37°C, and then in 1% SDS and 0.35 mg/mL Proteinase K for 30 minutes at 60°C. The homogenates were further lysed in a 60% volume of phenol:choloforom:isoamyl alcohol mixture (25:24:1) using a Mini Bead Beater 8 (Biospec; Bartleville, OK). DNA was isolated using a choloform:isoamyl alcohol

(24:1) solution and precipitated with 2.5X volumes of ethanol with 3 M sodium acetate pH 5.2 overnight at -20°C. The pellet was resuspended in Tris buffer (10 mM, pH 8) and a Qiagen DNAease Blood and Tissue kit (Qiagen) was used according to manufacturer protocol. Isolated DNA was subjected to real-time PCR as described above, using the following primers: universal *16s rDNA* (5'-GTGSTGCAYGGYTGTCGTCA-3' and 5'-ACGTCRTCCMCACCTTCCTC-3'), normalized to murine *Gapdh* (as above).

For bacterial cultures, harvested and weighed tissues were immediately homogenized with a polytron in sterile PBS. 10 µL of lysate was plated on sheep BHI plates (Remel; Lenexa, KA) in triplicate, and incubated overnight at 37°C. For anaerobic studies, plates were preconditioned overnight in an anaerobic chamber, and incubation of the plates was also done in an anaerobic chamber.

CMT-93 cell culture and stimulation

Murine rectal carcinoma cells (passage 33-59) (American Type Culture Collection (ATCC); Manassas, VA) were cultured in DMEM-high-glucose as described previously[241]. Cells were starved o/n in Opti-MEM and then treated with DALDA (10 µM) for the times indicated. Cells were directly lysed in 1X laemmli buffer and protein concentration was measured using Bio-Rad quantification assay.

Western blot analysis

Proteins (30 µg) were separated using 10% SDS-PAGE, transferred to nitrocellulose membranes and then probed with antibodies specific to pGSK3β(Ser9), GSK3β, pAKT(Ser473), Akt (all diluted at 1:1000 dilution, Cell

Signaling Technologies), and β-actin (1:10,000) (MP Biomedical; Solon, OH) in 5% BSA in TBS-Tween (0.1%), followed by the appropriate HRP-conjugated secondary antibody (GE Healthcare, Piscataway, NJ). The immune complexes were detected using chemiluminescence.

Migration and proliferation assays

Migration assays were performed as described previously[245]. Briefly, CMT-93 cells were plated to confluency in Opti-MEM and then were scratched with a P1000 pipette tip. 10 μM DALDA or PBS-vehicle alone was then immediately added to the plates. Wortmannin (1 μM; Sigma-Aldrich) or DMSO vehicle was added 5 minutes before addition of DALDA. 4 different regions per plate were demarked and images were taken at 0 and 8 hours post-wounding using an Olympus IX7 microscope. Images were analyzed with NIH ImageJ software. Each experiment was measured at 4 individual points, and was repeated independently at least 2 times.

Statistical analyses

Unless specifically noted, statistical analyses were performed using GraphPad Prism version 5.0a (GraphPad, La Jolla, CA). Comparisons of mouse studies were made with non-parametric, one-way analysis of variance (ANOVA), Kruskal-Wallis test with Dunn's Multiple Comparison post-test. Further comparisons made between mice were analyzed using a Mann-Whitney U test at a 95% confidence interval. *In vitro* migration data and cell counting were compared with student t-tests, at a 95% confidence interval. Radioligand binding assays were analyzed using a non-linear fit (single-binding site) function, built

into Prism. All graphs depict mean ± S.E.M. Experiments were considered statistically significant if $P<.05$. $P<.05$ denoted by *, $P<.01$ denoted by **, $P<.001$ denoted by ***.

Results

Generation of IEC-specific MOR gene deleted mice

To define the role of intestinal epithelial cell-derived MOR signaling in the intestine, we crossed floxed-MOR mice ($MOR^{f/f}$) to Villin-Cre mice to generate specific IEC gene deleted mice ($MOR^{IEC-/-}$, Figure 27A). PCR analysis showed MOR (*Oprm1*) mRNA accumulation in purified IECs and splenocytes from $MOR^{f/f}$ mice, whereas the transcript was absent in the IECs of $MOR^{IEC-/-}$ mice (Figure 27B). MOR mRNA accumulation was detected in splenocytes isolated from $MOR^{IEC-/-}$ mice, showing the specificity of MOR gene deletion (Figure 27C). Radioligand binding assays revealed a lacked of detectable binding of the MOR-specific ligand ^{3}H-DAMGO in IEC cells isolated from $MOR^{IEC-/-}$ mice compared to $MOR^{f/f}$ mice (Table 3). ^{3}H-DAMGO binding to brain (cortex) cell membrane extracts was not significantly altered in $MOR^{IEC-/-}$ mice. These findings confirmed that MOR signaling is functionally ablated in IEC in $MOR^{IEC-/-}$ mice.

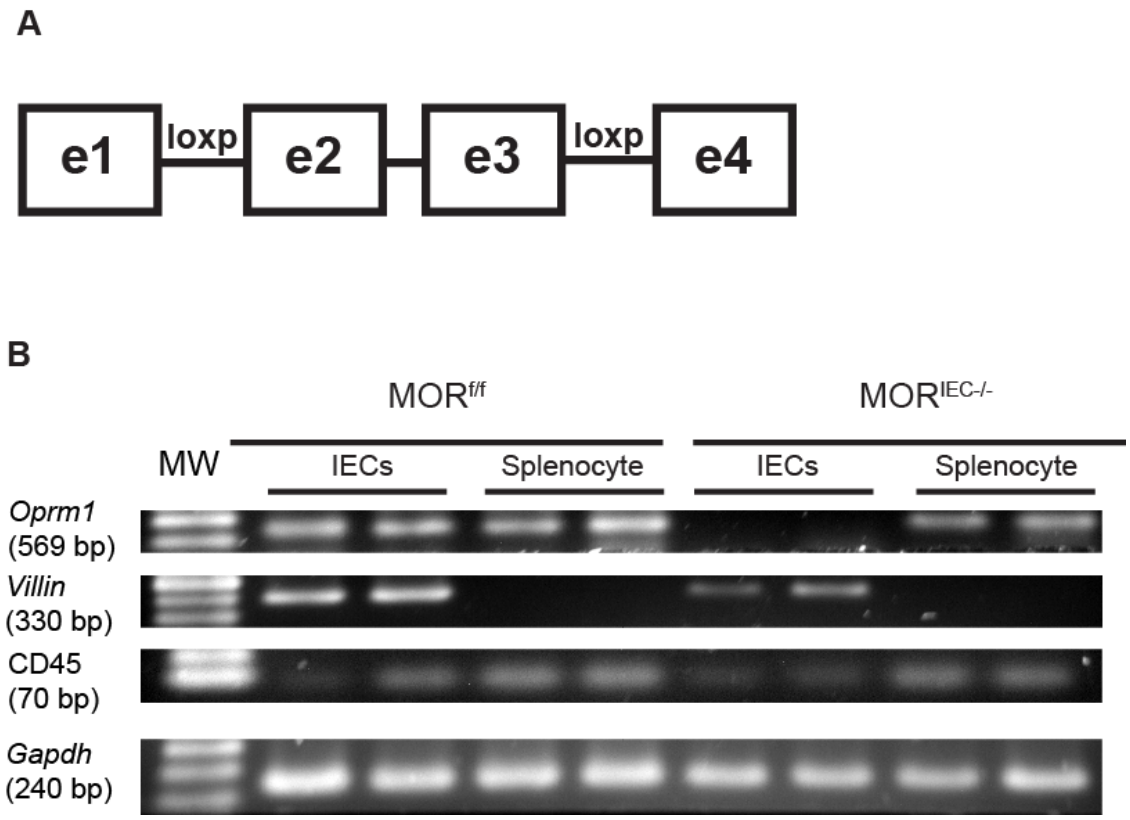

Figure 27. Generation of IEC-specific MOR gene deleted mice. A) Schematic representation of the exon-flanked *loxP* sites of $MOR^{f/f}$ mice. B) RT-PCR analysis of MOR (*oprm1*) mRNA accumulation from IECs and splenocytes obtained from $MOR^{f/f}$ and $MOR^{IEC-/-}$ mice. *Villin* and CD45 are used as marker of enterocytes and immune cells respectively. *Gapdh* is used as a loading control. Biological duplicates are shown.

Mouse Strain	Cortex DAMGO B_{max}	Enterocyte DAMGO B_{max}
$MOR^{f/f}$	165.6 +/- 16.10 fmol/mg	11.55 +/- 4.397 fmol/mg
$MOR^{IEC-/-}$	108.5 +/ 13.10 fmol/mg	No binding detected

Table 3: $MOR^{IEC-/-}$ enterocytes do not bind mu ligand. Radioligand binding assays using the MOR-specific agonist ^{3}H-DAMGO demonstrated an absence of intestinal binding in $MOR^{IEC-/-}$ mice. No statistically significant difference between $MOR^{f/f}$ and $MOR^{IEC-/-}$ binding was observed (P = 0.0705) in the cortex (brain) samples used as a positive control. N = 4 or 6 per group.

IEC mu-opioid signaling protects against ischemia/reperfusion injury

To address the cell-type specific role of MOR signaling in intestinal injury response, we subjected mice to episode of ischemia-reperfusion (I/R) where peripheral branches of the SMA were clamped for 60 minutes (ischemic phase), followed by 90 minutes of reperfusion. As seen in Figure 28, I/R induced epithelium denudement, with partial to complete ablation of the crypts, alongside immune cell infiltration into the lamina propria. Interestingly, administration of DALDA (50 μg/kg) dramatically reduced I/R mediated tissue damage compared to untreated mice, as shown by histological damage assessment (2.5 vs 0.6, $P<0.05$; (Figure 28A-B). However, DALDA was unable to protect $MOR^{IEC-/-}$ mice from I/R induced injury compared to $MOR^{f/f}$ mice (1.75 vs 2.58 $P=0.2920$) (Figure 28A-B).

Due to hypoxic conditions, I/R leads to increased IEC apoptosis with associated disruption of intestinal barrier function [3, 8, 9]. A fluorescent TUNEL assay showed enhancement of fragmented DNA indicative of apoptosis/necrosis in mice subjected to I/R injury, which was absent in mice treated with DALDA (Figure 28C). DALDA-mediated reduction of DNA fragmentation was ablated in $MOR^{IEC-/-}$ mice (Figure 28C). To specifically address the role of apoptosis in DALDA-mediated protection, we investigated the level of caspase-3 activation using IHC. Interestingly, caspase 3 activation was strongly reduced following DALDA treatment, an effect abrogated in $MOR^{IEC-/-}$ mice (Figure 28C). These findings indicate that IEC-derived MOR signaling is critical for the DALDA-mediated protective effect on the epithelium.

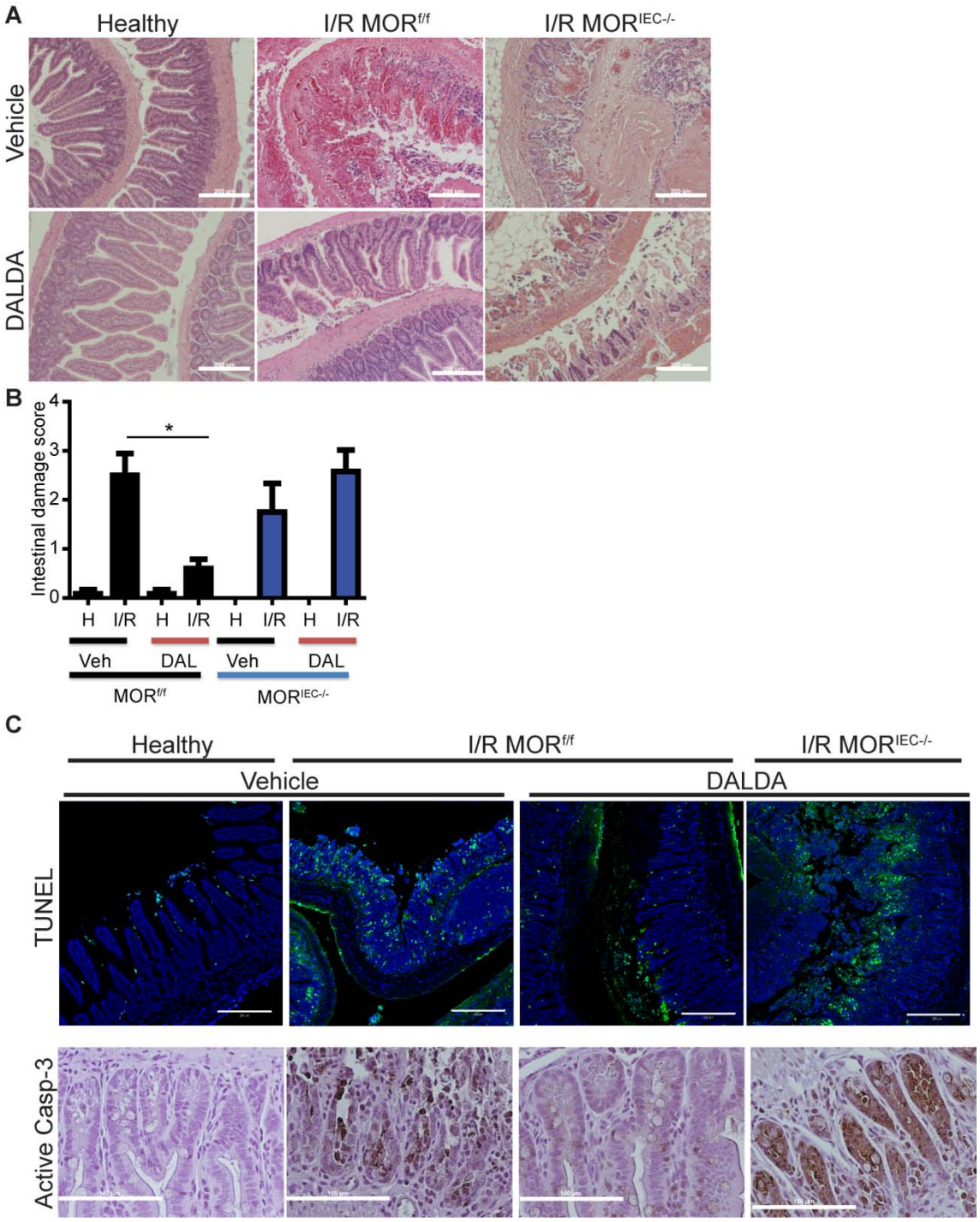

Figure 28. DALDA administration protects against ischemia-reperfusion induced injury. 50 µg/kg of DALDA was administered s.c to MOR$^{f/f}$ and MOR$^{IEC-/-}$ mice 10 minutes before ischemia/reperfusion (I/R) exposure. Healthy tissues (H) represent a non-ischemic region of the small bowel adjacent to the damaged area. A) Representative H&E images of ileal swiss rolls. Scale bars are 200 µm. N =5-6 per group. B) Histological damage scores show DALDA mediated protection from I/R injury only in mice with functional IEC-derived MOR signaling

($MOR^{f/f}$). N =5-6 per group. C) TUNEL assay demonstrates decreased apoptotic/necrotic IECs in DALDA-treated mice with functional IEC-derived MOR signaling. Cells with fragmented DNA are stained green while DAPI counterstained marked all intestinal cells. Scale bars are 200 μm. Representative of 3 sections per group, from two different mice. IHC analysis of activated caspase 3 from ileal section of DALDA-treated $MOR^{f/f}$ and $MOR^{IEC-/-}$ mice showed decrease caspase 3 staining in mice with functional IEC-derived MOR signaling. Images are representative of two different mice. Scale bars are 100 μm.

Interestingly, I/R induced *Il1b* and *Il6* mRNA accumulation was not modulated by DALDA administration, nor was it affected by the status of MOR expression (Figure 29). A similar, but less robust pattern of induction, was noticed with *Tnf* mRNA (data not shown).

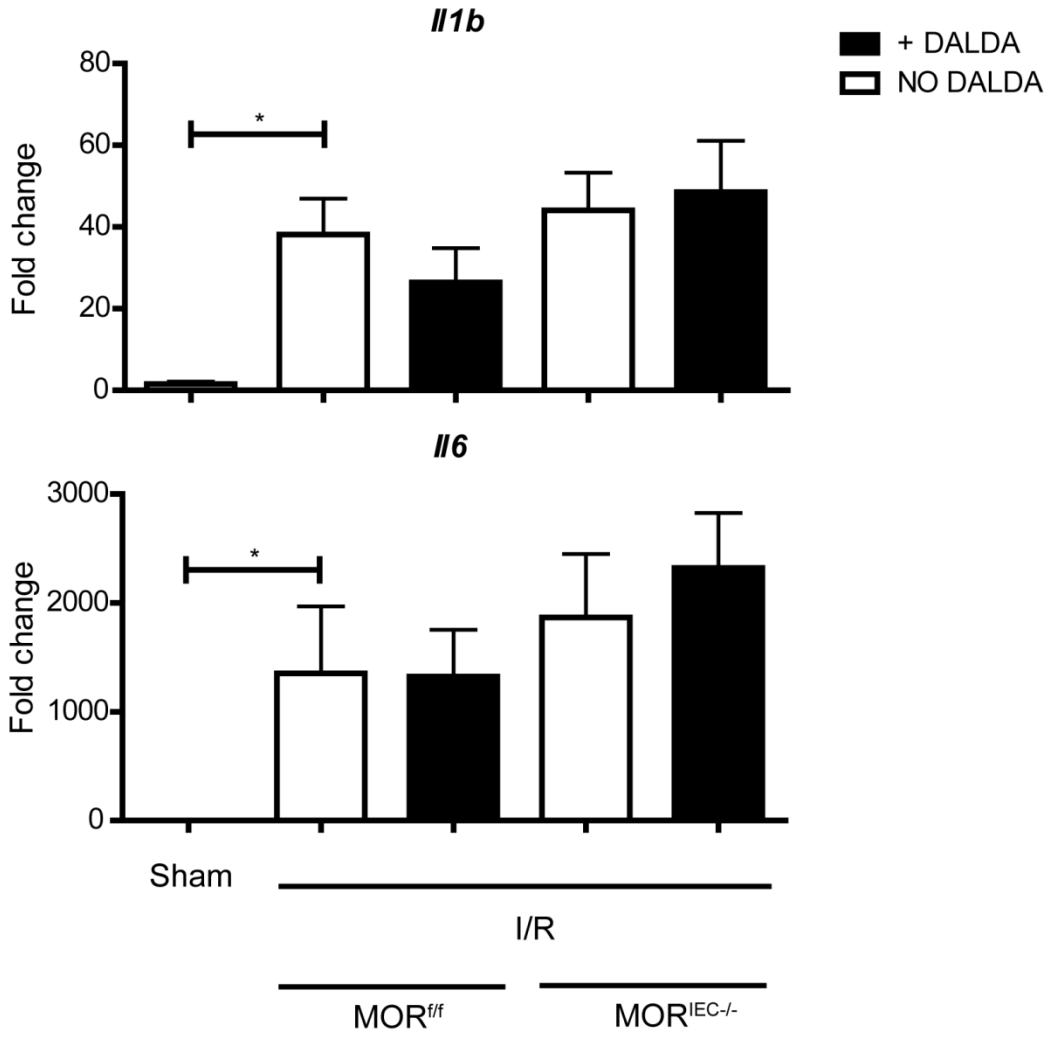

Figure 29. MOR-mediated cyto-protective effect does not correlate with decreased cytokine production. Mice were treated with DALDA and exposed to I/R as described in Figure 28. *Il1b, Il6, and Tnf* mRNA ileal tissue levels were determined using ABIPrism7900HT. Data was processed using the ΔΔCt method, normalized to *b-actin* and set relative to sham operated mouse tissue. No statistical significance was noted between any of the ischemic tissue groups. Comparing between sham and all ischemic groups, P <0.0317 for *Il1b*, P<0.0159 for *Il6*. N ≥3 per group.

Because I/R induced injury is a multi-phase process, we next investigated the role of MOR signaling during the early ischemic phase of intestinal injury. Administration of DALDA protected against the induction of intestinal damage during the ischemic phase (2.7 vs 1.5, $P<0.01$), an effect dependent on the presence of functional IEC-MOR signaling Figure 30A&B). These data suggest that IEC-derived MOR signaling protect against the deleterious effect of ischemia. TUNEL (data not shown) and IHC analysis of activated caspase-3 demonstrates that IEC-MOR signaling confers protection during the ischemic phase of injury through up-regulation of pro-survival/anti-apoptotic signals (Figure 30D).

One potentially serious outcome of intestinal ischemia is multi-organ dysfunction syndrome [6], which results from bacterial translocation and dissemination after loss of the intestinal barrier function [23]. To assess for the presence of extra-intestinal bacteria during I/R injury, we measured the bacterial 16S rDNA in the liver. Increased bacterial 16S rDNA (~4 fold) in the liver of I/R-exposed $MOR^{f/f}$ mice was significantly decreased in DALDA treated mice, while this beneficial effect was lost in $MOR^{IEC-/-}$ mice (Figure 30C). These findings indicate that DALDA prevented initial ischemia induced epithelial damage and prevent bacterial translocation to extra-intestinal organs.

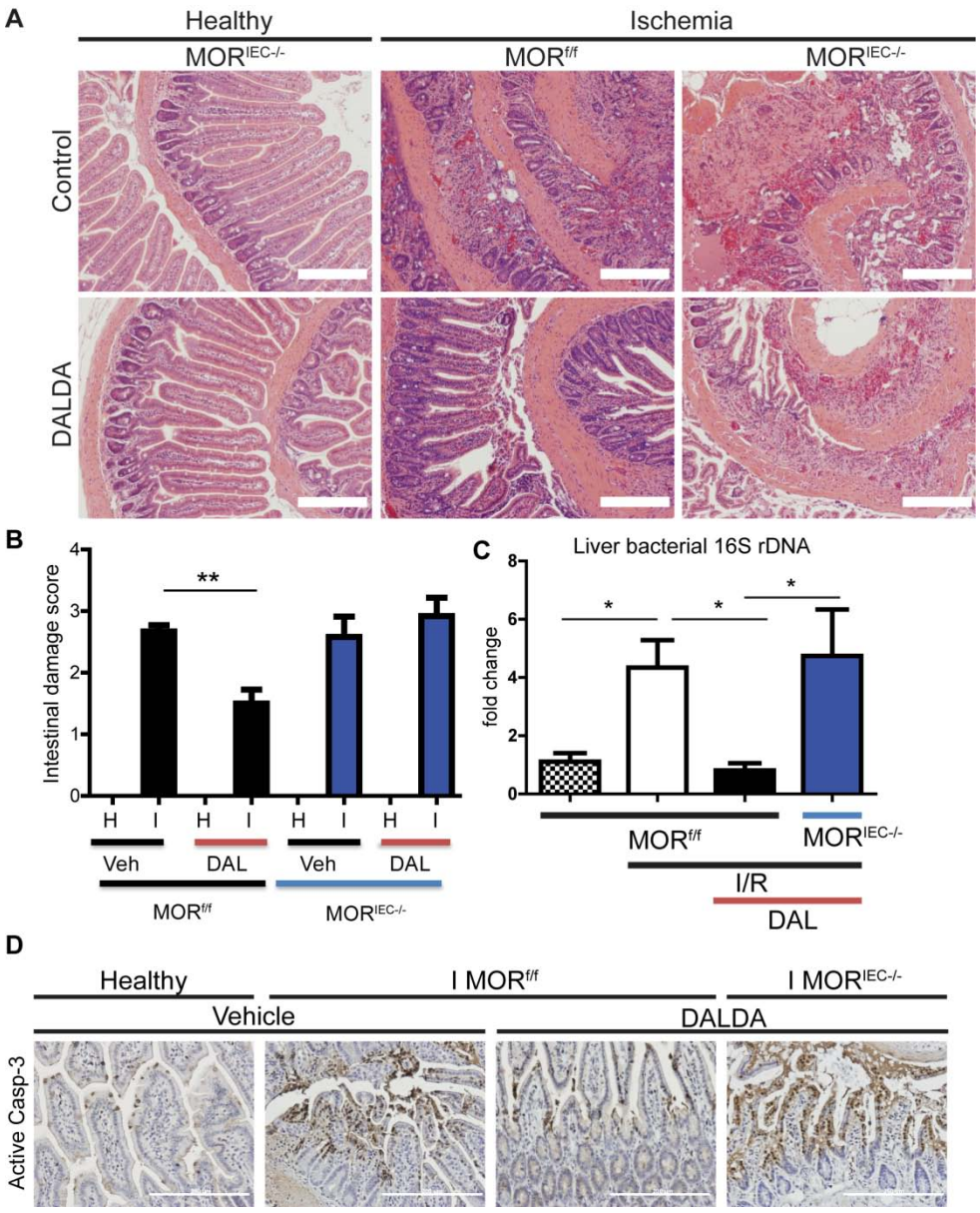

Figure 30. DALDA administration protects against ischemia induced injury and attenuates bacterial translocation. 50 µg/kg of DALDA was administered s.c to MOR$^{f/f}$ and MOR$^{IEC-/-}$ mice 10 minutes before ischemia (I) exposure (60min). Healthy tissues (H) represent a non-ischemic region of the small bowel adjacent to the damaged area. A) Representative H&E images of ileal swiss rolls. Scale bars are 200 µm. B) Histological damage scores show DALDA mediated protection from ischemia injury only in mice with functional IEC-derived MOR signaling (MOR$^{f/f}$). N =5-6 per group. C) PCR quantification of total bacterial 16S DNA at 4 hours of reperfusion shows that MOR-mediated protection results in decreased bacterial dissemination to the liver. Data was analyzed by the ΔΔCt method, normalized to murine *Gapdh*, and compared to control. N = 4 per group. D) IHC analysis of activated caspase 3 from ileal section of DALDA-treated MOR$^{f/f}$ and MOR$^{IEC-/-}$ mice shows that enterocyte MOR

signaling confirms protection from apoptosis during the ischemic phase of injury. Images are representative of three different mice. Scale bars are 200 μm.

MOR-mediated protection involves PI3K-mediated GSK3β phosphorylation

We previously showed *in vitro* that IEC wound healing responses are dependent on PI3K/GSK3β signaling [270]. To test the role of the PI3K/GSK3β pathway in MOR-mediated protective effect, we stimulated murine rectal-carcinoma CMT-93 cells with DALDA (10 μM) for variable period of time. Interestingly, DALDA increased GSK3β phosphorylation with a peak activation of 60 minutes (Figure 31A). DALDA-mediated GSK3β phosphorylation was dependent on PI3K/AKT signaling since the pan-PI3K inhibitor wortmannin blocked both AKT and GSK3β phosphorylation (Figure 31B). To functionally link PI3K/GSK3β activation to cellular restitution, we then performed migration scratch assays. DALDA mediated cellular migration was blocked by PI3K inhibition (Figure 31C).

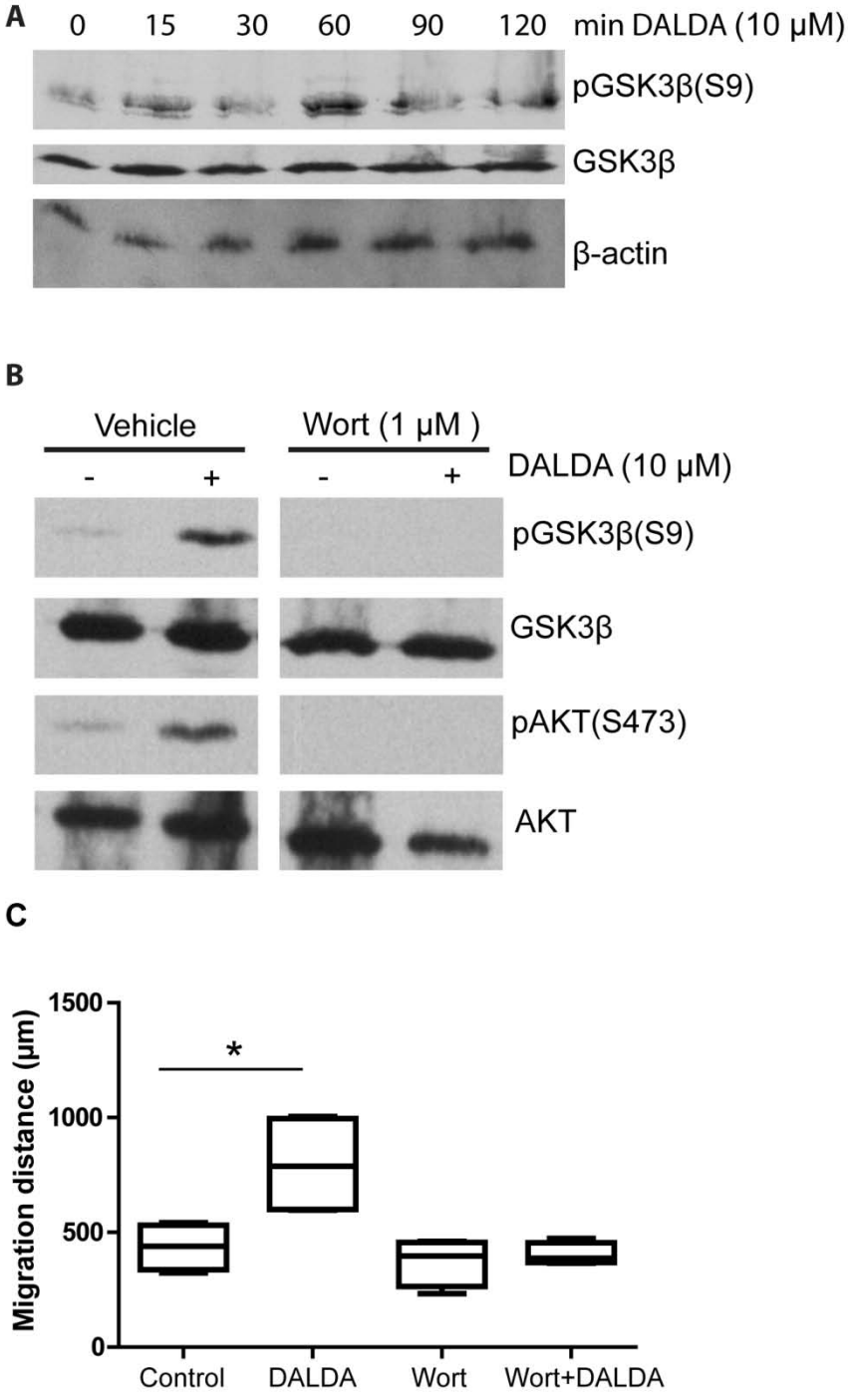

Figure 31. MOR signaling induces GSKβ phosphorylation and cell migration in a PI3K-dependent manner in CMT-93 cells. CMT-93 cells were stimulated DALDA (10 μM) for the indicated time in presence or absence of the PI3K inhibitor wortmannin (1 μM). Proteins were extracted and subjected to Western blot analysis. A) Kinetic analysis of GSK3β phosphorylation. Representative of 2 independent experiments. B) DALDA-mediated Akt/GSK3β phosphorylation is blocked in wortmannin treated cells. Representative of 3

independent experiments. C) DALDA-induced cell migration require PI3K signaling. CMT-93 cells were grown in a monolayer, treated with DALDA (10 μM) in presence or absence of Wortmannin (Wort; 1 μM). Cells were then scratched with a pipet tip and cellular migration from the wound-edge was measured 8 hours later. Four separate wounds were measure per group; data representative of 2 independent experiments.

To expand these observations *in vivo*, we performed IHC analysis on DALDA-treated mice. Interestingly, IEC-specific Akt and GSK3β phosphorylation is enhanced in DALDA-treated $MOR^{f/f}$ mice compared to the vehicle-treated mice (Figure 32A-B). We further quantified the pGSK3β staining, and found increased staining in the crypts of DALDA-treated $MOR^{f/f}$ mice compared to the vehicle-treated mice (7.2 vs 3.9, $P<.01$, Figure 32C). Finally, we observed that activation of these signaling pathways was abrogated in DALDA-treated $MOR^{IEC-/-}$ mice (Figure 32A-C), demonstrating that these effects were a result of direct enterocyte-mediated MOR signaling.

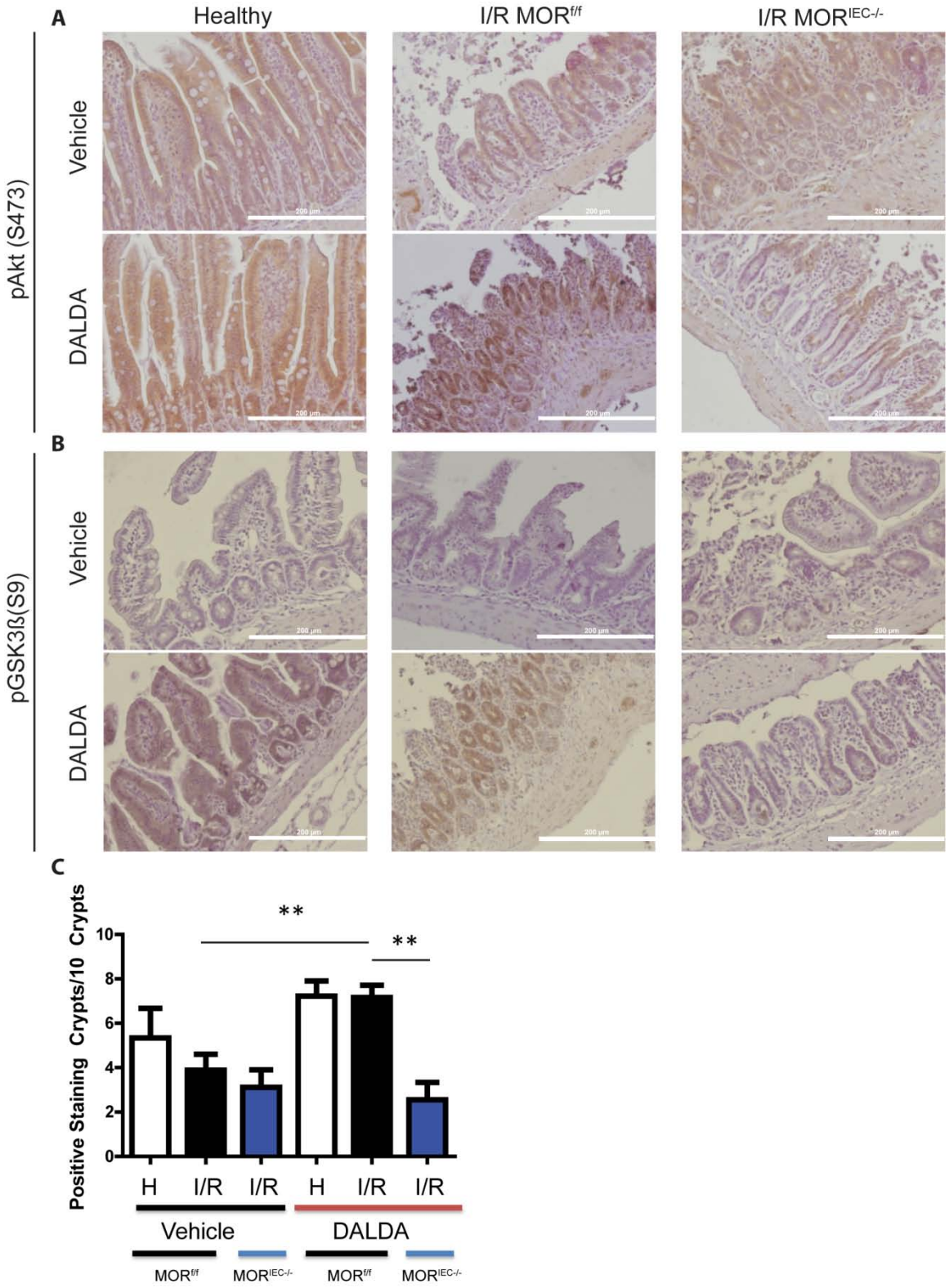

Figure 32. DALDA induced protection from I/R injury correlates with enterocyte AKT and GSK3β phosphorylation. Mice were treated with DALDA and exposed to I/R as described in Figure 28. Healthy tissues (H) represent a

non-ischemic region of the small bowel adjacent to the damaged area. A) Representative IHC of ileal swiss rolls stained for pAkt. Scale bars are 200 μm. N = 2 per group. B) Representative IHC of ileal swiss rolls stained for p-GSK3β. Scale bars are 200 μm. N = 3 per group. C) Number of p-GSK3β positive crypts per 10 crypts. N = 3 mice per group, with three random fields of view per mouse. Analysis by one-way ANOVA with Tukey's post-test.

To determine the functional role of PI3K signaling in DALDA mediated protective effect, $MOR^{f/f}$ mice were treated with the PI3K inhibitor Ly294002 (0.25 mg/kg, i.p). Interestingly, DALDA-mediated protective effect against I/R-injury was lost in mice treated with Ly294002 (Figure 33A&B). Additionally, the administration of Ly294002 resulted in decreased DALDA-mediated induction of GSK3β phosphorylation (Figure 33C&D), and reduction in baseline GSK3β phosphorylation levels (Figure 33D). These findings indicate that the DALDA-mediated cyto-protective effect in the intestine is mediated by IEC-dependent MOR signaling to the PI3K pathway, including downstream targets Akt and GS3K3β.

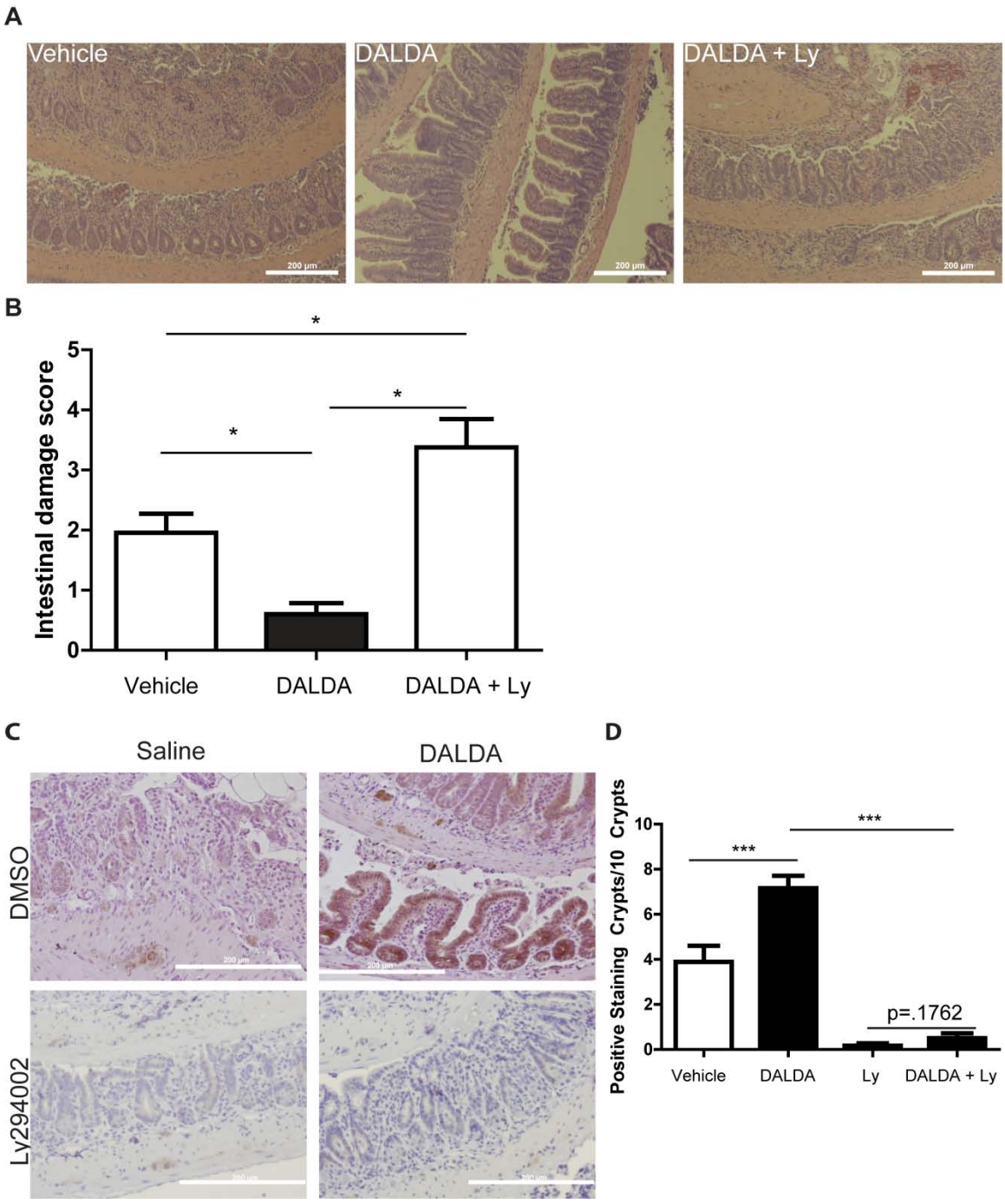

Figure 33. DALDA-mediated cyto-protection is PI3K-dependent. The PI3K inhibitor Ly294002 was administered to $MOR^{f/f}$ and $MOR^{IEC-/-}$ mice at 0.25 mg/kg i.p. 10 minutes before injection of vehicle or DALDA and then exposed to I/R as described in Figure 28. A) Histology (scale bars are 200 µm) and B) histological damage scores show that DALDA mediated protection from I/R injury requires functional PI3K signaling. N = 4-11 per group. C) DALDA-induced pGSK3β phosphorylation is ablated in mice treated with Ly294002. Scale bars are 200 µm. Positive staining pGSK3β crypts per 10 total crypts. Results are from 5-6

mice/group, with two random fields of view per mouse. Analysis by one-way ANOVA with Tukey's post-test.

Discussion

Intestinal ischemia/reperfusion injury is a serious pathology with potentially lethal sequelae, including necrotizing enterocolitis [21] and MODS [6]. Unfortunately, no therapeutic strategies are currently available to treat the underlying intestinal injury that drives many of these sequelae. Although opioid agonists have been shown to protect various organs against injury, including the intestine and heart, the cellular compartment(s) mediating these effects have remained elusive. Since IEC responses to various injurious insults including inflammation, radiation, and I/R are critical for the maintenance of intestinal barrier function [2, 23, 32, 40], we speculated that these cells drive DALDA-mediated protective effect. Indeed, selective genetic removal of MOR signaling in IECs abrogated the cyto-protective action of DALDA following I/R exposure. Since the extent of intestinal injury following I/R exposure is similar between $MOR^{f/f}$ and $MOR^{IEC-/-}$ mice, we conclude that MOR signaling is protective only in the presence of an exogenous ligand (e.g DALDA). Additionally, adjacent healthy tissue in mice subjected to I/R showed no alterations in villus length or crypt numbers in $MOR^{IEC-/-}$ mice. Furthermore, administration of DALDA did not result in increased villus length or crypt numbers in the healthy tissue of $MOR^{f/f}$ mice. These findings suggest that DALDA/MOR-mediated protection is a direct result of tightly-regulated MOR signaling that occurs only in injured tissue.

Interestingly, DALDA administration had no significant modulatory effect on I/R-induced *Il6*, *Il1b*, and *Tnf* mRNA expression levels. Since $MOR^{IEC-/-}$ mice have functional MOR in the immune compartment, these findings suggests that

DALDA/MOR primary therapeutic targets are not at the immune cell response level. Also, this suggests that the induction of inflammatory cytokines in the intestine in the early stages of I/R injury is driven by the presence of hypoxic conditions more than the extent of injury to the tissue itself. This is compatible with the reported effect of hypoxia on inflammatory gene expression observed in the intestine and may represent an adaptive response to promote IECs resistance to apoptosis [271] [272]. Together, these findings indicate that DALDA likely mediates its protective function by enhancing IEC resistance to cell death during hypoxic conditions and/or by enhancing the recovery of the intestinal barrier by increasing IEC restitution. The pro-migratory effect of DALDA on injury CMT-93 cells in conjunction with decreased epithelial apoptosis in both ischemic and ischemia/reperfusion phase are supportive of this mechanism.

Previous reports showed that MOR activates the pro-proliferative and survival signaling pathway PI3K/Akt/GSK3β in numerous *in vitro* systems [54] and during cardiac ischemia [89]. Here, we showed that DALDA enhanced AKT and GSK3β phosphorylation in the intestine both *in vivo* and *in vitro*, which correlated with protection from intestinal ischemia. The pharmacological agent Ly294002 demonstrated that MOR-mediated protection from I/R injury requires activation of PI3K signaling. PI3K is a heterodimer comprised of a catalytic (p110α, p110β, p110δ, or p110γ) and regulatory (p85, p55, or p50—or p101 for p110γ) subunit [273, 274]. Although Ly294002 is a fairly selective inhibitor of PI3K signaling, its inhibitory effect is not directed toward any specific subunit and therefore one cannot identify the PI3K subunit mediating the beneficial effects observed.

However, since IECs express the ubiquitous p110β catalytic subunit (known to couple to GPCRs [275]) and the regulatory p85α subunit, these subunits may be the target of DALDA effect. The regulatory p85α subunit has shown to be central to enterocyte PI3K signaling both at baseline and upon stimulation with parathyroid hormone [276, 277], and has been shown to promote mitogenic signals in enterocytes [278]. Further investigation would be necessary to identify the PI3K subunit responsible for DALDA-mediated protection.

Interestingly, we observed the protective effect of DALDA in the ischemic phase of injury where IECs typically undergo massive apoptosis due to prolonged hypoxia [3, 8, 9], suggesting that anti-apoptosis may be the primary mechanism of protection conferred by DALDA. The anti-apoptotic role of the PI3K signaling pathway has been observed in enterocytes [279], as well as in endothelial cells subjected to hypoxic conditions [280]. Downstream, phospholipid-dependent Akt pathway activation has been implicated in the anti-apoptotic effects of PI3K activation [266]. Akt activation can lead to enhancement of pro-survival signaling through IKK-mediated increases in NF-κB activity [266]. Akt activation can also directly inhibit apoptotic signals such as Fas-L, Bax, and p53 and promotes anti-apoptotic signals such as Bcl-XL, Bcl-2 [266]. Additionally, Akt activation results in GSK3β phosphorylation, which leads to inhibition of apoptotic signals mediated by MCL-1 and Bax, and enhancement of pro-survival signals such as β-catenin [266]. Since DALDA failed to directly activate NF-κB signaling in IECs [205], the Akt/GSK3β pathway is likely the candidate pathway activated in the intestine by this opioid agonist.

Regardless of the PI3K-dependent mechanism(s) involved, the functional impact of DALDA-mediated intestinal barrier enhancement through increased PI3K activity is clearly illustrated in the bacterial translocation assay. Presence of bacterial 16S rDNA in the liver of I/R exposed mice was strongly decreased by DALDA administration. This is an important finding, as bacterial translocation in the face of a damaged barrier is the main source of multi-organ failure in patients suffering from intestinal ischemia [6, 8, 9].

Overall, these studies demonstrate for the first time that activation of IEC-specific, PI3K-dependent MOR signaling is able to result in protection from ischemia/reperfusion-induced intestinal injury. The current lack of therapies for treating intestinal ischemia, combined with the wide availability of FDA-approved MOR-specific agonists to clinicians, makes this work of particular clinical relevance.

CHAPTER 6

DISCUSSION AND CONCLUSIONS

Mu opioid receptor signaling protects against intestinal injury

A significant strength of this work lies in its use of multiple models of acute intestinal injury across two species. Numerous GI pathologies including IBD [1, 11], I/R injury [3, 8, 9] and radiation injury [2, 7] involve loss of the intestinal barrier. The studies presented in this dissertation establish the ability of MOR-mediated signaling to protect against and enhance recovery from a variety acute intestinal injury events. Using the peripheral acting, highly specific MOR agonist DALDA, we demonstrated that MOR signaling can protect against glafenine-mediated injury in zebrafish, protect and enhance recovery from DSS-induced injury in mice, and prevent I/R-mediated injury in mice.

The ability for MOR signaling to affect a wide array of models is perhaps related to the fact that it is a GPCR, and can thus interact with numerous cellular signaling cascades. A good portion of the work in this dissertation focused on establishing some of these events. In these studies, we found that MOR-mediated protection affects enterocyte signaling. Our work in zebrafish demonstrated that administration of DALDA can restore proper UPR and autophagic responses that are blocked by glafenine administration, enhancing

cellular survival. S-XBP1, a gene that we demonstrated is up-regulated by DALDA-administration in zebrabfish, has recently been implicated in IBD pathogenesis due to an increased susceptibility to IEC apoptosis in the presence of ER stress [17, 19]. Genetic ablation of s-XBP1 in mice results in increased susceptibility to DSS colitis [19]—a model of acute injury treated by DALDA, which suggests a linkage and possible common mechanism of action across these various studies. The fact that MOR activation enhances s-XBP1 mRNA levels suggests that opioid therapy could be used to treat IBD patients with low-transcription polymorphisms of this gene [19], assuming that MOR activation could overcome the low basal transcription of s-XBP1; which remains to be determined.

Our murine studies demonstrated two further IEC-protective pathways driven by MOR signaling. Our DSS studies in mice demonstrated that DALDA enhances enterocyte STAT3 activation, which is known to be protective in enterocytes [32, 281-283]. Surprisingly, our I/R studies did not show increased STAT3 activation during the course of MOR-mediated protection; however, we did observe PI3K activation and AKT and GSK3β-phosphorylation. This suggests another pathway through which MOR can act to enhance epithelial restitution. Together, these works provide a picture of MOR-signaling as a broadly acting agent that enhances multiple enterocyte-protective pathways. These broad-based effects could account for its ability to protect against multiple models of injury. The work presented here establishes both the viability and molecular basis for MOR-mediated protection from intestinal injury.

Limitations, future directions and proposed mechanisms

One area that remains untouched in this research is the study of MOR-mediated protection from chronic colitis. In particular, it would be interesting to study the effect of DALDA on *Il10*$^{-/-}$ colitis. These mice develop spontaneous colitis within four weeks of being transferred from germ-free to specific pathogen free (spf) conditions, as a result inappropriate immune activation to commensal gut flora [284]. DALDA therapy has already been shown to abrogate other immune-mediated models of murine colitis [70, 71], and so it would be interesting to see if DALDA administration could protect against this human-disease-relevant [163, 285, 286] murine model of colitis. Specifically, DALDA would be administered concurrently with transfer of the germ-free mice to SPF conditions via osmotic pump, with conditions of the pump such that only a low dose (<50 μg/kg/day) would be administered (to ward off receptor desensitization). This work would show that MOR-mediated signaling can not only protect against acute epithelial injury and acute, immune-mediated injury [70, 71], but also chronic immune-mediated injury. This would establish pan-protective effects of MOR signaling in the intestine, and further build a case for the pursuit of clinical trials to study the use of opioids to treat gastrointestinal diseases such as IBD.

Molecularly, the studies presented in this dissertation have demonstrated that MOR-mediated signaling can affect multiple pathways within enterocytes: UPR/autophagy, STAT3 and PI3K/AKT/GSK3β. However, the exact mechanisms by which these pathways are activated and their specific molecular consequences have yet to be fully determined. While the use of MOR$^{IEC-/-}$ mice

in the I/R studies demonstrated that in this system MOR-mediated protection occurs through direct action on enterocytes, further studies need to be performed in the other models utilized in this dissertation to determine if MOR-mediated protection occurs via direct signaling on enterocyte-MOR or indirectly through other mediators such IL-22 (an inducer of STAT3) that then act upon the enterocytes. Specifically, the DSS studies need to be repeated using the $MOR^{IEC-/-}$ mice, including evaluation of enterocyte STAT3 activation upon DALDA administration in the face of DSS-injury. In our zebrafish system, a tissue-specific $MOR^{IEC-/-}$ strain would need to be developed, to establish the cell compartment responsible for MOR-mediated protection from glafenine-induced injury. However, the intestine-specific nature of glafenine-injury, as well as the rapid kinetics of injury in the system (within one hour of drug administration) suggests that DALDA acts on enterocytes directly.

Assuming the effects we have observed in these studies are a result of direct action on enterocytes, more work still needs to be done to map out the pathways between MOR activation and end-result enhancement of proliferation, migration enhancement, autophagy and cell survival. Specifically, the importance of STAT3 activation in MOR-mediated protection needs to be further assessed. While our work with DSS suggested the involvement of enterocyte-STAT3 activation in MOR-mediated protection, we did not see STAT3 enhancement in our I/R studies. In the DSS system, $STAT3^{IEC-/-}$ knockout mice should be employed to determine the importance of STAT3 in MOR-mediated protection. However, this study will have its own limits as these mice exhibit exacerbated

DSS-damage due to their loss of enterocyte STAT3 [32], and consequently MOR-mediated protection may not be sufficient to overcome enterocyte-specific loss of STAT3 even if STAT3 is not central to MOR-mediated protection in this model. Additionally, while STAT3 activation was not observed in the I/R studies, activation of STAT3 signaling has been linked to PI3K activation [287], which was observed in the I/R studies. This suggests integration between STAT3 activation and the PI3K/Akt/GS3Kβ pathway in MOR-mediated signaling. This is supported by both the literature (in particular the cardio-protective studies of opioids [89]), as well as our own studies *in vitro*, which showed that pharmacological inhibition of either JAK2 or PI3K resulted in loss of DALDA-induced STAT3 and GS3Kβ phosphorylation (Figure 34). The fact that STAT3 activation was not observed in the I/R studies could also be a matter of kinetics and/or the fact that the ischemic tissues used in the Western blot analyses had high levels of innate proteolysis, which could have preferentially masked STAT3 activation; consequently, IHC studies should be undertaken. Use of the $STAT3^{IEC-/-}$ mice in the I/R system could also beneficial in sorting out this unresolved issue.

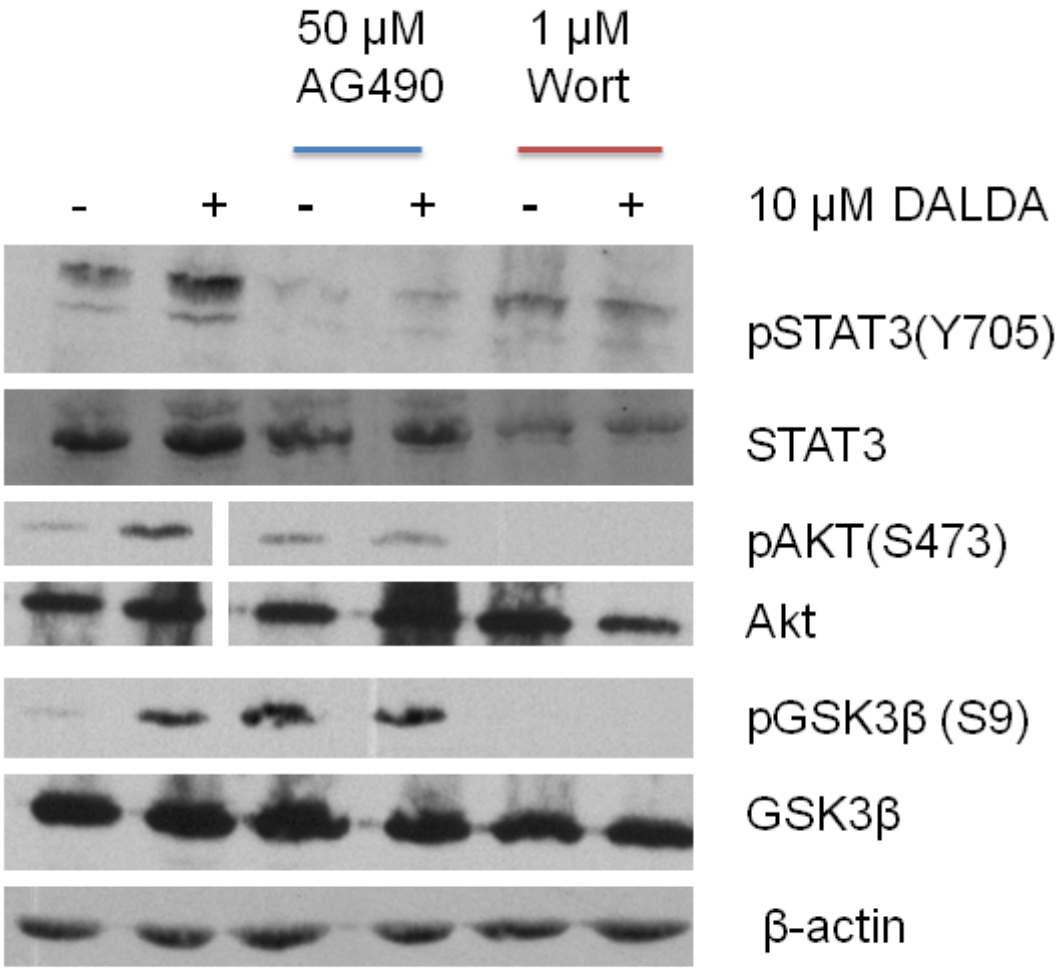

Figure 34. Phosphorylation of STAT3 and GSK3β by DALDA in CMT-93 cells are both dependent on PI3K and JAK2 activity. CMT-93 cells were stimulated with DALDA for 60 minutes, with 10 minutes of inhibitor pre-treatment where indicated. Cells were directly lysed in 1X laemelli buffer and subjected to Western blot analysis. AG490 is a JAK2 inhibitor. Wortmannin (Wort) is a PI3K inhibitor. Representative of 3 independent experiments.

A combined interpretation of the DSS and I/R studies alongside the *in vitro* work suggests that PI3K could serve as the central mechanism for the wide variety of intestinal protective effects induced by MOR signaling, including STAT3 activation. However, questions remain regarding the steps between MOR activation and STAT3 phosphorylation. While MOR has been well-established to activate PI3K/Akt signaling [54, 89] and the cardio-protection literature suggests that MOR activates JAK2 (leading to STAT3 phosphorylation) [89], more work needs to be performed in the systems presented in this dissertation to link these two pathways.

The zebrafish glafenine studies also present evidence that PI3K may be the mediator of MOR-induced enhancement of autophagy, the proposed mechanism of DALDA-mediated protection in this system. Wortmannin administration blockaded DALDA-mediated protection from glafenine-injury in zebrafish, and PI3K signaling is known to induce autophagy [224]. Specifically, the PI3K regulatory subunit p85α has been shown in mouse embryonic fibroblasts to increase resolution of endoplasmic reticulum (ER) stress and prevent apoptosis via enhancement of s-XBP1 nuclear transport and activity [288], one of the UPR molecules modulated by DALDA in our zebrafish studies. However, further work needs to be performed to fully map out how MOR signaling up-regulates UPR and autophagy responses—including the involvement of PI3K activation, and the p85α subunit in particular, in these processes.

Despite the aforementioned remaining holes, this work paints a picture of MOR-mediated protection that involves a central role for PI3K signaling, which then induces numerous downstream protective signaling events, including Akt, GS3Kβ and STAT3 phosphorylation, and engagement of protective autophagy pathways. An outline of the proposed mechanisms by which MOR signaling induces cyto-protection are presented in Figure 35.

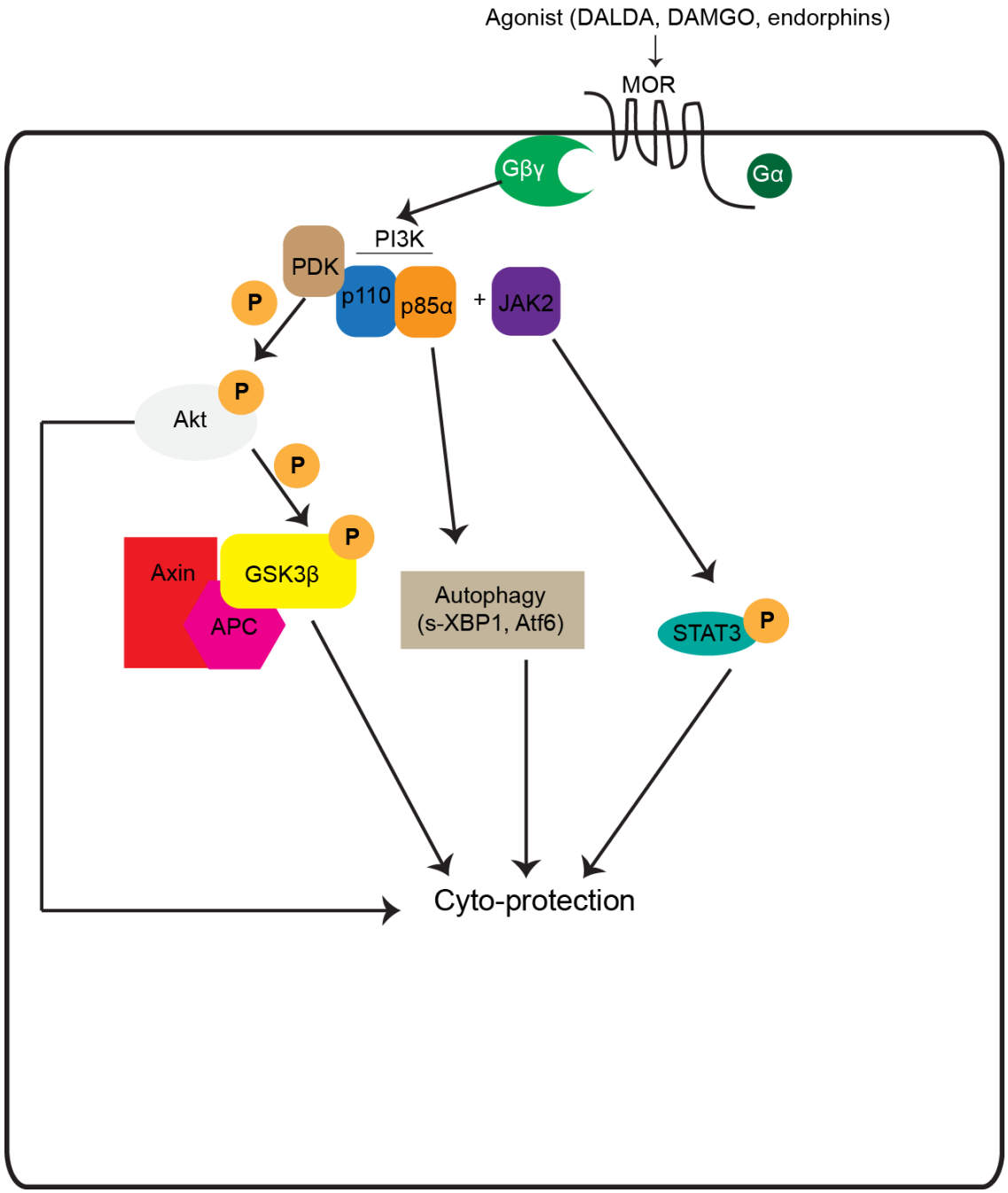

Figure 35. Proposed mechanisms by which MOR signaling engages cyto-protection. After activation of MOR by a ligand, we propose that the coupled $G_{\beta\gamma}$ G-protein engages and activates PI3K. This in turn engages three cyto-protective cascades: 1) the PDK/Akt/GSK3β cascade, through the catalytic p110 PI3K subunit, 2) enhancement of autophagy genes, through the PI3K p85α regulatory subunit, and 3) STAT3 phosphorylation through synergy between PI3K activation and JAK2 activation.

MOR therapy in humans: a case for the pursuit of clinical trials

As discussed above, numerous GI pathologies including IBD [1, 11], I/R injury [3, 8, 9] and radiation injury [2, 7] involve loss of the intestinal barrier as a principal component of their pathogenesis. Existing treatments of these pathologies do not address the intestinal damage directly, but either try to stop the source of the damage (via immunosuppression in the case of IBD [13-16, 289]), or are merely supportive [6, 8]. Consequently, the ability to activate epithelial restitution represents a completely unexplored but potentially vital treatment modality that directly targets intestinal injury. Currently, there are significant limitations to targeting epithelial restitution, as most recombinant growth factors (such as EGF) are very expensive and can have significant off-target side effects. While opioids also have noteworthy side effects, including the risk of dependency [54], narcotic bowel syndrome [91], and toxic megacolon [91], the class of compounds are also clinically well-understood and highly used, mitigating much of their risk. Opioids are additionally relatively cheap and widely available. The presence of multiple mu-opioid agonists in the pharmacopeia is another benefit of pursuing opioid-mediated therapy, as clinical trials (Phase I and some Phase II) could largely be skipped, as the toxicity and side effects of these drugs are already known. Even more importantly, there already exists a peripheral-only acting MOR agonist that is highly used to treat diarrhea and is available over-the-counter: loperamide (Imodium®). Consequently, clinical trials studying peripheral-MOR therapy (just like what is accomplished with DALDA in

our systems) could be easily undertaken, and a relatively low cost since drug develop is not a concern.

Specifically, it would be ideal to pursue the use of loperamide (1-2 2 mg doses/day) to treat ulcerative colitis in patients that still have rectal/sigmoidal ulceration resulting in bleeding, despite 5-ASA and/or immunosuppressive therapy. Since diarrhea is treated by loperamide therapy, this could not be an outcome of this study. Rather, epithelial healing would be the primary outcome, as measured by colonoscopy imaging (with pathology samples) performed both before therapy was initiated and 4 weeks into therapy. A secondary, clinical outcome would be the presence of visible blood in the stool. The cost of performing a randomized, double-blind trial on 30 patients has already been estimated, and is approximately $50,000. If this trial were successful, it would be provide sufficient evidence to pursue a full-fledged Phase III trial, and also provide evidence to support the pursuit of loperamide for the study of intestinal I/R injury and radiation injury.

The strong protection we observed with DALDA administration during ischemia-reperfusion injury is of great clinical interest as well. I/R injury is a serious complication of surgeries and in pre-mature infants in the form of necrotizing enterocolitis, potentially leading to sepsis and multi-organ dysfunction syndrome [6, 8, 9, 21]. New therapies are desperately needed for the treatment of intestinal I/R injury, as current approaches are only supportive [6, 8]. Opiates have already been demonstrated to confer significant cardio-protection during ischemia/reperfusion injury in studies in both rodents and humans [86-89, 290],

including in randomized, double-blind clinical trials [265]. This work extends the protective observations to the intestinal system, and suggests that clinical trials to study the use of opioids to treat intestinal I/R injury would be viable.

Summary

This works establishes that MOR signaling is protective against multiple models of acute intestinal injury. Engaging MOR signaling, likely in the enterocytes directly, results in the activation of multiple cell programs to enhance epithelial restitution and stave off IEC apoptosis. This work provides sufficient evidence to warrant extending these observations into the clinic, with the initiation of clinical trials. Numerous opioids are already commercially available and pharmacologically well understood, making the pursuit of clinical trials relatively inexpensive and easy to undertaken. Such work could have profound benefits for patients suffering from a variety of intestinal diseases.

APPENDIX 1

OTHER DATA

Other data were produced during this dissertation, which either did not make into a manuscript, or still needs further work before being published. These are presented below. Each figure includes in its legend the relevant methods, and are cited elsewhere in the manuscript as appropriate.

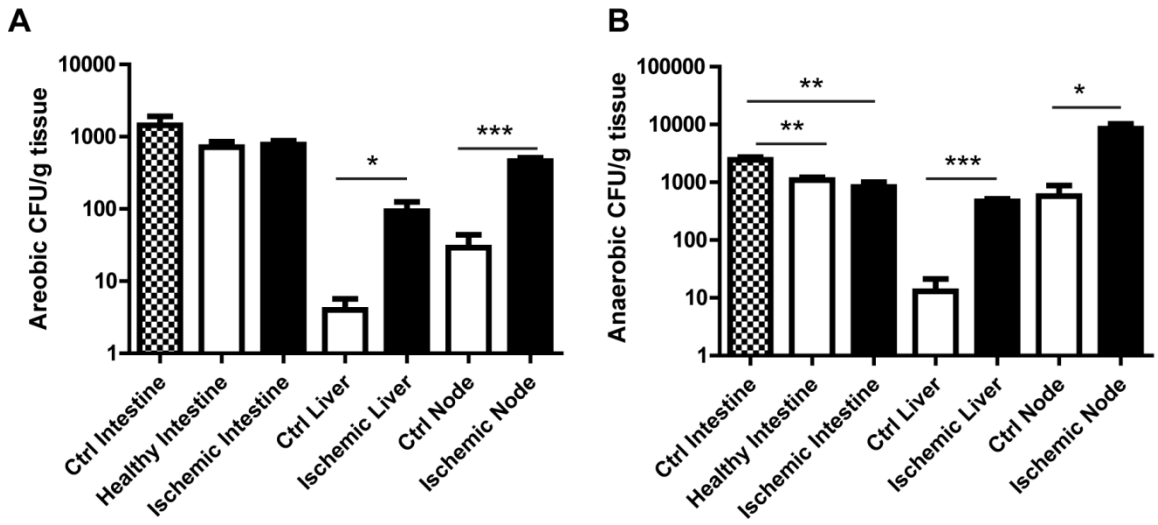

Figure 36: DALDA administration reduces bacterial dissemination to the liver and spleen. Mice were subjected to ileal ischemia for 1 hour, followed by reperfusion for 4 hours before sacrifice. Control samples are from mice sacrificed without ischemia being performed. Healthy tissues were taken from ileum adjacent to the ischemic area. A&B) Tissue homogenates were plated on sheep BHI plates overnight in aerobic (A) or anaerobic (B) conditions and CFUs were counted and normalized to the grams of tissue in each homogenate. Representative of 3 or 4 mice per group.

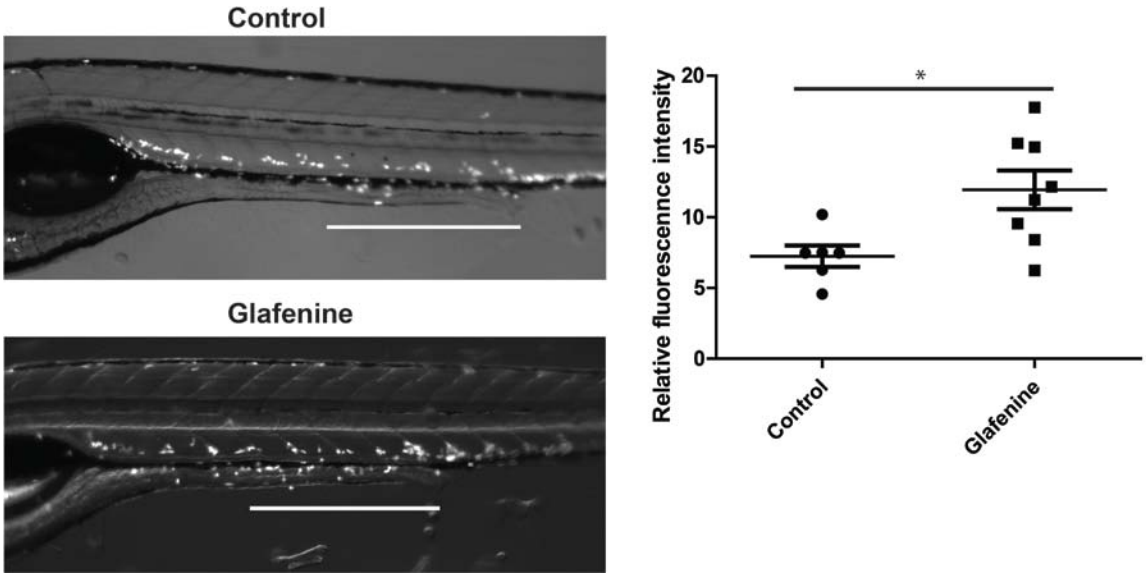

Figure 37: Tg(MPO:EGFP) zebrafish demonstrate increased neutrophil signal overlaying the intestine. Zebrafish were administered glafenine using the same protocol as described elsewhere in this work. Bars are 1 mm in length. Relative fluorescence intensity was analyzed over segment 2. Representative of 3 independent experiments, N as portrayed. Wide-field fluorescence images were captured and analyzed using the same methodology as described in the text.

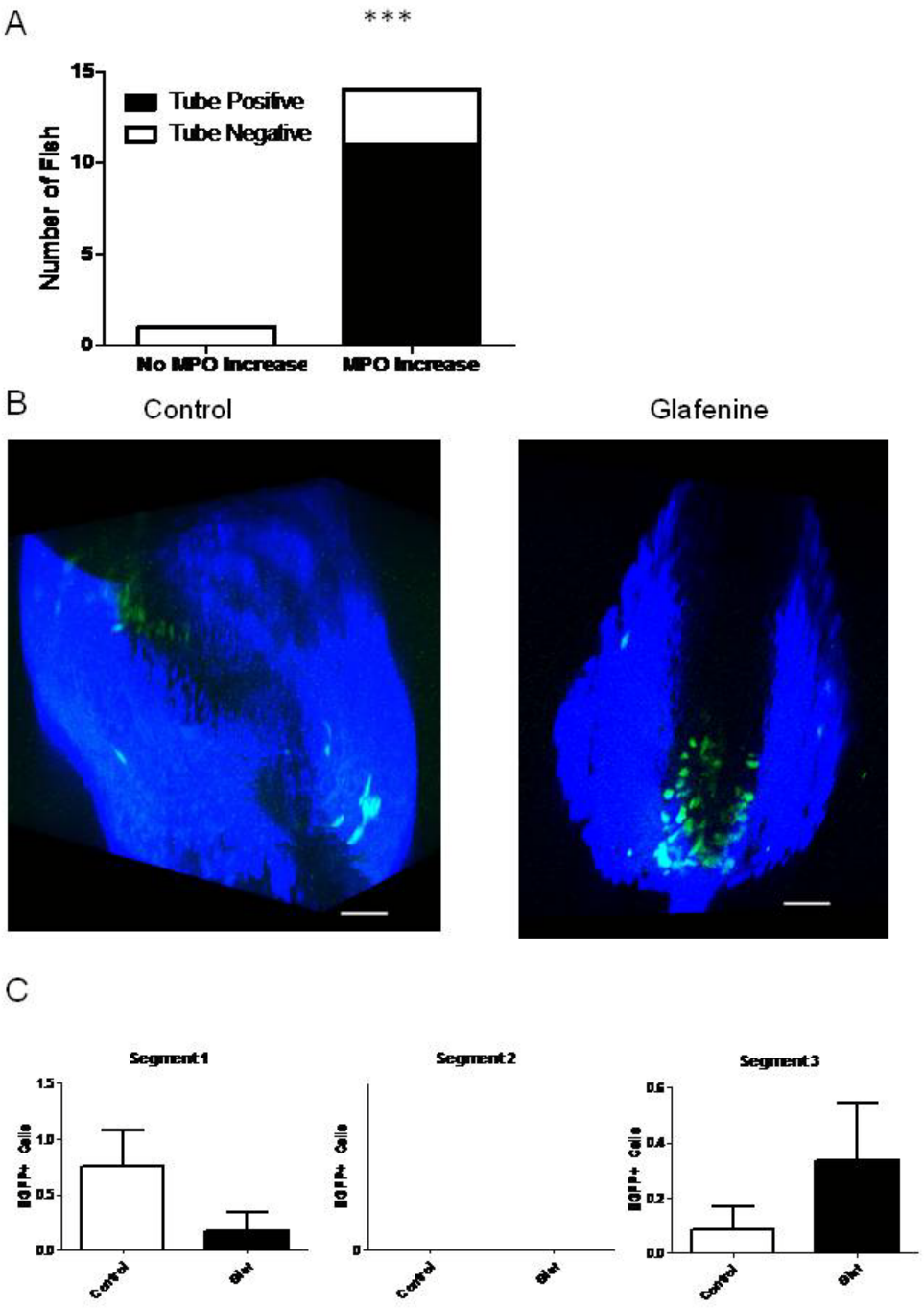

Figure 38: Neutrophils are near, but not in the gut compartment. Zebrafish larvae were administered 25 µM glafenine for 12 hours as described elsewhere. A) Correlation between formation of apoptotic tubes and tg(MPO:EGFP) signal increase. N based on height of bars, pooled from 3 independent experiments. B) 3D confocal reconstructions of tg(MPO:EGFP) zebrafish with and without glafenine treatment. Images are representative of 2 different fish per condition;

bars equal 50 μm. Confocal images were captured with 1% agar embedded, anesthetized (alive) fish, using the same imaging setup as used for the confocal imaging of murine intestines described in the text. C) EGFP positive cells from gut micro-dissections of tg(MPO:EGFP) zebrafish. No significant difference between groups was found. N≥6, pooled from 2 replicate groups. Gut micro-dissections were performed as described in the text and analyzed by eye with wide-field fluorescence microscopy.

APPENDIX 2

HUMAN STUDIES IN IBS PATIENTS

Manuscript to be written (data collection completed)—clinical data not presented here.

Introduction and overview

Probiotics have been shown to be beneficial in alleviating various functional GI symptoms, however, the mechanisms of these effects are unknown. The probiotic bacterium L-NCFM has been shown to increase expression of MOR in the intestinal mucosa and decrease intestinal pain sensation in animal studies [143], and recent clinical studies of IBS patients with diarrhea (IBS-D) demonstrated decreased levels of *lactobacillus* strains in patients suffering from IBS-D compared to healthy controls [291]. Other studies have demonstrated an important role for commensal bacteria in the protection from inflammatory pain [144].

Materials and methods

Caucasian women (N=17) 18-70 years with mild to moderate abdominal pain were investigated. Colonic biopsies were collected during un-sedated, un-prepped flexible sigmoidoscopy pre- and post- 21 days consumption of the probiotics at a total dose of 1.0 x 1010 CFU bid. Cellular RNA was extracted from the mucosal biopsies and reverse transcribed to cDNA. mRNA expression of mucosal MOR receptors was determined by RT-PCR on an ABI Prism HT7700 Thermocycler (Applied Biosystems) via SybrGreen. Relative fold-changes were

determined using the ΔΔCT calculation method. Immunohistochemistry (IHC) for pSTAT3 was performed on paraffin-embedded sections of mucosal biopsies with monocloncal antibodies for pSTAT3(Y705) (Cell Signaling Technology Inc) were used at a 1:50 dilution. Slides were developed using horseradish peroxidase-conjugated secondary antibody and a VectaStain Elite ABC Kit (Vector Laboratories Inc).

Results

Preliminary analysis of patients treated with the L-NCFM bacterium demonstrated a statistically significant decrease in bloating symptoms (data unavailable, in final processing). Pre- to post-intervention with L-NCFM and B-LBi07 or L-NCFM alone was associated with a 5.5-fold increase in MOR expression (8.2E-6 vs 1.5E-6 fold-over-β-actin, P=0.014; n=13). The increase in MOR expression was significantly (~10-fold) greater with L-NCFM alone compared to the combination of B-LBi07 and L-NCFM (1.1E-5 vs1.8E-6 fold-over-β-actin post-treatment increase, P=0.022). Analysis of MOR expression on a per-patient-basis showed that patients treated with L-NCFM alone had a 39.9-fold pre- to post-intervention increase in the levels of the receptor (P =0.0313). IHC for pStat3 showed increase in mucosal biopsies only in the L-NCFM group.

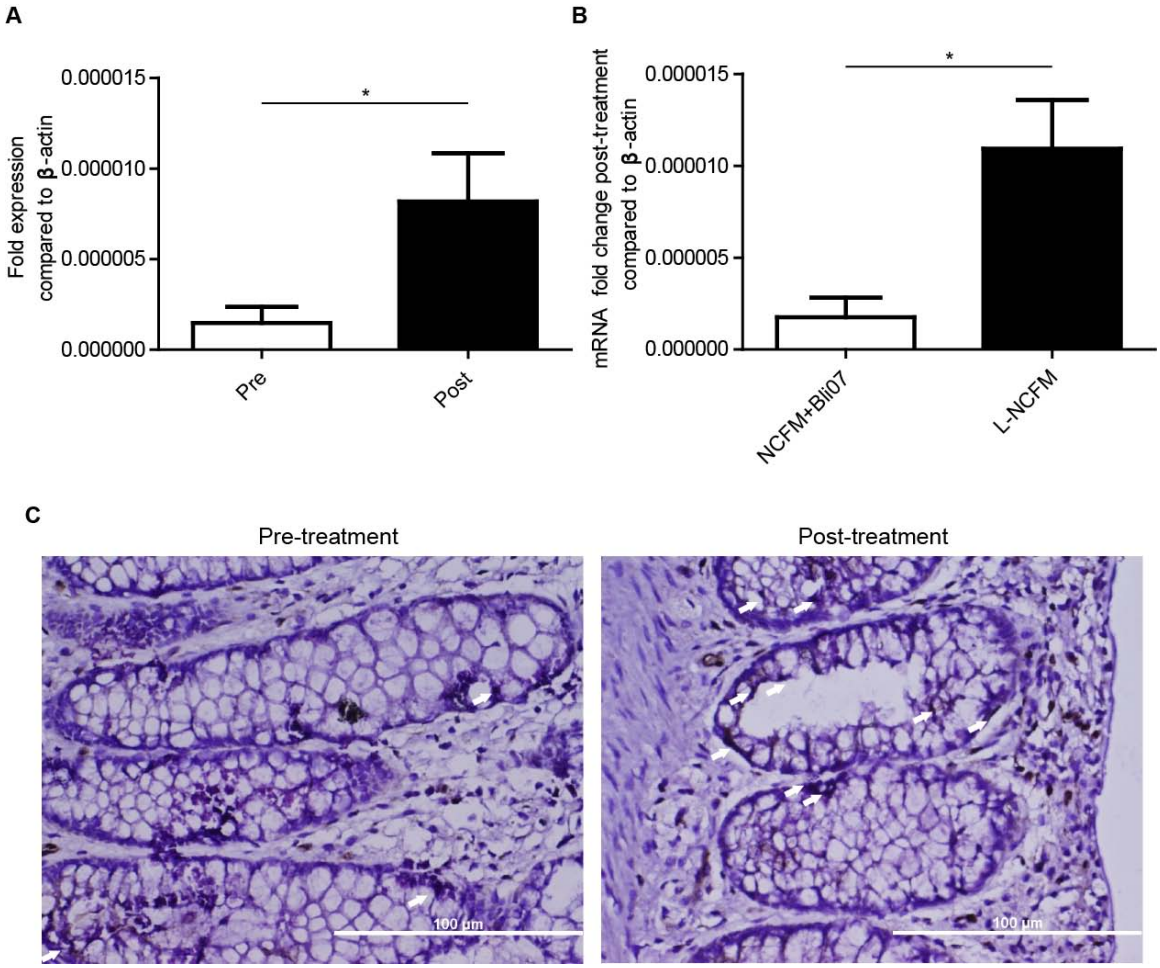

Figure 39: **Administration of L-NCFM results in increased MOR expression and downstream signaling in humans.** A&B) Real-time PCR for MOR expression relative to β-actin expression in colonic mucosa biopsies from human patients. Analyzed using the ΔΔCt method. A) Pre verses post-treatment analysis demonstrates an induction of MOR expression with probiotic administration. N = 13 per group B) Analysis of NCFM + Bli07 vs NCFM alone demonstrates that NCFM alone is responsible for MOR induction, and that Bli07 serves as a competitive agent for NCFM colonization. N = 7 per group C) IHC analysis of mucosal biopsies demonstrates downstream activation of MOR signaling with NCFM treatment, as measured by increased levels of STAT3 phosphorylation. Representative image from 3 separate samples per group. Scale bars are 100 µm.

Conclusions

These results replicate in humans an observation seen in mice, with promising initial clinical findings. It demonstrates the modulation of MOR signaling by pro-biotics, in addition to direct receptor activation, could be a viable avenue for MOR-mediated therapy in patients. A pro-biotic approach has several advantages over pharmacological interventions, including less systemic side effects.

WORKS CITED

1. Sartor, R.B., *Microbial Influences in Inflammatory Bowel Diseases.* Gastroenterology, 2008. **134**(2): p. 577-594.

2. Packey, C.D. and M.A. Ciorba, *Microbial influences on the small intestinal response to radiation injury.* Curr Opin Gastroenterol, 2009. **26**(2): p. 88-94.

3. Kinross, J., et al., *Intestinal ischemia/reperfusion injury: defining the role of the gut microbiome.* Biomarkers in Medicine, 2009. **3**(2): p. 175-192.

4. Morteau, O., et al., *Impaired mucosal defense to acute colonic injury in mice lacking cyclooxygenase-1 or cyclooxygenase-2.* J Clin Invest, 2000. **105**(4): p. 469-478.

5. Williams, K.L., et al., *Enhanced survival and mucosal repair after dextran sodium sulfate-induced colitis in transgenic mice that overexpress growth hormone.* Gastroenterology, 2001. **120**(4): p. 925-937.

6. Gustot, T., *Multiple organ failure in sepsis: prognosis and role of systemic inflammatory response.* Curr Opin Crit Care, 2011. **17**(2): p. 153-9.

7. Potten, C.S., *Radiation, the ideal cytotoxic agent for studying the cell biology of tissues such as the small intestine.* Radiat Res, 2004. **161**(2): p. 123-36.

8. Haglund, U., *Gut ischaemia.* Gut, 1994. **35**(1 Suppl): p. S73-6.

9. Parks, D.A. and D.N. Granger, *Ischemia-reperfusion injury: a radical view.* Hepatology, 1988. **8**(3): p. 680-2.

10. Karrasch, T. and C. Jobin, *Wound healing responses at the gastrointestinal epithelium: a close look at novel regulatory factors and investigative approaches.* Z Gastroenterol, 2009. **47**(12): p. 1221-1229.

11. Sartor, R.B. and M. Muehlbauer, *Microbial host interactions in IBD: implications for pathogenesis and therapy.* Curr Gastroenterol Rep, 2007. **9**(6): p. 497-507.

12. Loftus, E.V., Jr., *Clinical epidemiology of inflammatory bowel disease: Incidence, prevalence, and environmental influences.* Gastroenterology, 2004. **126**(6): p. 1504-17.

13. Pithadia, A.B. and S. Jain, *Treatment of inflammatory bowel disease (IBD).* Pharmacol Rep, 2011. **63**(3): p. 629-42.

14. Sandborn, W.J., *Current Directions in IBD Therapy: What Goals Are Feasible With Biological Modifiers?* Gastroenterology, 2008. **135**(5): p. 1442-1447.

15. Rutgeerts, P., et al., *Infliximab for induction and maintenance therapy for ulcerative colitis.* N Engl J Med, 2005. **353**(23): p. 2462-76.

16. Hanauer, S.B., et al., *Maintenance infliximab for Crohn's disease: the ACCENT I randomised trial.* Lancet, 2002. **359**(9317): p. 1541-9.

17. Kaser, A., E. Martinez-Naves, and R.S. Blumberg, *Endoplasmic reticulum stress: implications for inflammatory bowel disease pathogenesis.* Curr Opin Gastroenterol, 2010. **26**(4): p. 318-26.

18. Stappenbeck, T.S., et al., *Crohn disease: a current perspective on genetics, autophagy and immunity.* Autophagy, 2010. **7**(4): p. 355-74.

19. Kaser, A., et al., *XBP1 links ER stress to intestinal inflammation and confers genetic risk for human inflammatory bowel disease.* Cell, 2008. **134**(5): p. 743-56.

20. Ravikumar, B., et al., *Regulation of Mammalian Autophagy in Physiology and Pathophysiology.* Physiological Reviews, 2010. **90**(4): p. 1383-1435.

21. Young, C.M., S.D. Kingma, and J. Neu, *Ischemia-reperfusion and neonatal intestinal injury.* J Pediatr, 2011. **158**(2 Suppl): p. e25-8.

22. Koury, J., et al., *Persistent HIF-1alpha activation in gut ischemia/reperfusion injury: potential role of bacteria and lipopolysaccharide.* Shock, 2004. **22**(3): p. 270-7.

23. Chen, L.W., et al., *The two faces of IKK and NF-kappaB inhibition: prevention of systemic inflammation but increased local injury following intestinal ischemia-reperfusion.* Nat Med, 2003. **9**(5): p. 575-81.

24. Meinzen-Derr, J., et al., *Epidemiology of necrotizing enterocolitis temporal clustering in two neonatology practices.* J Pediatr, 2009. **154**(5): p. 656-61.

25. Slonim, A.E., et al., *A Preliminary Study of Growth Hormone Therapy for Crohn's Disease.* N Engl J Med, 2000. **342**(22): p. 1633-1637.

26. Theiss, A.L., S. Fruchtman, and P.K. Lund, *Growth factors in inflammatory bowel disease. The actions and interactions of growth hormone and insulin-like growth factor-I.* Inflammatory Bowel Diseases, 2004. **10**(6): p. 871-880.

27. Iizuka, M. and S. Konno, *Wound healing of intestinal epithelial cells.* World J Gastroenterol, 2011. **17**(17): p. 2161-71.

28. Sturm, A. and A.U. Dignass, *Epithelial restitution and wound healing in inflammatory bowel disease.* World J Gastroenterol, 2008. **14**(3): p. 348-353.

29. Marchiando, A.M., et al., *The epithelial barrier is maintained by in vivo tight junction expansion during pathologic intestinal epithelial shedding.* Gastroenterology, 2011. **140**(4): p. 1208-1218 e1-2.

30. Ciacci, C., S.E. Lind, and D.K. Podolsky, *Transforming growth factor beta regulation of migration in wounded rat intestinal epithelial monolayers.* Gastroenterology, 1993. **105**(1): p. 93-101.

31. Dignass, A.U. and D.K. Podolsky, *Cytokine modulation of intestinal epithelial cell restitution: central role of transforming growth factor beta.* Gastroenterology, 1993. **105**(5): p. 1323-1332.

32. Pickert, G., et al., *STAT3 links IL-22 signaling in intestinal epithelial cells to mucosal wound healing.* J. Exp. Med., 2009. **206**(7): p. 1465-1472.

33. Kim, J.W. and C. Jobin, *Nod2/GSK3b signaling protects the small intestine against ischemia-reperfusion induced injury in mice.* Gastroenterology, 2010. **138**.

34. Huang, C.-Y., et al., *Anti-apoptotic PI3K/Akt signaling by sodium/glucose transporter 1 reduces epithelial barrier damage and bacterial translocation in intestinal ischemia.* Lab Invest. **91**(2): p. 294-309.

35. Wirtz, S., et al., *Chemically induced mouse models of intestinal inflammation.* Nat Protoc, 2007. **2**(3): p. 541-6.

36. Farooq, S.M., et al., *Therapeutic effect of blocking CXCR2 on neutrophil recruitment and dextran sodium sulfate-induced colitis.* J Pharmacol Exp Ther, 2009. **329**(1): p. 123-9.

37. Qualls, J.E., et al., *Suppression of experimental colitis by intestinal mononuclear phagocytes.* J Leukoc Biol, 2006. **80**(4): p. 802-15.

38. Dieleman, L.A., et al., *Dextran sulfate sodium-induced colitis occurs in severe combined immunodeficient mice.* Gastroenterology, 1994. **107**(6): p. 1643-52.

39. Hahm, K.-B., et al., *Loss of transforming growth factor {beta} signalling in the intestine contributes to tissue injury in inflammatory bowel disease.* Gut, 2001. **49**(2): p. 190-198.

40. Steinbrecher, K.A., et al., *Loss of Epithelial RelA Results in Deregulated Intestinal Proliferative/Apoptotic Homeostasis and Susceptibility to Inflammation.* J Immunol, 2008. **180**(4): p. 2588-2599.

41. Koch, S., et al., *The Wnt antagonist Dkk1 regulates intestinal epithelial homeostasis and wound repair.* Gastroenterology, 2011. **141**(1): p. 259-68, 268 e1-8.

42. Kitajima, S., et al., *Dextran sodium sulfate-induced colitis in germ-free IQI/Jic mice.* Exp Anim, 2001. **50**(5): p. 387-95.

43. Araki, A., et al., *MyD88-deficient mice develop severe intestinal inflammation in dextran sodium sulfate colitis.* J Gastroenterol, 2005. **40**(1): p. 16-23.

44. Richardson, W.M., et al., *Nucleotide-binding oligomerization domain-2 inhibits toll-like receptor-4 signaling in the intestinal epithelium.* Gastroenterology, 2010. **139**(3): p. 904-17, 917 e1-6.

45. Victoni, T., et al., *Local and remote tissue injury upon intestinal ischemia and reperfusion depends on the TLR/MyD88 signaling pathway.* Med Microbiol Immunol, 2010. **199**(1): p. 35-42.

46. Moses, T., L. Wagner, and S.D. Fleming, *TLR4-mediated Cox-2 expression increases intestinal ischemia/reperfusion-induced damage.* J Leukoc Biol, 2009. **86**(4): p. 971-80.

47. Lieschke, G.J. and P.D. Currie, *Animal models of human disease: zebrafish swim into view.* Nat Rev Genet, 2007. **8**(5): p. 353-367.

48. Mathias, J.R., et al., *Resolution of inflammation by retrograde chemotaxis of neutrophils in transgenic zebrafish.* J Leukoc Biol, 2006. **80**(6): p. 1281-8.

49. Niethammer, P., et al., *A tissue-scale gradient of hydrogen peroxide mediates rapid wound detection in zebrafish.* Nature, 2009. **459**(7249): p. 996-9.

50. Rieger, S. and A. Sagasti, *Hydrogen peroxide promotes injury-induced peripheral sensory axon regeneration in the zebrafish skin.* PLoS Biol, 2011. **9**(5): p. e1000621.
51. Roy, S. and H.H. Loh, *Effects of opioids on the immune system.* Neurochem Res, 1996. **21**(11): p. 1375-86.

52. Roy, S., R.A. Barke, and H.H. Loh, *MU-opioid receptor-knockout mice: role of [mu]-opioid receptor in morphine mediated immune functions.* Molecular Brain Research, 1998. **61**(1-2): p. 190-194.

53. Wang, J., et al., *The immunosuppressive effects of chronic morphine treatment are partially dependent on corticosterone and mediated by the mu-opioid receptor.* J Leukoc Biol, 2002. **71**(5): p. 782-790.

54. Law, P.-Y., Y.H. Wong, and H.H. Loh, *Molecular Mechanisms and Regulation of Opioid Receptor Signaling.* Annual Review of Pharmacology and Toxicology, 2000. **40**(1): p. 389-430.

55. Chen, Y.L., P.Y. Law, and H.H. Loh, *Nuclear factor kappaB signaling in opioid functions and receptor gene expression.* J Neuroimmune Pharmacol, 2006. **1**(3): p. 270-9.

56. D Smart, R.A.H., K Hirota, D K Grandy, D G Lambert,, *The effects of recombinant rat mu-opioid receptor activation in CHO cells on phospholipase C, [Ca2+] and adenylyl cyclase.* British Journal of Pharmacology, 1997. **120**(6): p. 1165-1171.

57. Xie, W., et al., *Genetic alteration of phospholipase C beta3 expression modulates behavioral and cellular responses to mu opioids.* Proc Natl Acad Sci U S A, 1999. **96**(18): p. 10385-90.

58. Wang, H.Y., et al., *Ultra-low-dose naloxone suppresses opioid tolerance, dependence and associated changes in mu opioid receptor-G protein coupling and G[beta][gamma] signaling.* Neuroscience, 2005. **135**(1): p. 247-261.

59. Chakrabarti, S., A. Regec, and A.R. Gintzler, *Biochemical demonstration of mu-opioid receptor association with Gs[alpha]: enhancement following morphine exposure.* Molecular Brain Research, 2005. **135**(1-2): p. 217-224.

60. Wang, J., et al., *Morphine Negatively Regulates Interferon-{gamma} Promoter Activity in Activated Murine T Cells through Two Distinct Cyclic AMP-dependent Pathways.* J. Biol. Chem., 2003. **278**(39): p. 37622-37631.

61. Li, L. and K. Chang, *The stimulatory effect of opioids on mitogen-activated protein kinase in Chinese hamster ovary cells transfected to express mu-opioid receptors.* Mol Pharmacol, 1996. **50**(3): p. 599-602.
62. Chuang, L.F., K.F. Killam Jr., and R.Y. Chuang, *Induction and Activation of Mitogen-activated Protein Kinases of Human Lymphocytes as One of the Signaling Pathways of the Immunomodulatory Effects of Morphine Sulfate.* J. Biol. Chem., 1997. **272**(43): p. 26815-26817.

63. Edelblum, K.L., et al., *Raf Protects Against Colitis by Promoting Mouse Colon Epithelial Cell Survival Through NF-[kappa]B.* Gastroenterology, 2008. **135**(2): p. 539-551.e3.

64. Ye, R.D., *Regulation of nuclear factor {kappa}B activation by G-protein-coupled receptors.* J Leukoc Biol, 2001. **70**(6): p. 839-848.

65. Polakiewicz, R.D., et al., *μ-Opioid Receptor Activates Signaling Pathways Implicated in Cell Survival and Translational Control.* J. Biol. Chem., 1998. **273**(36): p. 23534-23541.

66. Liu, H., et al., *Mechanisms involved in phosphatidylinositol 3-kinase pathway mediated up-regulation of the mu opioid receptor in lymphocytes.* Biochemical Pharmacology. **79**(3): p. 516-523.

67. Drake, M.T., S.K. Shenoy, and R.J. Lefkowitz, *Trafficking of G Protein-Coupled Receptors.* Circ Res, 2006. **99**(6): p. 570-582.

68. Pierce, K.L. and R.J. Lefkowitz, *Classical and new roles of [beta]-arrestins in the regulation of G-Protein-Coupled receptors.* Nat Rev Neurosci, 2001. **2**(10): p. 727-733.

69. Schiller, P.W., et al., *Dermorphin analogs carrying an increased positive net charge in their "message" domain display extremely high .mu.-opioid receptor selectivity.* Journal of Medicinal Chemistry, 1989. **32**(3): p. 698-703.

70. Philippe, D., et al., *Anti-inflammatory properties of the mu opioid receptor support its use in the treatment of colon inflammation.* J Clin Invest, 2003. **111**(9): p. 1329-38.

71. Philippe, D., et al., *Mu opioid receptor expression is increased in inflammatory bowel diseases: implications for homeostatic intestinal inflammation.* Gut, 2006. **55**(6): p. 815-823.

72. Matters, G.L., et al., *The opioid antagonist naltrexone improves murine inflammatory bowel disease.* J Immunotoxicol, 2008. **5**(2): p. 179-187.

73. Smith, J.P., et al., *Low-dose naltrexone therapy improves active Crohn's disease.* Am J Gastroenterol, 2007. **102**(4): p. 820-828.
74. Largent-Milnes, T.M., et al., *Oxycodone Plus Ultra-Low-Dose Naltrexone Attenuates Neuropathic Pain and Associated [mu]-Opioid Receptor-Gs Coupling.* The Journal of Pain, 2008. **9**(8): p. 700-713.

75. Kai, Y., et al., *Colitis in mice lacking the common cytokine receptor [gamma] chain is mediated by IL-6-producing CD4+ T cells.* Gastroenterology, 2005. **128**(4): p. 922-934.

76. Kraus, J., et al., *Regulation of mu-Opioid Receptor Gene Transcription by Interleukin-4 and Influence of an Allelic Variation within a STAT6 Transcription Factor Binding Site.* J. Biol. Chem., 2001. **276**(47): p. 43901-43908.

77. Borner, C., et al., *Transcriptional Regulation of the Human mu-opioid Receptor Gene by Interleukin-6.* 2004. **66**(6): p. 1719-1726.

78. Beltran, J.A., A. Pallur, and S.L. Chang, *HIV-1 gp120 up-regulation of the mu opioid receptor in TPA-differentiated HL-60 cells.* International Immunopharmacology, 2006. **6**(9): p. 1459-1467.

79. Pol, O., F. Alameda, and M.M. Puig, *Inflammation Enhances mu-Opioid Receptor Transcription and Expression in Mice Intestine.* 2001. **60**(5): p. 894-899.

80. Páldy, E., et al., *CB2 cannabinoid receptor antagonist SR144528 decreases mu-opioid receptor expression and activation in mouse brainstem: Role of CB2 receptor in pain.* Neurochemistry International, 2008. **53**(6-8): p. 309-316.

81. Welters, I.D., et al., *Morphine inhibits NF-kappaB nuclear binding in human neutrophils and monocytes by a nitric oxide-dependent mechanism.* Anesthesiology, 2000. **92**(6): p. 1677-84.

82. Roy, S., et al., *Morphine Modulates NF[kappa]B Activation in Macrophages.* Biochemical and Biophysical Research Communications, 1998. **245**(2): p. 392-396.

83. Cho, M.-L., et al., *STAT3 and NF-{kappa}B Signal Pathway Is Required for IL-23-Mediated IL-17 Production in Spontaneous Arthritis Animal Model IL-1 Receptor Antagonist-Deficient Mice.* J Immunol, 2006. **176**(9): p. 5652-5661.

84. He, J.C., et al., *Role of the Go/i signaling network in the regulation of neurite outgrowth.* Can J Physiol Pharmacol, 2006. **84**(7): p. 687-94.

85. Lo, R.K.H. and Y.H. Wong, *Signal Transducer and Activator of Transcription 3 Activation by the {delta}-Opioid Receptor via G{alpha}14 Involves Multiple Intermediates.* Mol Pharmacol, 2004. **65**(6): p. 1427-1439.

86. Li, R., et al., *Intrathecal Morphine Preconditioning Induces Cardioprotection via Activation of Delta, Kappa, and Mu Opioid Receptors in Rats.* Anesth Analg, 2009. **108**(1): p. 23-29.

87. Lin, J.-Y.M.D., et al., *Kappa-Opioid Receptor Agonist Protects the Microcirculation of Skeletal Muscle From Ischemia Reperfusion Injury.* Annals of Plastic Surgery, 2008. **61**(3): p. 330-336.

88. Yang, Y., et al., *delta-Opioid receptor activation attenuates oxidative injury in the ischemic rat brain.* BMC Biology, 2009. **7**(1): p. 55.

89. Gross, E.R., A.K. Hsu, and G.J. Gross, *The JAK/STAT pathway is essential for opioid-induced cardioprotection: JAK2 as a mediator of STAT3, Akt, and GSK-3beta.* Am J Physiol Heart Circ Physiol, 2006. **291**(2): p. H827-834.

90. Bueno, L. and J. Fioramonti, *Action of opiates on gastrointestinal function.* Baillieres Clin Gastroenterol, 1988. **2**(1): p. 123-39.

91. Grunkemeier, D.M., et al., *The narcotic bowel syndrome: clinical features, pathophysiology, and management.* Clin Gastroenterol Hepatol, 2007. **5**(10): p. 1126-39; quiz 1121-2.

92. Fire, A., et al., *Potent and specific genetic interference by double-stranded RNA in Caenorhabditis elegans.* Nature, 1998. **391**(6669): p. 806-11.

93. Yuan, J., et al., *The C. elegans cell death gene ced-3 encodes a protein similar to mammalian interleukin-1Î²-converting enzyme.* Cell, 1993. **75**(4): p. 641-652.

94. Hansson, G.r.K. and K. Edfeldt, *Toll To Be Paid at the Gateway to the Vessel Wall.* Arteriosclerosis, Thrombosis, and Vascular Biology, 2005. **25**(6): p. 1085-1087.

95. Barut, B.A. and L.I. Zon, *Realizing the potential of zebrafish as a model for human disease.* Physiol Genomics, 2000. **2**(2): p. 49-51.

96. Shin, J.T., et al., *Human-zebrafish non-coding conserved elements act in vivo to regulate transcription.* Nucleic Acids Res, 2005. **33**(17): p. 5437-45.

97. Moens, C.B., et al., *Reverse genetics in zebrafish by TILLING.* Brief Funct Genomic Proteomic, 2008. **7**(6): p. 454-9.

98. White, R.M., et al., *Transparent adult zebrafish as a tool for in vivo transplantation analysis.* Cell Stem Cell, 2008. **2**(2): p. 183-9.

99. Lieschke, G.J., et al., *Morphologic and functional characterization of granulocytes and macrophages in embryonic and adult zebrafish.* Blood, 2001. **98**(10): p. 3087-3096.

100. Meeker, N.D. and N.S. Trede, *Immunology and zebrafish: Spawning new models of human disease.* Developmental & Comparative Immunology, 2008. **32**(7): p. 745-757.

101. Novoa, B., et al., *Zebrafish: Model for the Study of Inflammation and the Innate Immune Response to Infectious Diseases: Current Topics in Innate Immunity II*. 2012, Springer New York. p. 253-275.

102. Raya, A., et al., *Activation of Notch signaling pathway precedes heart regeneration in zebrafish.* Proc Natl Acad Sci U S A, 2003. **100 Suppl 1**: p. 11889-95.

103. Belousov, V.V., et al., *Genetically encoded fluorescent indicator for intracellular hydrogen peroxide.* Nat Methods, 2006. **3**(4): p. 281-6.

104. Pan, Q., et al., *Low levels of hydrogen peroxide stimulate corneal epithelial cell adhesion, migration, and wound healing.* Invest Ophthalmol Vis Sci, 2011. **52**(3): p. 1723-34.

105. Toth, T., et al., *Evaluation of LHP(R) (1% hydrogen peroxide) cream versus petrolatum and untreated controls in open wounds in healthy horses: a randomized, blinded control study.* Acta Vet Scand, 2011. **53**: p. 45.

106. Weiss, J., et al., *Evaluation of Hydrogen Peroxide as an Intraprocedural Hemostatic Agent in Manual Dermabrasion.* Dermatologic Surgery, 2010. **36**(10): p. 1601-1603.

107. Poss, K.D., L.G. Wilson, and M.T. Keating, *Heart regeneration in zebrafish.* Science, 2002. **298**(5601): p. 2188-90.

108. Lien, C.-L., et al., *Gene Expression Analysis of Zebrafish Heart Regeneration.* PLoS Biol, 2006. **4**(8): p. e260.

109. Ng, A.N., et al., *Formation of the digestive system in zebrafish: III. Intestinal epithelium morphogenesis.* Dev Biol, 2005. **286**(1): p. 114-35.
110. Wallace, K.N., et al., *Intestinal growth and differentiation in zebrafish.* Mech Dev, 2005. **122**(2): p. 157-73.

111. H. William Detrich, I., M. Westerfield, and L. Zon, *The Zebrafish: Cellular and Developmental Biology*. Vol. 2. 2011: Academic Press.

112. Haramis, A.P., et al., *Adenomatous polyposis coli-deficient zebrafish are susceptible to digestive tract neoplasia.* EMBO Rep, 2006. **7**(4): p. 444-9.

113. Lam, S.H. and Z. Gong, *Modeling liver cancer using zebrafish: a comparative oncogenomics approach.* Cell Cycle, 2006. **5**(6): p. 573-7.

114. Rekha, R.D., et al., *Thioacetamide accelerates steatohepatitis, cirrhosis and HCC by expressing HCV core protein in transgenic zebrafish Danio rerio.* Toxicology, 2008. **243**(1-2): p. 11-22.

115. Park, S.W., et al., *Oncogenic KRAS induces progenitor cell expansion and malignant transformation in zebrafish exocrine pancreas.* Gastroenterology, 2008. **134**(7): p. 2080-90.

116. Fleming, A., J. Jankowski, and P. Goldsmith, *In vivo analysis of gut function and disease changes in a zebrafish larvae model of inflammatory bowel disease: A feasibility study.* Inflammatory Bowel Diseases, 2010. **16**(7): p. 1162-1172.

117. Oehlers, S.H., et al., *A chemical enterocolitis model in zebrafish larvae that is dependent on microbiota and responsive to pharmacological agents.* Developmental Dynamics, 2011. **240**(1): p. 288-298.

118. Brugman, S., et al., *Oxazolone-Induced Enterocolitis in Zebrafish Depends on the Composition of the Intestinal Microbiota.* Gastroenterology, 2009. **137**(5): p. 1757-1767.e1.

119. Cinaroglu, A., et al., *Activating transcription factor 6 plays protective and pathological roles in steatosis due to endoplasmic reticulum stress in zebrafish.* Hepatology, 2011. **54**(2): p. 495-508.

120. Amali, A.A., et al., *Thioacetamide induced liver damage in zebrafish embryo as a disease model for steatohepatitis.* J Biomed Sci, 2006. **13**(2): p. 225-32.

121. Passeri, M.J., et al., *Hepatic steatosis in response to acute alcohol exposure in zebrafish requires sterol regulatory element binding protein activation.* Hepatology, 2009. **49**(2): p. 443-52.

122. Groden, J., et al., *Identification and characterization of the familial adenomatous polyposis coli gene.* Cell, 1991. **66**(3): p. 589-600.

123. Kinzler, K.W., et al., *Identification of FAP locus genes from chromosome 5q21.* Science, 1991. **253**(5020): p. 661-5.

124. Su, L.K., et al., *Multiple intestinal neoplasia caused by a mutation in the murine homolog of the APC gene.* Science, 1992. **256**(5057): p. 668-70.

125. Jemal, A., et al., *Cancer Statistics, 2010.* CA: A Cancer Journal for Clinicians, 2010. **60**(5): p. 277-300.

126. Bosch, F.X., et al., *Primary liver cancer: Worldwide incidence and trends.* Gastroenterology, 2004. **127**(5, Supplement 1): p. S5-S16.

127. El-Serag, H.B., et al., *The continuing increase in the incidence of hepatocellular carcinoma in the United States: an update.* Ann Intern Med, 2003. **139**(10): p. 817-23.

128. Lee, M.N., et al., *Hepatitis C virus core protein represses the p21 promoter through inhibition of a TGF-beta pathway.* J Gen Virol, 2002. **83**(Pt 9): p. 2145-51.

129. Molodecky, N.A., et al., *Increasing Incidence and Prevalence of the Inflammatory Bowel Diseases With Time, Based on Systematic Review.* Gastroenterology, 2012. **142**(1): p. 46-54.e42.

130. Saleh, M. and C.O. Elson, *Experimental inflammatory bowel disease: insights into the host-microbiota dialog.* Immunity, 2011. **34**(3): p. 293-302.

131. Boirivant, M., et al., *Oxazolone colitis: A murine model of T helper cell type 2 colitis treatable with antibodies to interleukin 4.* J Exp Med, 1998. **188**(10): p. 1929-39.

132. Fichtner-Feigl, S., et al., *Cytokines mediating the induction of chronic colitis and colitis-associated fibrosis.* Mucosal Immunol, 2008. **1**(1s): p. S24-S27.

133. Goldsmith, J.R., J.F. Rawls, and C. Jobin, *The Neuropeptide DALDA Protects Against NSAID-Induced Acute Intestinal Injury in Zebrafish Larvae.* Gastroenterology, 2011. **140**(5): p. S-474.

134. Kim, W.R., et al., *Burden of liver disease in the United States: summary of a workshop.* Hepatology, 2002. **36**(1): p. 227-42.

135. Lazo, M. and J.M. Clark, *The Epidemiology of Nonalcoholic Fatty Liver Disease: A Global Perspective.* Semin Liver Dis, 2008. **28**(04): p. 339,350.

136. Williams, R., *Global challenges in liver disease.* Hepatology, 2006. **44**(3): p. 521-526.

137. Neuschwander-Tetri, B.A. and S.H. Caldwell, *Nonalcoholic steatohepatitis: summary of an AASLD Single Topic Conference.* Hepatology, 2003. **37**(5): p. 1202-19.

138. Sadler, K.C., et al., *A genetic screen in zebrafish identifies the mutants vps18, nf2 and foie gras as models of liver disease.* Development, 2005. **132**(15): p. 3561-72.

139. Lieber, C.S., *Alcoholic fatty liver: its pathogenesis and mechanism of progression to inflammation and fibrosis.* Alcohol, 2004. **34**(1): p. 9-19.

140. Pham, L.N., et al., *Methods for generating and colonizing gnotobiotic zebrafish.* Nat Protoc, 2008. **3**(12): p. 1862-75.

141. Uronis, J.M. and C. Jobin, *Microbes and colorectal cancer: is there a relationship?* Curr Oncol, 2009. **16**(4): p. 22-4.

142. Ley, R.E., *Obesity and the human microbiome.* Current Opinion in Gastroenterology, 2010. **26**(1): p. 5-11 10.1097/MOG.0b013e328333d751.

143. Rousseaux, C., et al., *Lactobacillus acidophilus modulates intestinal pain and induces opioid and cannabinoid receptors.* Nat Med, 2007. **13**(1): p. 35-37.

144. Amaral, F.A., et al., *Commensal microbiota is fundamental for the development of inflammatory pain.* Proceedings of the National Academy of Sciences, 2008. **105**(6): p. 2193-2197.

145. van der Sar, A.M., et al., *A star with stripes: zebrafish as an infection model.* Trends Microbiol, 2004. **12**(10): p. 451-7.

146. Kanther, M. and J.F. Rawls, *Host-microbe interactions in the developing zebrafish.* Curr Opin Immunol, 2010. **22**(1): p. 10-9.

147. Jault, C., L. Pichon, and J. Chluba, *Toll-like receptor gene family and TIR-domain adapters in Danio rerio.* Molecular Immunology, 2004. **40**(11): p. 759-771.

148. Oehlers, S.H., et al., *The inflammatory bowel disease (IBD) susceptibility genes NOD1 and NOD2 have conserved anti-bacterial roles in zebrafish.* Dis Model Mech, 2011. **4**(6): p. 832-41.

149. Hall, C., et al., *Transgenic zebrafish reporter lines reveal conserved Toll-like receptor signaling potential in embryonic myeloid leukocytes and adult immune cell lineages.* J Leukoc Biol, 2009. **85**(5): p. 751-65.

150. Fan, S., et al., *Zebrafish TRIF, a Golgi-localized protein, participates in IFN induction and NF-kappaB activation.* J Immunol, 2008. **180**(8): p. 5373-83.

151. Correa, R.G., et al., *Zebrafish IkappaB kinase 1 negatively regulates NF-kappaB activity.* Curr Biol, 2005. **15**(14): p. 1291-5.

152. Correa, R.G., et al., *Characterization of NF-kappa B/I kappa B proteins in zebra fish and their involvement in notochord development.* Mol Cell Biol, 2004. **24**(12): p. 5257-68.

153. Medzhitov, R., *Toll-like receptors and innate immunity.* Nat Rev Immunol, 2001. **1**(2): p. 135-45.

154. Janssens, S. and R. Beyaert, *A universal role for MyD88 in TLR/IL-1R-mediated signaling.* Trends in biochemical sciences, 2002. **27**(9): p. 474-482.

155. Doyle, S., et al., *IRF3 mediates a TLR3/TLR4-specific antiviral gene program.* Immunity, 2002. **17**(3): p. 251-63.

156. Bates, J.M., et al., *Intestinal alkaline phosphatase detoxifies lipopolysaccharide and prevents inflammation in zebrafish in response to the gut microbiota.* Cell Host Microbe, 2007. **2**(6): p. 371-82.

157. Stockhammer, O.W., et al., *Transcriptome profiling and functional analyses of the zebrafish embryonic innate immune response to Salmonella infection.* J Immunol, 2009. **182**(9): p. 5641-53.

158. Hall, C., et al., *The zebrafish lysozyme C promoter drives myeloid-specific expression in transgenic fish.* BMC Dev Biol, 2007. **7**: p. 42.

159. Sepulcre, M.P., et al., *Evolution of lipopolysaccharide (LPS) recognition and signaling: fish TLR4 does not recognize LPS and negatively regulates NF-kappaB activation.* J Immunol, 2009. **182**(4): p. 1836-45.

160. Sullivan, C., et al., *The gene history of zebrafish tlr4a and tlr4b is predictive of their divergent functions.* J Immunol, 2009. **183**(9): p. 5896-908.

161. Hugot, J.P., et al., *Association of NOD2 leucine-rich repeat variants with susceptibility to Crohn's disease.* Nature, 2001. **411**(6837): p. 599-603.

162. Eckmann, L. and M. Karin, *NOD2 and Crohn's disease: loss or gain of function?* Immunity, 2005. **22**(6): p. 661-7.
163. Noguchi, E., et al., *A Crohn's disease-associated NOD2 mutation suppresses transcription of human IL10 by inhibiting activity of the nuclear ribonucleoprotein hnRNP-A1.* Nat Immunol, 2009. **10**(5): p. 471-9.

164. Karrasch, T. and C. Jobin, *NF-kappaB and the intestine: friend or foe?* Inflamm Bowel Dis, 2008. **14**(1): p. 114-124.

165. Kanther, M., et al., *Microbial Colonization Induces Dynamic Temporal and Spatial Patterns of NF-kappaB Activation in the Zebrafish Digestive Tract.* Gastroenterology, 2011. **141**(1): p. 197-207.

166. Dolin, P.J., M.C. Raviglione, and A. Kochi, *Global tuberculosis incidence and mortality during 1990-2000.* Bull World Health Organ, 1994. **72**(2): p. 213-20.

167. Cohn, D.L., F. Bustreo, and M.C. Raviglione, *Drug-Resistant Tuberculosis: Review of the Worldwide Situation and the WHO/IUATLD Global Surveillance Project.* Clinical Infectious Diseases, 1997. **24**(Supplement 1): p. S121-S130.

168. Gandhi, N.R., et al., *Multidrug-resistant and extensively drug-resistant tuberculosis: a threat to global control of tuberculosis.* The Lancet, 2010. **375**(9728): p. 1830-1843.

169. Davis, J.M., et al., *Real-time visualization of mycobacterium-macrophage interactions leading to initiation of granuloma formation in zebrafish embryos.* Immunity, 2002. **17**(6): p. 693-702.

170. Clay, H., et al., *Dichotomous role of the macrophage in early Mycobacterium marinum infection of the zebrafish.* Cell Host Microbe, 2007. **2**(1): p. 29-39.

171. Davis, J.M. and L. Ramakrishnan, *The role of the granuloma in expansion and dissemination of early tuberculous infection.* Cell, 2009. **136**(1): p. 37-49.

172. Driever, W., et al., *A genetic screen for mutations affecting embryogenesis in zebrafish.* Development, 1996. **123**: p. 37-46.

173. Haffter, P., et al., *The identification of genes with unique and essential functions in the development of the zebrafish, Danio rerio.* Development, 1996. **123**: p. 1-36.

174. Amsterdam, A., et al., *A large-scale insertional mutagenesis screen in zebrafish.* Genes Dev, 1999. **13**(20): p. 2713-24.
175. Amsterdam, A., et al., *Identification of 315 genes essential for early zebrafish development.* Proc Natl Acad Sci U S A, 2004. **101**(35): p. 12792-7.

176. Emery, A.E., *The muscular dystrophies.* Lancet, 2002. **359**(9307): p. 687-95.

177. Granato, M., et al., *Genes controlling and mediating locomotion behavior of the zebrafish embryo and larva.* Development, 1996. **123**(1): p. 399-413.

178. Bassett, D.I., et al., *Dystrophin is required for the formation of stable muscle attachments in the zebrafish embryo.* Development, 2003. **130**(23): p. 5851-60.

179. Ong, A.C. and D.N. Wheatley, *Polycystic kidney disease--the ciliary connection.* Lancet, 2003. **361**(9359): p. 774-6.

180. Sun, Z., et al., *A genetic screen in zebrafish identifies cilia genes as a principal cause of cystic kidney.* Development, 2004. **131**(16): p. 4085-93.

181. Hershberger, R.E., A. Morales, and J.D. Siegfried, *Clinical and genetic issues in dilated cardiomyopathy: a review for genetics professionals.* Genet Med, 2010. **12**(11): p. 655-67.

182. Rakar, S., et al., *Epidemiology of dilated cardiomyopathy.* European Heart Journal, 1997. **18**(1): p. 117-123.

183. Jiang, H. and J. Ge, *Epidemiology and clinical management of cardiomyopathies and heart failure in China.* Heart, 2009. **95**(21): p. 1727-1731.

184. Chen, J.N., et al., *Mutations affecting the cardiovascular system and other internal organs in zebrafish.* Development, 1996. **123**: p. 293-302.

185. Stainier, D.Y., et al., *Mutations affecting the formation and function of the cardiovascular system in the zebrafish embryo.* Development, 1996. **123**: p. 285-92.

186. Sehnert, A.J., et al., *Cardiac troponin T is essential in sarcomere assembly and cardiac contractility.* Nat Genet, 2002. **31**(1): p. 106-10.

187. Xu, X., et al., *Cardiomyopathy in zebrafish due to mutation in an alternatively spliced exon of titin.* Nat Genet, 2002. **30**(2): p. 205-9.

188. Hennekam, R.C.M., *Hutchinson–Gilford progeria syndrome: Review of the phenotype.* American Journal of Medical Genetics Part A, 2006. **140A**(23): p. 2603-2624.

189. Koshimizu, E., et al., *Embryonic senescence and laminopathies in a progeroid zebrafish model.* PLoS One, 2011. **6**(3): p. e17688.

190. Parng, C., et al., *Zebrafish: A Preclinical Model for Drug Screening.* ASSAY and Drug Development Technologies, 2002. **1**(1): p. 41-48.

191. Weinstein, B.M., et al., *Gridlock, a localized heritable vascular patterning defect in the zebrafish.* Nat Med, 1995. **1**(11): p. 1143-7.

192. Kenny, D. and Z.M. Hijazi, *Coarctation of the aorta: from fetal life to adulthood.* Cardiol J. **18**(5): p. 487-95.

193. Zhong, T.P., et al., *gridlock, an HLH gene required for assembly of the aorta in zebrafish.* Science, 2000. **287**(5459): p. 1820-4.

194. Zhong, T.P., et al., *Gridlock signalling pathway fashions the first embryonic artery.* Nature, 2001. **414**(6860): p. 216-20.

195. Peterson, R.T., et al., *Chemical suppression of a genetic mutation in a zebrafish model of aortic coarctation.* Nat Biotechnol, 2004. **22**(5): p. 595-9.

196. Ren, B., et al., *ERK1/2-Akt1 crosstalk regulates arteriogenesis in mice and zebrafish.* J Clin Invest, 2010. **120**(4): p. 1217-28.

197. Roden, D.M., *Drug-induced prolongation of the QT interval.* N Engl J Med, 2004. **350**(10): p. 1013-22.

198. Langheinrich, U., G. Vacun, and T. Wagner, *Zebrafish embryos express an orthologue of HERG and are sensitive toward a range of QT-prolonging drugs inducing severe arrhythmia.* Toxicol Appl Pharmacol, 2003. **193**(3): p. 370-82.

199. Milan, D.J., et al., *Drugs that induce repolarization abnormalities cause bradycardia in zebrafish.* Circulation, 2003. **107**(10): p. 1355-8.

200. Woods, I.G., et al., *A comparative map of the zebrafish genome.* Genome Res, 2000. **10**(12): p. 1903-14.

201. Etchin, J., J.P. Kanki, and A.T. Look, *Zebrafish as a model for the study of human cancer.* Methods Cell Biol, 2011. **105**: p. 309-37.

202. Lee, L.M., et al., *The fate of human malignant melanoma cells transplanted into zebrafish embryos: assessment of migration and cell division in the absence of tumor formation.* Dev Dyn, 2005. **233**(4): p. 1560-70.

203. Stoletov, K., et al., *High-resolution imaging of the dynamic tumor cell vascular interface in transparent zebrafish.* Proc Natl Acad Sci U S A, 2007. **104**(44): p. 17406-11.

204. Topczewska, J.M., et al., *Embryonic and tumorigenic pathways converge via Nodal signaling: role in melanoma aggressiveness.* Nat Med, 2006. **12**(8): p. 925-32.

205. Goldsmith, J.R., J.M. Uronis, and C. Jobin, *Mu Opioid Signaling Protects Against Acute Murine Intestinal Injury in a Manner Involving Stat3 Signaling.* The American Journal of Pathology, 2011. **179**(2): p. 673-683.

206. Meeker, N.D. and N.S. Trede, *Immunology and zebrafish: spawning new models of human disease.* Dev Comp Immunol, 2008. **32**(7): p. 745-57.

207. Maiden, L., et al., *A quantitative analysis of NSAID-induced small bowel pathology by capsule enteroscopy.* Gastroenterology, 2005. **128**(5): p. 1172-8.

208. Grosser, T., et al., *Developmental expression of functional cyclooxygenases in zebrafish.* Proceedings of the National Academy of Sciences of the United States of America, 2002. **99**(12): p. 8418-8423.

209. Flynn, E.J., 3rd, C.M. Trent, and J.F. Rawls, *Ontogeny and nutritional control of adipogenesis in zebrafish (Danio rerio).* J Lipid Res, 2009. **50**(8): p. 1641-52.

210. Jin, S.W., et al., *Cellular and molecular analyses of vascular tube and lumen formation in zebrafish.* Development, 2005. **132**(23): p. 5199-209.

211. Traver, D., et al., *Transplantation and in vivo imaging of multilineage engraftment in zebrafish bloodless mutants.* Nat Immunol, 2003. **4**(12): p. 1238 - 1246.

212. Abramoff, M., P. Magelhaes, and S. Ram, *Image Processing with ImageJ.* Biophotonics International, 2004. **11**(7): p. 36 - 42.

213. Trotter, A.J., A.C. Parslow, and J.K. Heath, *Morphologic analysis of the zebrafish digestive system.* Methods Mol Biol, 2009. **546**: p. 289-315.

214. Russel, L. and S. Burguet, *Ultrastructure of leydig cells as revealed by secondary tissue treatment with a ferrocyanide-osmium mixture.* Tissue Cell, 1977. **9**(4): p. 751-66.

215. Reynolds, E.S., *The use of lead citrate at high pH as an electron-opaque stain in electron microscopy.* J Cell Biol, 1963. **17**: p. 208-12.

216. Senghaas, N. and R.W. KÃ¶ster, *Culturing and Transfecting Zebrafish PAC2 Fibroblast Cells.* Cold Spring Harbor Protocols, 2009. **2009**(6): p. pdb.prot5235.

217. Teraoka, H., et al., *Role of the cyclooxygenase 2-thromboxane pathway in 2,3,7,8-tetrachlorodibenzo-p-dioxin-induced decrease in mesencephalic vein blood flow in the zebrafish embryo.* Toxicol Appl Pharmacol, 2009. **234**(1): p. 33-40.

218. Stricker, B.H., R.R. de Groot, and J.H. Wilson, *Anaphylaxis to glafenine.* Lancet, 1990. **336**(8720): p. 943-4.

219. van der Klauw, M.M., et al., *A population based case-cohort study of drug-induced anaphylaxis.* Br J Clin Pharmacol, 1993. **35**(4): p. 400-8.

220. North, T.E., et al., *PGE2-regulated wnt signaling and N-acetylcysteine are synergistically hepatoprotective in zebrafish acetaminophen injury.* Proceedings of the National Academy of Sciences, 2010. **107**(40): p. 17315-17320.

221. Ootani, A., et al., *Sustained in vitro intestinal epithelial culture within a Wnt-dependent stem cell niche.* Nat Med, 2009. **15**(6): p. 701-706.

222. Zhao, J., et al., *R-spondin1, A Novel Intestinotrophic Mitogen, Ameliorates Experimental Colitis in Mice.* Gastroenterology, 2007. **132**(4): p. 1331-1343.

223. Shen, J., et al., *Stable binding of ATF6 to BiP in the endoplasmic reticulum stress response.* Mol Cell Biol, 2005. **25**(3): p. 921-32.

224. Codogno, P. and A.J. Meijer, *Autophagy and signaling: their role in cell survival and cell death.* Cell Death Differ, 2005. **12 Suppl 2**: p. 1509-18.

225. Franceschelli, S., et al., *In the Huh7 Hepatoma Cells Diclofenac and Indomethacin Activate Differently the Unfolded Protein Response and Induce ER Stress Apoptosis.* Open Biochem J, 2011. **5**: p. 45-51.

226. Hama, K., et al., *In vivo imaging of zebrafish digestive organ function using multiple quenched fluorescent reporters.* American Journal of Physiology - Gastrointestinal and Liver Physiology, 2009. **296**(2): p. G445-G453.

227. Somasundaram, et al., *Uncoupling of intestinal mitochondrial oxidative phosphorylation and inhibition of cyclooxygenase are required for the development of NSAID-enteropathy in the rat.* Alimentary Pharmacology & Therapeutics, 2000. **14**(5): p. 639-650.

228. Pang, Y. and W. Ge, *Epidermal Growth Factor and TGFβ Promote Zebrafish Oocyte Maturation in Vitro: Potential Role of the Ovarian Activin Regulatory System.* Endocrinology, 2002. **143**(1): p. 47-54.

229. Pozios, K.C., et al., *IGFs stimulate zebrafish cell proliferation by activating MAP kinase and PI3-kinase-signaling pathways.* American Journal of Physiology - Regulatory, Integrative and Comparative Physiology, 2001. **280**(4): p. R1230-R1239.

230. Borner, C., et al., *Mechanisms of Opioid-Mediated Inhibition of Human T Cell Receptor Signaling.* J Immunol, 2009. **183**(2): p. 882-889.

231. Mani, A.R. and K.P. Moore, *New insights into the role of endogenous opioids in the pathogenesis of gastrointestinal and liver disease.* Gut, 2009. **58**(7): p. 893-895.

232. Gainetdinov, R.R., et al., *Desensitization of G protein-coupled receptors and neuronal functions.* Annu Rev Neurosci, 2004. **27**: p. 107-144.

233. Kieffer, B.L. and C. Gavériaux-Ruff, *Exploring the opioid system by gene knockout.* Progress in Neurobiology, 2002. **66**(5): p. 285-306.

234. Wirtz, S., et al., *Chemically induced mouse models of intestinal inflammation.* Nat Protoc, 2007. **2**(3): p. 541-546.

235. Menéndez, L., et al., *Analgesic effects of loperamide in bone cancer pain in mice.* Pharmacology Biochemistry and Behavior, 2005. **81**(1): p. 114-121.

236. Murthy, S.N., et al., *Treatment of dextran sulfate sodium-induced murine colitis by intracolonic cyclosporin.* Dig Dis Sci, 1993. **38**(9): p. 1722-1734.

237. Uronis, J.M., et al., *Modulation of the intestinal microbiota alters colitis-associated colorectal cancer susceptibility.* PLoS ONE, 2009. **4**(6): p. e6026.

238. Cooper, H.S., et al., *Clinicopathologic study of dextran sulfate sodium experimental murine colitis.* Lab Invest, 1993. **69**(2): p. 238-249.

239. Dieleman, L.A., et al., *Chronic experimental colitis induced by dextran sulphate sodium (DSS) is characterized by Th1 and Th2 cytokines.* Clin Exp Immunol, 1998. **114**(3): p. 385-391.

240. Williams, K.L., et al., *Enhanced survival and mucosal repair after dextran sodium sulfate-induced colitis in transgenic mice that overexpress growth hormone.* Gastroenterology, 2001. **120**(4): p. 925-937.

241. Haller, D., et al., *IKK-beta and Phosphatidylinositol 3-Kinase/Akt Participate in Non-pathogenic Gram-negative Enteric Bacteria-induced RelA Phosphorylation and NF-κB Activation in Both Primary and Intestinal Epithelial Cell Lines.* Journal of Biological Chemistry, 2002. **277**(41): p. 38168-38178.

242. Haller, D., et al., *Transforming Growth Factor-{beta}1 Inhibits Non-pathogenic Gramnegative Bacteria-induced NF-{kappa}B Recruitment to the Interleukin-6 Gene Promoter in Intestinal Epithelial Cells through Modulation of Histone Acetylation.* J. Biol. Chem., 2003. **278**(26): p. 23851-23860.

243. Joo, Y., et al., *Tomato lycopene extract prevents lipopolysaccharide-induced NF-κB signaling but worsens dextran sulfate sodium-induced colitis in NF-κB^{EGFP} mice.* PLoS ONE, 2009. **4**(2): p. e4562.

244. Snider, A.J., et al., *A role for sphingosine kinase 1 in dextran sulfate sodium-induced colitis.* FASEB J., 2009. **23**(1): p. 143-152.

245. Karrasch, T., et al., *Wound-induced p38MAPK-dependent histone H3 phosphorylation correlates with increased COX-2 expression in enterocytes.* Journal of Cellular Physiology, 2006. **207**(3): p. 809-815.

246. Cook, J.A. and J.B. Mitchell, *Viability measurements in mammalian cell systems.* Analytical Biochemistry, 1989. **179**(1): p. 1-7.

247. Kovacic, J.C., et al., *Stat3-dependent acute Rantes production in vascular smooth muscle cells modulates inflammation following arterial injury in mice.* J Clin Invest. **120**(1): p. 303-314.

248. Karrasch, T., et al., *Gnotobiotic IL-10-/-;NF-kappa B(EGFP) mice reveal the critical role of TLR/NF-kappa B signaling in commensal bacteria-induced colitis.* J Immunol, 2007. **178**(10): p. 6522-6532.

249. Karrasch, T., et al., *The Flavonoid Luteolin Worsens Chemical-Induced Colitis in NF-{kappa}BTransgenic Mice through Blockade of NF-{kappa}B-Dependent Protective Molecules.* PLoS ONE, 2007. **2**(7): p. e596.

250. Zheng, H., H.H. Loh, and P.-Y. Law, *Beta-Arrestin-Dependent Mu-Opioid Receptor-Activated Extracellular Signal-Regulated Kinases (ERKs) Translocate to Nucleus in Contrast to G Protein-Dependent ERK Activation.* Molecular Pharmacology, 2008. **73**(1): p. 178-190.

251. Almela, P., M.V. Milanés, and M.L. Laorden, *Activation of the ERK signalling pathway contributes to the adaptive changes in rat hearts during naloxone-induced morphine withdrawal.* British Journal of Pharmacology, 2007. **151**(6): p. 787-797.

252. Jun-Li, C., et al., *Activation of the spinal ERK signaling pathway contributes naloxone-precipitated withdrawal in morphine-dependent rats.* Pain, 2005. **118**(3): p. 336-349.

253. Granata, R., et al., *Growth hormone-releasing hormone promotes survival of cardiac myocytes in vitro and protects against ischaemiaâ€“reperfusion injury in rat heart.* Cardiovascular Research, 2009. **83**(2): p. 303-312.

254. Ma, J., et al., *Morphine Disrupts Interleukin-23 (IL-23)/IL-17-Mediated Pulmonary Mucosal Host Defense against Streptococcus pneumoniae Infection.* Infect. Immun. **78**(2): p. 830-837.

255. Wei, G., J. Moss, and C.-S. Yuan, *Opioid-induced immunosuppression: is it centrally mediated or peripherally mediated?* Biochemical Pharmacology, 2003. **65**(11): p. 1761-1766.

256. Egan, L.J., et al., *IkappaB-kinasebeta-dependent NF-kappaB activation provides radioprotection to the intestinal epithelium.* Proc Natl Acad Sci U S A, 2004. **101**(8): p. 2452-7.

257. Greten, F.R., et al., *IKKbeta links inflammation and tumorigenesis in a mouse model of colitis-associated cancer.* Cell, 2004. **118**(3): p. 285-96.

258. Nenci, A., et al., *Epithelial NEMO links innate immunity to chronic intestinal inflammation.* Nature, 2007. **446**(7135): p. 557-561.

259. Joo Sung Kim, C.J., *The flavonoid luteolin prevents lipopolysaccharide-induced NF-{kappa};B signalling and gene expression by blocking*

I{kappa}B kinase activity in intestinal epithelial cells and bone-marrow derived dendritic cells. Immunology, 2005. **115**(3): p. 375-387.

260. Grivennikov, S., et al., *IL-6 and Stat3 are required for survival of intestinal epithelial cells and development of colitis-associated cancer.* Cancer Cell, 2009. **15**(2): p. 103-113.

261. Grivennikov, S., et al., *IL-6 and Stat3 Are Required for Survival of Intestinal Epithelial Cells and Development of Colitis-Associated Cancer.* Cancer Cell, 2009. **15**(2): p. 103-113.

262. Yu, H., D. Pardoll, and R. Jove, *STATs in cancer inflammation and immunity: a leading role for STAT3.* Nat Rev Cancer, 2009. **9**(11): p. 798-809.

263. Sturm, A. and A.U. Dignass, *Epithelial restitution and wound healing in inflammatory bowel disease.* World J Gastroenterol, 2008. **14**(3): p. 348-53.

264. Guslandi, M., *Exacerbation of inflammatory bowel disease by nonsteroidal anti-inflammatory drugs and cyclooxygenase-2 inhibitors: fact or fiction?* World J Gastroenterol, 2006. **12**(10): p. 1509-10.

265. Wong, G.T., et al., *Remifentanil reduces the release of biochemical markers of myocardial damage after coronary artery bypass surgery: a randomized trial.* J Cardiothorac Vasc Anesth, 2010. **24**(5): p. 790-6.

266. Duronio, V., *The life of a cell: apoptosis regulation by the PI3K/PKB pathway.* Biochem J, 2008. **415**(3): p. 333-44.

267. Jilling, T., et al., *Intestinal Epithelial Apoptosis Initiates Gross Bowel Necrosis in an Experimental Rat Model of Neonatal Necrotizing Enterocolitis.* Pediatric Research, 2004. **55**(4): p. 622-629.

268. Hoentjen, F., et al., *STAT3 regulates NF-kappaB recruitment to the IL-12p40 promoter in dendritic cells.* Blood, 2005. **105**(2): p. 689-96.

269. Roth, B.L., M.B. Laskowski, and C.J. Coscia, *Evidence for distinct subcellular sites of opiate receptors. Demonstration of opiate receptors in smooth microsomal fractions isolated from rat brain.* J Biol Chem, 1981. **256**(19): p. 10017-23.

270. Karrasch, T., et al., *PI3K-dependent GSK3B(Ser9)-phosphorylation is implicated in the intestinal epithelial cell wound-healing response.* PLoS ONE, 2011. **6**(10): p. e26340.

271. Feinman, R., et al., *HIF-1 mediates pathogenic inflammatory responses to intestinal ischemia-reperfusion injury.* Am J Physiol Gastrointest Liver Physiol, 2010. **299**(4): p. G833-43.

272. Rollwagen, F.M., et al., *IL-6 protects enterocytes from hypoxia-induced apoptosis by induction of bcl-2 mRNA and reduction of fas mRNA.* Biochem Biophys Res Commun, 2006. **347**(4): p. 1094-8.

273. Uno, J.K., et al., *Altered macrophage function contributes to colitis in mice defective in the phosphoinositide-3 kinase subunit p110delta.* Gastroenterology, 2010. **139**(5): p. 1642-53, 1653 e1-6.

274. Vanhaesebroeck, B., et al., *Synthesis and function of 3-phosphorylated inositol lipids.* Annu Rev Biochem, 2001. **70**: p. 535-602.

275. Guillermet-Guibert, J., et al., *The p110beta isoform of phosphoinositide 3-kinase signals downstream of G protein-coupled receptors and is functionally redundant with p110gamma.* Proc Natl Acad Sci U S A, 2008. **105**(24): p. 8292-7.

276. Gentili, C., S. Morelli, and A. Russo De Boland, *Involvement of PI3-kinase and its association with c-Src in PTH-stimulated rat enterocytes.* J Cell Biochem, 2002. **86**(4): p. 773-83.

277. Laprise, P., et al., *Phosphatidylinositol 3-kinase controls human intestinal epithelial cell differentiation by promoting adherens junction assembly and p38 MAPK activation.* J Biol Chem, 2002. **277**(10): p. 8226-34.

278. Moran, A.E., et al., *Apc Deficiency Is Associated with Increased Egfr Activity in the Intestinal Enterocytes and Adenomas of C57BL/6J-Min/+ Mice.* Journal of Biological Chemistry, 2004. **279**(41): p. 43261-43272.

279. Leone, V., et al., *PGE2 inhibits apoptosis in human adenocarcinoma Caco-2 cell line through Ras-PI3K association and cAMP-dependent kinase A activation.* American Journal of Physiology - Gastrointestinal and Liver Physiology, 2007. **293**(4): p. G673-G681.

280. Hung, S.-C., et al., *Angiogenic Effects of Human Multipotent Stromal Cell Conditioned Medium Activate the PI3K-Akt Pathway in Hypoxic Endothelial Cells to Inhibit Apoptosis, Increase Survival, and Stimulate Angiogenesis.* Stem Cells, 2007. **25**(9): p. 2363-2370.

281. Alonzi, T., et al., *Induced somatic inactivation of STAT3 in mice triggers the development of a fulminant form of enterocolitis.* Cytokine, 2004. **26**(2): p. 45-56.

282. Sugimoto, K., *Role of STAT3 in inflammatory bowel disease.* World J Gastroenterol, 2008. **14**(33): p. 5110-4.

283. Sugimoto, K., et al., *IL-22 ameliorates intestinal inflammation in a mouse model of ulcerative colitis.* J Clin Invest, 2008. **118**(2): p. 534-544.

284. Sellon, R.K., et al., *Resident enteric bacteria are necessary for development of spontaneous colitis and immune system activation in interleukin-10-deficient mice.* Infect Immun, 1998. **66**(11): p. 5224-31.

285. Grundtner, P., et al., *The IL-10R1 S138G loss-of-function allele and ulcerative colitis.* Genes Immun, 2008. **10**(1): p. 84-92.

286. Scheinn, T., et al., *Validation of the interleukin-10 knockout mouse model of colitis: antitumour necrosis factor-antibodies suppress the progression of colitis.* Clinical & Experimental Immunology, 2003. **133**(1): p. 38-43.

287. Vogt, P.K. and J.R. Hart, *PI3K and STAT3: A New Alliance.* Cancer Discovery, 2011. **1**(6): p. 481-486.

288. Park, S.W., et al., *The regulatory subunits of PI3K, p85[alpha] and p85[beta], interact with XBP-1 and increase its nuclear translocation.* Nat Med, 2010. **16**(4): p. 429-437.

289. Barrie, A. and S. Plevy, *Treatment of Immune-Mediated Extraintestinal Manifestations of Inflammatory Bowel Disease with Infliximab.* Gastroenterology Clinics of North America, 2006. **35**(4): p. 883-893.

290. Rentoukas, I., et al., *Cardioprotective role of remote ischemic periconditioning in primary percutaneous coronary intervention: enhancement by opioid action.* JACC Cardiovasc Interv, 2010. **3**(1): p. 49-55.

291. Carroll, I.M., et al., *Luminal and mucosal-associated intestinal microbiota in patients with diarrhea-predominant irritable bowel syndrome.* Gut Pathog, 2010. **2**(1): p. 19.